

RD-R141 369

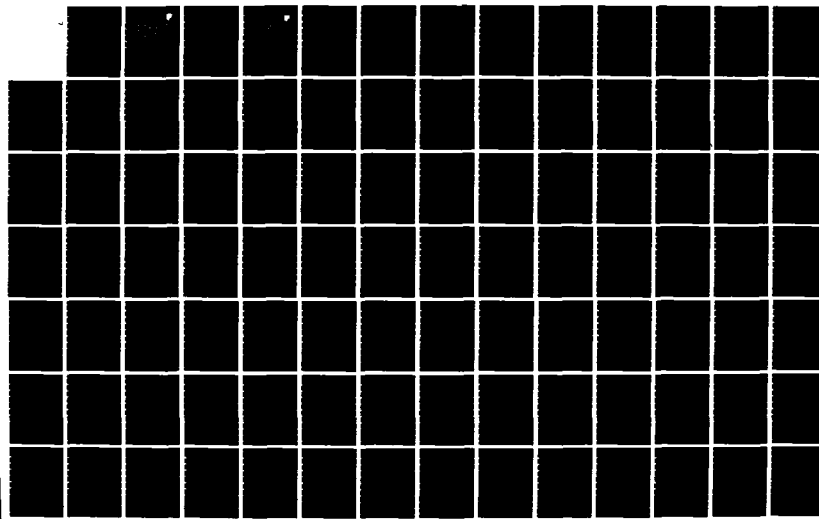
BASIC EMC (ELECTROMAGNETIC COMPATIBILITY) TECHNOLOGY
ADVANCEMENT FOR C3 S. (U) SOUTHEASTERN CENTER FOR
ELECTRICAL ENGINEERING EDUCATION INC S.

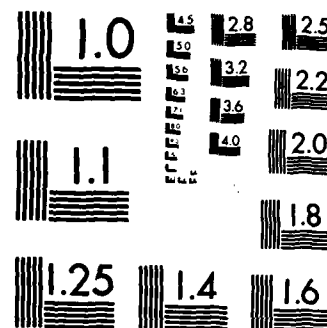
1/2

UNCLASSIFIED

G K CHEN ET AL. DEC 83 RADC-TR-82-286-VOL-1 F/G 9/5

NL





MICROCOPY RESOLUTION TEST CHART
NATIONAL BUREAU OF STANDARDS-1963-A

1:2
RADC-TR-82-286, Vol I (of six)
Final Technical Report
December 1983



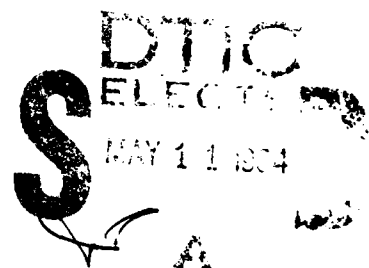
BASIC EMC TECHNOLOGY ADVANCEMENT FOR C³ SYSTEMS - A Nonlinear Macromodel of the Bipolar Integrated Circuit Operational Amplifier for Electromagnetic Interference Analysis

AD-A141 369

DTIC FILE COPY

Southeastern Center for Electrical Engineering Education

Gordon Kowa-Cheng Chen and James J. Whalen



APPROVED FOR PUBLIC RELEASE; DISTRIBUTION UNLIMITED

**ROME AIR DEVELOPMENT CENTER
Air Force Systems Command
Griffiss Air Force Base, NY 13441**

This report has been reviewed by the RADC Public Affairs Office (PA) and is releasable to the National Technical Information Service (NTIS). At NTIS it will be releasable to the general public, including foreign nations.

RADC-TR-82-286, Volume I (of six) has been reviewed and is approved for publication.

APPROVED:

by R. S. Stratton

ROY F. STRATTON
Project Engineer

APPROVED:

W. S. Tuthill

W. S. TUTHILL, Colonel, USAF
Chief, Reliability & Compatibility Division

FOR THE COMMANDER:

John P. Huss

JOHN P. HUSS
Acting Chief, Plans Office

If your address has changed or if you wish to be removed from the RADC mailing list, or if the addressee is no longer employed by your organization, please notify RADC (RBCT) Griffiss AFB NY 13441. This will assist us in maintaining a current mailing list.

Do not return copies of this report unless contractual obligations or notices on a specific document requires that it be returned.

RADC-TR-82-286, Vol 1 (of six)

Final Technical Report

December 1983



***BASIC EMC TECHNOLOGY ADVANCEMENT
FOR C³ SYSTEMS - A Nonlinear
Macromodel of the Bipolar Integrated
Circuit Operational Amplifier for
Electromagnetic Interference Analysis***

Southeastern Center for Electrical Engineering Education

Gordon Kow-Cheng Chen and James J. Whalen

APPROVED FOR PUBLIC RELEASE; DISTRIBUTION UNLIMITED

**ROME AIR DEVELOPMENT CENTER
Air Force Systems Command
Griffiss Air Force Base, NY 13441**

This report has been reviewed by the RADC Public Affairs Office (PA) and is releasable to the National Technical Information Service (NTIS). At NTIS it will be releasable to the general public, including foreign nations.

RADC-TR-82-286, Volume I (of six) has been reviewed and is approved for publication.

APPROVED:

By F. S. Stratton

ROY F. STRATTON
Project Engineer

APPROVED:

W. S. Tuthill

W. S. TUTHILL, Colonel, USAF
Chief, Reliability & Compatibility Division

FOR THE COMMANDER:

John P. Huss

JOHN P. HUSS
Acting Chief, Plans Office

If your address has changed or if you wish to be removed from the RADC mailing list, or if the addressee is no longer employed by your organization, please notify RADC (RBCT) Griffiss AFB NY 13441. This will assist us in maintaining a current mailing list.

Do not return copies of this report unless contractual obligations or notices on a specific document requires that it be returned.

UNCLASSIFIED

SECURITY CLASSIFICATION OF THIS PAGE (When Data Entered)

REPORT DOCUMENTATION PAGE		READ INSTRUCTIONS BEFORE COMPLETING FORM RECIPIENT'S CATALOG NUMBER
1. REPORT NUMBER	2. GOVT ACCESSION NO.	A141369
3. RADC-TR-82-286, Vol I (of six)		5. TYPE OF REPORT & PERIOD COVERED Final Technical Report Jun 81 - Jun 82
4. TITLE (and Subtitle) BASIC EMC TECHNOLOGY ADVANCEMENT FOR C ³ SYSTEMS-A NONLINEAR MACROMODEL OF THE BIPOLAR INTEGRATED CIRCUIT OPERATIONAL AMPLI- FIER FOR ELECTROMAGNETIC INTERFERENCE ANALYSIS		6. PERFORMING ORG. REPORT NUMBER N/A
7. AUTHOR(s) Gordon Kowa-Cheng Chen James J. Whalen		8. CONTRACT OR GRANT NUMBER(s) F30602-81-C-0062
9. PERFORMING ORGANIZATION NAME AND ADDRESS Southeastern Center for Electrical Engineering Education 1101 Massachusetts Ave. St Cloud FL 32706		10. PROGRAM ELEMENT, PROJECT, TASK AREA & WORK UNIT NUMBERS 62702F 23380335
11. CONTROLLING OFFICE NAME AND ADDRESS Rome Air Development Center (RBCT) Griffiss AFB NY 13441		12. REPORT DATE December 1983
13. NUMBER OF PAGES 142		14. SECURITY CLASS. (of this report) UNCLASSIFIED
15. DECLASSIFICATION DOWNGRADING SCHEDULE N/A		16. DISTRIBUTION STATEMENT (of this Report) Approved for public release; distribution unlimited.
17. DISTRIBUTION STATEMENT (of the abstract entered in Block 20, if different from Report) Same		
18. SUPPLEMENTARY NOTES RADC Project Engineers: Roy F. Stratton; Gerard T. Capraro (RBCT) This investigation was performed at the State University of New York at Buffalo, Dept of Electrical Engineering, Buffalo NY 14226. Additional Volumes II - VI are being published.		
19. KEY WORDS (Continue on reverse side if necessary and identify by block number) Electromagnetic Compatibility Nonlinear Response Electromagnetic Interference Nonlinear Transfer Functions Operational Amplifiers Nonlinear Circuit Analysis Program Macromodel (NCAP) SPICE		
20. ABSTRACT (Continue on reverse side if necessary and identify by block number) A macromodel containing two transistors can accurately predict how amplitude modulated RF signals with RF carrier frequencies in the 0.05 to 100.0 MHz range are demodulated in bipolar operational amplifiers (uA741 and LM10 op amps) to cause undesired low frequency responses related to the modulation envelope of the RF signals. The original op amp macromodel which was developed by Boyle et al was modified by adding four capacitors C _{sub} to account for parasitic capacitance effects in integrated circuit		

UNCLASSIFIED

SECURITY CLASSIFICATION OF THIS PAGE(When Data Entered)

op amps. A procedure for assigning C_{sub} values is given. The macromodel can be used when the RFI signals are incident upon the op amp input terminals. The use of the macromodel leads to substantial reduction in computer time and expense.

The ability of the nonlinear macromodel to represent the overall integrated circuit nonlinear response with only two transistors at the input stage is explained using the feedback theory of cascaded nonlinear transfer functions. In an operational amplifier with a linear feedback in its second stage, the nonlinear response of the second stage is suppressed. The overall nonlinear response is dominated by the nonlinearities of the input stage.

UNCLASSIFIED

SECURITY CLASSIFICATION OF THIS PAGE(When Data Entered)

ABSTRACT

A macromodel containing two transistors can accurately predict how amplitude modulated RF signals with RF carrier frequencies in the .05 to 100 MHz range are demodulated in bipolar operational amplifiers (μ A741 and LM10 op amps) to cause undesired low frequency responses related to the modulation envelope of the RF signals. The original op amp macromodel which was developed by Boyle et al. was modified by adding four capacitors C_{sub} to account for parasitic capacitance effects in integrated circuit op amps. A procedure for assigning C_{sub} values is given. The macromodel can be used when the RFI signals are incident upon the op amp input terminals. The use of the macromodel leads to a substantial reduction in computer time and expense.

The ability of the nonlinear macromodel to represent the overall integrated circuit nonlinear response with only two transistors at the input stage is explained using the feedback theory of cascaded nonlinear transfer functions. In an operational amplifier with a linear feedback in its second stage, the nonlinear response of the second stage is suppressed. The overall nonlinear response is dominated by the nonlinearities of the input stage.



ACKNOWLEDGEMENTS

There are many who have contributed to the investigation and to the preparation of the report. At RADC Mr. Carmen A. Paludi, Jr. has followed the investigation from its inception and has provided encouragement and suggestions. Both he and Dr. Roy F. Stratton have read drafts of the manuscripts and have provided valuable criticism. The contributions of Mr. Jon B. Valenti deserve special consideration. With his assistance, many NCAP simulations were made on the RADC computing system. His aid was invaluable. At the State University of New York at Buffalo, Mr. Robert Bennett and Mr. Kun-Nau Chen assisted with the experiment and other technical matters. Mrs. Joan G. Bennett and Mrs. Mary M. Hill typed numerous drafts. Mr. Peter Talarico performed the photographic work. Miss Beth Whalen, Miss Cathy Whalen and Miss Paula Gilmour prepared the figures. To all who have contributed to the investigation and to the report goes a well-deserved thank you.

TABLE OF CONTENTS

	<u>Page</u>
LIST OF ILLUSTRATIONS	vii
LIST OF TABLES	xi
1. INTRODUCTION	1
1.1 EMI, Nonlinearity, and Nonlinear Transfer Function. . .	3
1.2 System Nonlinearity of the Integrated BJT Operational Amplifier	17
1.3 Macromodeling of BJT ICs.	24
2. THE NONLINEAR MACROMODEL FOR EMI ANALYSIS OF THE BIPOLAR IC OPERATIONAL AMPLIFIER.	31
2.1 The Nonlinear Macromodel Based on a Two-Transistor Physical Representation	31
2.2 NCAP Intermodulation Predictions with the Nonlinear Macromodel and Experimental Verification.	37
2.3 Substrate Capacitances in Nonlinear Macromodeling . . .	45
3. MACROMODELING PROCEDURE AND APPLICATION.	51
3.1 The Macromodeling Procedure	52
3.2 Macromodeling of the LM10 Bipolar IC Op Amp	53
3.3 Calculation of the Macromodel Parameters.	56
3.4 NCAP Predictions for the Second Order Transfer Function $H_2(f_2, -f_1)$ Based on the Nonlinear Macromodel.	61

TABLE OF CONTENTS (Continued)

	<u>Page</u>
4. NETWORK THEORY FOR THE NONLINEAR MACROMODEL.	74
4.1 Cascade Configuration for the IC Operational Amplifier.	74
4.2 The Effect of Internal Feedback on a Cascade Nonlinear Transfer Function	81
4.3 Nonlinear Modeling of the Input Stage	86
5. CONCLUSIONS AND RECOMMENDATIONS.	91
5.1 Conclusions	91
5.2 Recommendations	93
REFERENCES	96
Appendix A. Reprint of Paper "Macromodel Predictions for EMI in Bipolar Operational Amplifiers"	104
Appendix B. LM10 Op Amp and Voltage Reference Data Sheets. . .	117

LIST OF ILLUSTRATIONS

<u>FIGURE</u>		<u>PAGE</u>
1-1	Intermodulation Type of EMI Arising from Second Degree Nonlinearity of a Receiver.	4
1-2	A Small-Signal Nonlinear Incremental T-Model for the BJT	6
1-3	Experimental System for Measuring Second Order Intermodulation Effect at Frequency $f_{AF} = f_2 - f_1$	6
1-4	Representative Intermodulation Data Obtained with Experimental System Shown in Figure 1-3	11
1-5	Interfering Signal Strength versus RF Frequency for an Electronic Circuit with Second Order Nonlinearity . . .	11
1-6	Frequency Response of Second Order Nonlinear Transfer Function.	15
1-7	Experimental System for Measuring Third Order Transfer Functions $H_3(-f_1, f_2, f_2)$	16
1-8	Schematic Diagram of the 741 Op Amp	18
1-9	NCAP Input Coding Diagram for the 741 Op Amp in the Buffer Amplifier Configuration.	18
1-10	Predicted and Measured Values for a 741 Op Amp Buffer Amplifier First Order Transfer Function	20
1-11	Measured and Predicted Values for a 741 Op Amp Buffer Amplifier Second Order Transfer Function.	20
1-12	A Macromodel for the 741 Type BJT IC Op Amp for DC, Small-Signal and Transient Analyses	26
1-13	A Small-Signal Macromodel	26

LIST OF ILLUSTRATIONS (Continued)

<u>FIGURE</u>		<u>PAGE</u>
1-14	Op Amp Macromodel for AC, Transient, and Thermal Analysis.	28
2-1	Schematic Representation of the 741 Type Op Amp	33
2-2	Nonlinear Macromodel for the BJT IC Op Amp in Small-Signal Operation.	33
2-3	Unity Gain Buffer Amplifier with IC Op Amp as the Active Device	38
2-4	Macromodel Circuit of the 741 Buffer Amplifier.	38
2-5	Experimental System for a Buffer Amplifier Second Order Intermodulation Measurement	39
2-6	NCAP Coding Circuit Diagram for the Voltage Follower Circuit with Op Amp Macromodel.	41
2-7	Experimental and NCAP Predicted Values for the Second Order Transfer Function for the 741 Buffer Amplifier. .	44
2-8	A Nonlinear Macromodel for the 741 IC Op Amp which Includes Substrate Capacitances	47
2-9	Effect of the BJT Substrate Capacitance Value on NCAP Prediction of the Second Order Transfer Function Based on the Nonlinear Macromodel of the 741 Buffer Amplifier	49
3-1	LM10 Pin Configuration and Functional Diagram	54
3-2	LM10 Op Amp IC Schematic.	55
3-3	Essential Details of the LM10 Op Amp.	57
3-4	Macromodel for the LM10 Op Amp.	57
3-5	LM10 Buffer Amp NCAP Coding Diagram	62

LIST OF ILLUSTRATIONS (Continued)

<u>FIGURE</u>	<u>PAGE</u>
3-6 Comparison of Experimental Results and NCAP Predictions Made Using the LM10 Op Amp Macromodel in a Buffer Amplifier Configuration	64
3-7 Small-Signal Equivalent Circuit of the Lateral pnp Transistor with Base-Substrate Capacitance C_{BS}	65
3-8 Effect of Emitter to Substrate Capacitance on the Second Order Nonlinear Transfer Function of the LM10 Voltage Follower.	67
3-9 Effect of Base to Substrate Capacitance on the Second Order Transfer Function of the LM10 Voltage Follower. .	68
3-10 NCAP Macromodel Prediction and Experimental Results for the First Order Transfer Function of LM10 Buffer Amplifier	69
3-11 NCAP Macromodel Prediction and Experimental Results for the Second Order Transfer Function of LM10 Buffer Amplifier	70
3-12 Experimental Values for the Second Order Transfer Function $H_2(f_2, -f_1)$ vs Frequency for the 741 and LM10 Op Amps	72
4-1 741 Op Amp Simplified Schematic Diagram	75
4-2 Small-Signal Equivalent Circuit of the IC Op Amp. . . .	75
4-3 Small-Signal Nonlinear Transfer Function Representation of an Amplifier Stage	77
4-4 Diagrammatic Representation of Cascaded Stages Making up an Op Amp.	78
4-5 A Two-Stage Cascade Nonlinear Transfer Function Repre- sentation	79

LIST OF ILLUSTRATIONS (Continued)

<u>FIGURE</u>		<u>PAGE</u>
4-6	Block Diagram Illustrating Nonlinear Transfer Functions with Feedback in the Second Stage	79
4-7	The Small-Signal Equivalent Circuit of the Gain Stage of 741.	83
4-8	The Nonlinear Cascaded Transfer Function of Figure 4-6 with Second and Higher Orders of the Second Stage Neglected	83
4-9	Full Model of the 741 Input Stage	87
4-10	Nonlinear Equivalent Circuit for the CC-CB Cascode Formed by the Transistor Pair Q1-Q3 (or Q2-Q4).	89

LIST OF TABLES

<u>TABLE</u>		<u>PAGE</u>
1-1	NONLINEAR COEFFICIENTS FOR 2N5109 BJT	8
1-2	NCAP INPUT PARAMETERS FOR 2N5109 BJT.	10
1-3	NCAP μ A741 BJT PARAMETER VALUES	22
2-1	MACROMODEL PARAMETERS FOR 741	35
2-2	NCAP INPUT PARAMETER VALUES FOR 741 OP AMP MACROMODEL .	36
2-3	NCAP INPUT CODE FOR SECOND ORDER INTERMODULATION ANALYSIS OF THE EXPERIMENT OF FIGURE 2-8.	42
3-1	NCAP INPUT CODE FOR THE MACROMODEL LM10 VOLTAGE FOLLOWER.	63

CHAPTER ONE

INTRODUCTION

Progress in the prediction of electromagnetic interference (EMI) has occurred on many fronts in recent years. A particularly important development in EMI prediction involves the nonlinear modeling of the Bipolar Junction Transistor (BJT) and computer-aided analysis procedures. [1-13] A large number of pioneering research efforts have culminated in the successful EMI analysis of the bipolar integrated circuit (IC) operational amplifier (Op Amp). [14] The engineering effort and computer time, and hence the cost, required for EMI analysis of the full IC Op Amp are large. The high costs involved in predicting EMI using a full IC Op Amp model may affect the wide application of the powerful computer-aided EMI analysis techniques which have been developed. The research which will be described in this report uses a simplified model called a macromodel for EMI analysis of Op Amps. In using the Op Amp macromodel for EMI analysis, the situation of the practicing electromagnetic compatibility (EMC) engineer is considered. An important goal of the present research is that techniques generally not available to the EMC engineer (such as the laboratory characterization of integrated electronic devices) are to be circumvented.

This report is organized in the following manner. Chapter One contains a review of material relevant to this report. An introduction to the theory and techniques of analysis of a weakly nonlinear system is presented. Next, an analysis of EMI in the 741 IC Op Amp made with a full model is reviewed.^[18] Finally, the IC Op Amp macromodel developed by Boyle et al. is presented and discussed.^[29] In Chapter Two the nonlinear macromodel for the BJT IC Op Amp derived from the Boyle model is presented. Predictions made using the Nonlinear Circuit Analysis Program (NCAP)^[19] and the nonlinear macromodel for the 741 Op Amp are compared with full model predictions and experimental results. Substrate effects on macromodeling accuracy are also presented. In Chapter Three, nonlinear macromodeling techniques are presented in detail. The LM10^[57] IC Op Amp is used as a concrete example. It is shown how the macromodel BJT parameters and circuit parameters are extracted from published information. The NCAP predictions on how amplitude modulated RF signals are demodulated in an LM10 buffer amplifier are compared with experimental results. In Chapter Four the network theory for the nonlinear macromodel is developed. Based on the nonlinear transfer function approach, it is shown that an IC Op Amp which consists of cascaded stages with internal feedback has nonlinear characteristics dominated by the input stage. The analysis shows that the input BJTs which are in two cascade configurations can be represented with a pair of single BJTs. Chapter Five is the conclusion. The effectiveness and validity of the non-

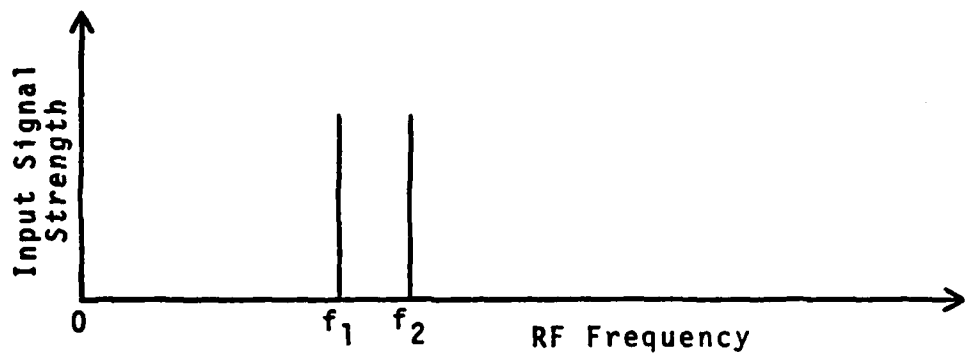
linear macromodel is discussed. A number of new research topics arising from this research are suggested.

1.1 EMI, Nonlinearity, and Nonlinear Transfer Function.

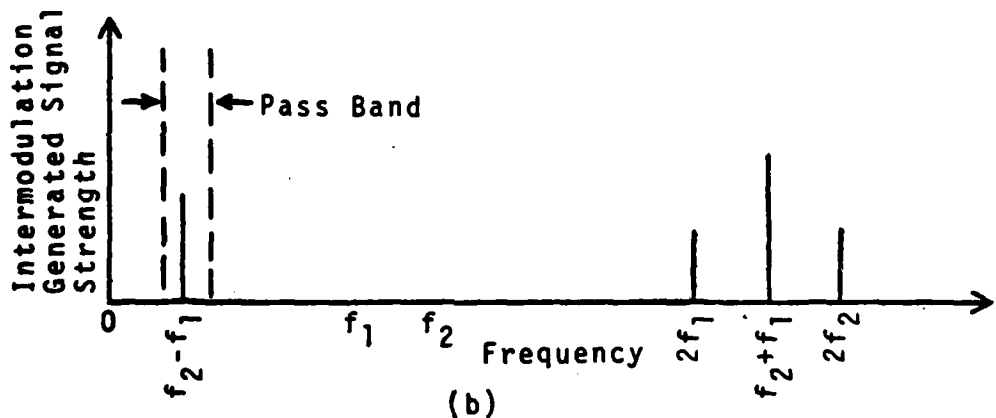
As communication channels become increasingly crowded, unwanted signals often accompany the desired signal. The unwanted signals can cause interference which can be classified as being caused by either linear effects or nonlinear effects. Linear interference effects may occur when the frequency of the interfering signal is very close to that of the desired signal. Nonlinear interference effects may occur when the unwanted signals cause new signals to be generated by the nonlinearities in the electronic devices and the new signal frequencies are close to that of the desired signal. Linear interference effects can often be avoided by improved tuning and selectivity. The nonlinear interference effects are more complex and not subject to any universal solution.

Among the nonlinear electromagnetic interference effects, intermodulation is an important example. Intermodulation interference may occur when signals with frequencies outside of a receiver's pass-band are combined nonlinearly to produce signals with new frequencies which then fall within the receiver's passband.

Intermodulation EMI is a result of electronic device nonlinearity. As illustrated in Figure 1-1, two sinusoidal signals with frequencies



(a)



(b)

Figure 1-1. Intermodulation Type of EMI Arising from Second Degree Nonlinearity of a Receiver.

- (a) frequency content at input
- (b) frequency content generated by second degree nonlinearity

f_1 and f_2 falling outside the passband of a receiver having second degree nonlinearities produce signals with new frequencies.^[17] Some of these new frequencies may fall within the receiver's passband and become interfering signals. The nonlinearities being referred to in this work are termed "weak" as opposed to the switching type of nonlinearity found, for example, in a modulator.^[16]

In order to analyse an electronic circuit to predict EMI, equivalent circuits are used in which the electronic devices are represented by nonlinear models. The BJT can be represented by the Nonlinear Incremental T-model shown in Figure 1.2, for a device exhibiting weak nonlinearities under small-signal operation.^[17,22] In this model, the nonlinear base-emitter resistor is represented by the nonlinear incremental current generator $K(v_2)$. The nonlinear collector capacitance is represented by the nonlinear incremental current generator $\gamma_c(v_3-v_2)$. The dependent current source in the collector circuit containing the h_{FE} nonlinearity and the avalanche nonlinearity is represented by the nonlinear current generator $g(v_2, v_3-v_2)$. The nonlinear emitter capacitance is represented by the nonlinear incremental current generator $\gamma_e(v_2)$. The resistors r_b and r_c are the incremental base and collector resistances respectively. For the case of low-level interference (usually labeled as weak interference), the nonlinear incremental current generators are represented by Taylor series.^[15] This is a basic difference between the small-signal linear^[45] and nonlinear BJT models.

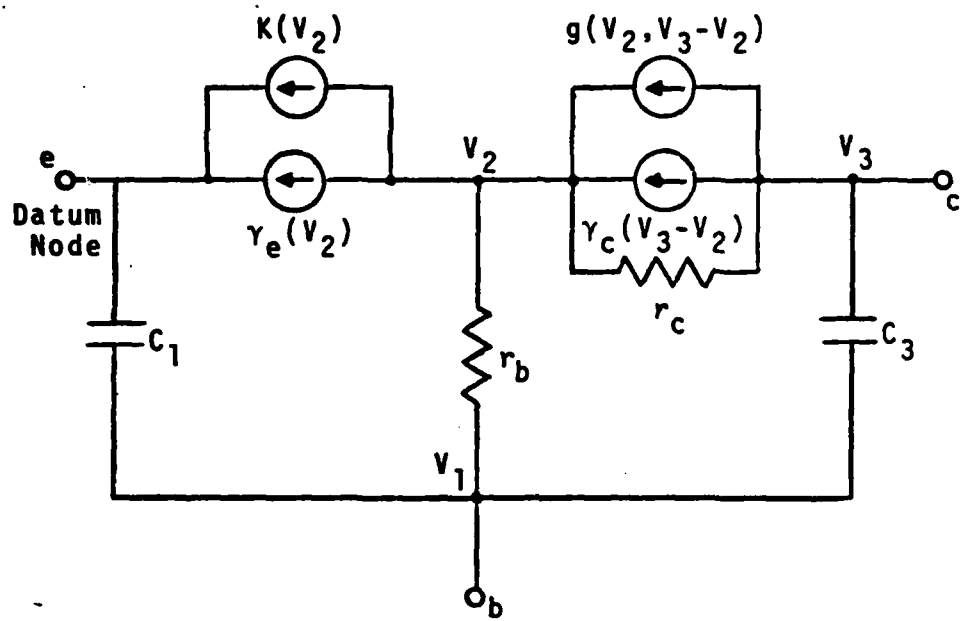
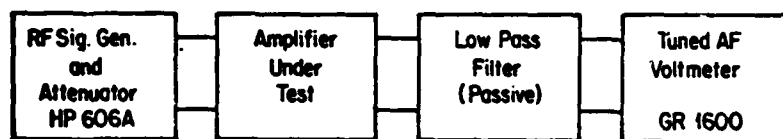


Figure 1-2. A Small-Signal Nonlinear Incremental T-model for the BJT.



$f_2 = f_{RF}$ $f_{RF} = \text{RF frequency}$

$f_1 = f_{RF} - f_{AF}$ $f_{AF} = \text{AF frequency}$

Modulation: 50% AM at f_{AF}

Figure 1-3. Experimental System for Measuring Second Order Intermodulation Effect at frequency
 $f_{AF} = f_2 - f_1$

For example [18]

$$i_e = K(v_2) = i_E - I_E = \sum_{j=1}^n k_j (v_{BE} - v_{BE})^j = \sum_{j=1}^n k_j v_2^j \quad (1-1)$$

is the Taylor expansion for the base-emitter nonlinear current about the operating point (I_E, v_{BE}) . The currents i_E , I_E , and i_e are the total instantaneous, dc and incremental emitter currents and the voltages v_{BE} , v_{BE} , and v_2 are total instantaneous, dc, and incremental base-emitter voltages respectively. The nonlinear current source representing the collector capacitance nonlinearity is given by

$$r_c(v_3 - v_2) = \sum_{j=1}^n C_j \frac{d}{dt} (v_3 - v_2)^j, \quad (1-2)$$

where C_j 's are the coefficients of the series. The collector dependent current source is expressed as

$$g(v_2, v_3 - v_2) = \sum_{j=0}^n \sum_{k=0}^j g_{jk} v_2^j (v_3 - v_2)^k, \quad (1-3)$$

where the g_{jk} 's are the coefficients of the series, and $g_{00}=0$. The nonlinear current source representing the emitter capacitance nonlinearity is

$$r_e(v_2) = \tau_F I_E \sum_{i=1}^n \left(\frac{1}{i!}\right) \left(\frac{q}{kT}\right)^i \frac{d}{dt} (v_2)^i + C_{je} \frac{dv_2}{dt}, \quad (1-4)$$

where τ_F is the emitter capacitance time constant, C_{je} the base-emitter junction space charge capacitance and (kT/q) the equivalent thermal potential. The BJT device nonlinearities therefore are represented by series expansions. An example of the series coefficients appear in

TABLE 1-1
NONLINEAR COEFFICIENTS FOR 2N5109 BJT^a

Nonlinear Incremental Current Generator	Coefficient	Value
$K(v_2)$	K_1 (mho)	1.9724
	K_2 (mho/V)	38.419
	K_3 (mho/V ²)	498.87
$\gamma_C(v_3-v_2)$	C_1 (F)	0.26549×10^{-12}
	C_2 (F/V)	-0.75664×10^{-14}
	C_3 (F/V ²)	0.64819×10^{-15}
$s(v_2, v_3-v_1)$	s_{01} (mho)	0.22851×10^{-6}
	s_{10} (mho)	1.9446
	s_{02} (mho/V)	0.11426×10^{-6}
	s_{20} (mho/V)	37.754
	s_{11} (mho/V)	-0.28734×10^{-7}
	s_{03} (mho/V ²)	0.30475×10^{-7}
	s_{30} (mho/V ²)	487.88
	s_{12} (mho/V ²)	-0.14367×10^{-7}
	s_{21} (mho/V ²)	-0.2718×10^{-6}

^aValues reported by Fang, Ref. 18, p.46.

Table 1-1. The computation of the nonlinear coefficients indicated was made by the Nonlinear Circuit Analysis Program (NCAP)^[19] which has a built-in device model for the BJT. The computer code requires only that the BJT model parameters be entered. An example of NCAP input parameters for a BJT is shown in Table 1-2. The parameters are determined experimentally^[18] utilizing several parameter extraction methods.^[15]

The purpose of an NCAP analysis is to predict quantitative EMI effects. By comparing the NCAP predicted results with laboratory measured interference effects, the modeling accuracy can be evaluated. An experimental system for measuring a second-order intermodulation effect is shown in Figure 1-3^[20]. This experimental system which simulates directly a practical interference situation has the advantage of being controlled and therefore amenable to analysis. The experimental data may be plotted as shown in Figure 1-4. The data points represent the strength of the interfering signal at the new frequency $f_2 - f_1$ as a function of the input RF power at RF frequencies 50 kHz, 1 MHz, and 10 MHz. The AF voltage which is the interfering signal is proportional to the available input RF power, as expected, at low RF power levels.

Measurements can be carried out at a fixed input RF power while the RF frequency is varied. The result of such an experiment is illustrated in Figure 1-5. The most susceptible RF frequency interval where the largest magnitude interference is obtained is apparent.

It is desirable that the interference phenomena be expressed as a

TABLE 1-2
NCAP INPUT PARAMETERS FOR 2N5109 BJT^a

Parameter Name	Description	Value
n	Avalanche exponent	6.0
V_{CB} (V)	Collector base bias voltage	5.0
V_{CBO} (V)	Avalanche voltage	40.0
M_1	Collector capacitance exponent	0.285
I_C (mA)	Collector bias current	50.0
I_{Cmax} (mA)	Collector current at maximum	18.0
	Dc current gain	
a	h_{FG} nonlinearity coefficient	0.363
h_{T2max}	Maximum d.c. current gain	84.6
k (pF-V $^{1/2}$)	Collector capacitor scale factor	0.42
R_{df}	Diode nonlinearity factor	1.0
C_{je} (pF)	Base-emitter junction space charge capacitance	10.0
C'_{je} (pF/mA)	Derivative of base-emitter diffusion capacitance	3.6
r_b (Ω)	Base resistance	15
r_c (k Ω)	Collector resistance	32.9
C_1 (pF)	Base-emitter capacitance	0.1
C_3 (pF)	Base-collector and overlap capacitance	0.56

^aParameter values reported by Fang, Ref. 18, p. 45.

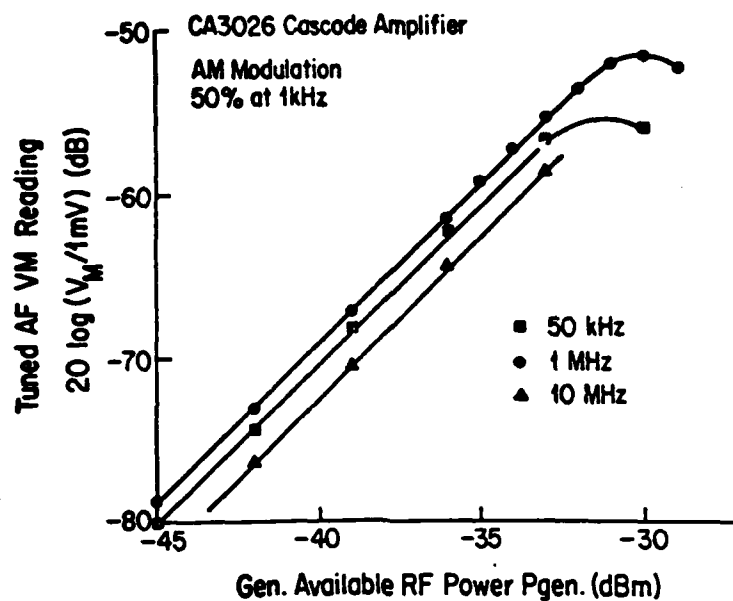


Figure 1-4. Representative Intermodulation Data[18]
Obtained With Experimental System Shown
in Figure 1-3.

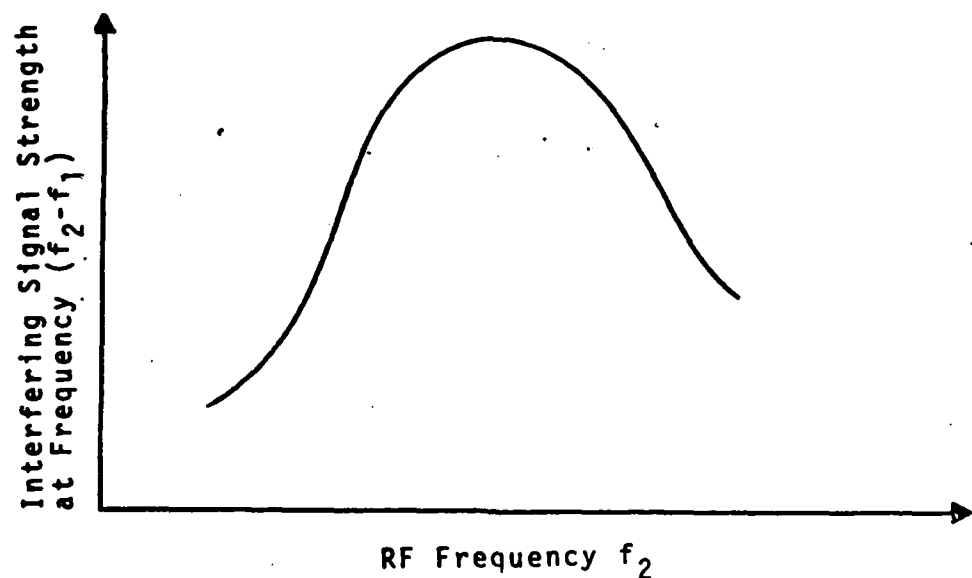


Figure 1-5. Interfering Signal Strength versus RF Frequency for an Electronic Circuit with Second Order Nonlinearity.

parameter of the electronic circuit or system in a manner similar to the linear voltage gain parameter. The "Nonlinear Transfer Function" derived from the Volterra Series kernel^[21] has been used by Graham and Ehrman^[17] as such a parameter. Consider a weakly nonlinear network with input $x(t)$ and output $y(t)$. Let $X(f)$ and $Y(f)$ be the Fourier transforms of $x(t)$ and $y(t)$. Then $Y(f)$ is related to $X(f)$ by the expression^[17]

$$Y(f) = \sum_n \int \int \dots \int_{-\infty}^{+\infty} H_n(f_1, \dots, f_n) X(f_1) \dots X(f_n) \cdot \delta(f - f_1 - f_2 - \dots - f_n) df_1 df_2 \dots df_n . \quad (1-5)$$

In the above equation $Y(f)$ is the sum of all orders of nonlinear responses; $X(f)$ is the input signal spectrum, $\delta(f - f_1 - f_2 - \dots - f_n)$ is the delta function defined by the integral

$$\delta(f - f_1 - f_2 - \dots - f_n) = \int_{-\infty}^{\infty} \exp \{-j2\pi(f - f_1 - f_2 - \dots - f_n)t\} dt . \quad (1-6)$$

and $H_n(f_1, f_2, \dots, f_n)$ is the nth order nonlinear transfer function. The first order (linear) transfer function can be expressed as^[17]

$$H_1(f_i) = [Y(f_i)]^{-1} J_d(f_i), \quad i = 1, 2, \dots, n \quad (1-7)$$

where $Y(f_i)$ is the network admittance matrix evaluated at f_i , and $J_d(f_i)$ the first order current source vector that excites the network. The second order nonlinear transfer function $H_2(f_1, f_2)$ can be expressed as^[17]

$$H_2(f_i, f_j) = (1/2) [Y(f_i + f_j)]^{-1} J_d(f_i, f_j) ; \\ \text{for } i = 1, 2, \dots, n; j = 1, 2, \dots, n \quad (1-8)$$

where $Y(f_i + f_j)$ is the network admittance matrix evaluated at the frequency $(f_i + f_j)$, and $J_d(f_i, f_j)$ is the second order nonlinear current source vector that excites the network. The third order nonlinear transfer function $H_3(f_i, f_j, f_k)$ can be expressed as^[18]

$$H_3(f_i, f_j, f_k) = \left(\frac{1}{6}\right) [Y(f_i + f_j + f_k)]^{-1} \overline{J_d(f_i, f_j, f_k)}; \\ i = 1, 2, \dots, n; j = 1, 2, \dots, n; k = 1, 2, \dots, n \quad (1-9)$$

where $Y(f_i + f_j + f_k)$ is the admittance matrix evaluated at the frequency $(f_i + f_j + f_k)$, and $\overline{J_d(f_i, f_j, f_k)}$ is the average* nonlinear third order current source vector that excites the network. Higher order nonlinear transfer functions can be expressed in a similar manner.

The experimental system of Figure 1-3 is used to measure the second order nonlinear transfer function. Let the two input signal frequencies f_1 and f_2 be denoted as $f_2 = f_{RF}$ and $f_1 = (f_{RF} - f_{AF})$ where f_{RF} is the RF carrier frequency and f_{AF} is the AM modulation frequency. The AF voltmeter is tuned to the frequency $f_{AF} = f_2 - f_1 = f_2 + (-f_1)$. The component of the output voltage at $f_2 - f_1$ can be expressed as^[15]

$$v(t) = mA^2 H_2(f_2, -f_1) \cos[2\pi(f_2 - f_1)t] \quad (1-10)$$

where A is the amplitude of the RF carrier at $f_2 = f_{RF}$, and m is the modulation index. The rms voltage read on the AF voltmeter is

$$V = 0.707mA^2 |H_2(f_2, -f_1)|. \quad (1-11)$$

* For the third order current vector averaging process, see Chapter 5 of Reference 15.

Expressed in dB with respect to a 1 mV reference level, Equation 1-11 becomes

$$\begin{aligned} 20\log|V/1mV| &= 20\log[0.707 mA^2 |H_2(f_2, -f_1)|] - 20\log(10^{-3}) \\ &= 57 + 20\log m + 20\log |H_2(f_2, -f_1)| \end{aligned} \quad (1-12)$$

When the RF generator impedance equals 50Ω , the RF carrier amplitude A is related to the available generator power by $P_{gen} = A^2/400$. [18]

With $m = 0.5$, Equation (1-12) can be written as

$$20\log|V/1mV| = 2P_{gen}(\text{dBm}) + 43 + 20\log |H_2(f_2, -f_1)|, \quad (1-13)$$

or

$$20\log |H_2(f_2, -f_1)| = 20\log|V/1mV| - 43 - 2P_{gen}(\text{dBm}) \quad (1-14)$$

Equation 1-13 indicates that the AF voltmeter reading V is proportional to P_{gen} . At low values of P_{gen} the data plotted in Fig. 1-4 obey Equation (1-13). Using Equation (1-14) and the data in Figure 1-4 at low P_{gen} values, values of the second order transfer function $H_2(f_2, -f_1)$ can be determined. Values of $H_2(f_2, -f_1)$ vs frequency f_2 are plotted as illustrated in Figure 1-6. It is to be noted that in both Figures 1-5 and 1-6 the frequency $(-f_1)$ is varied in step with f_2 to keep $(f_2 - f_1)$ a constant at a value $f_{AF} = f_2 - f_1$.

An experimental system for measuring a third order nonlinear transfer function is shown in Figure 1-7. [20] For an electronic circuit with third degree nonlinearities, two tone excitation can give rise to the following third order frequency mixes: $(2f_1 - f_2)$, $(2f_2 - f_1)$, $(3f_1)$, $(2f_1 + f_2)$, $(2f_2 + f_1)$, and $(3f_2)$. Since any one of the third order

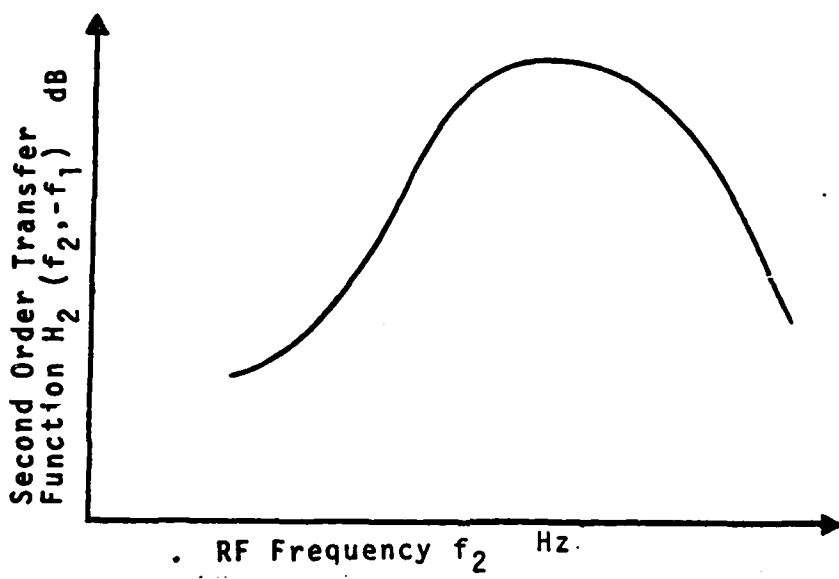


Figure 1-6. Frequency Response of Second Order Non-linear Transfer Function.

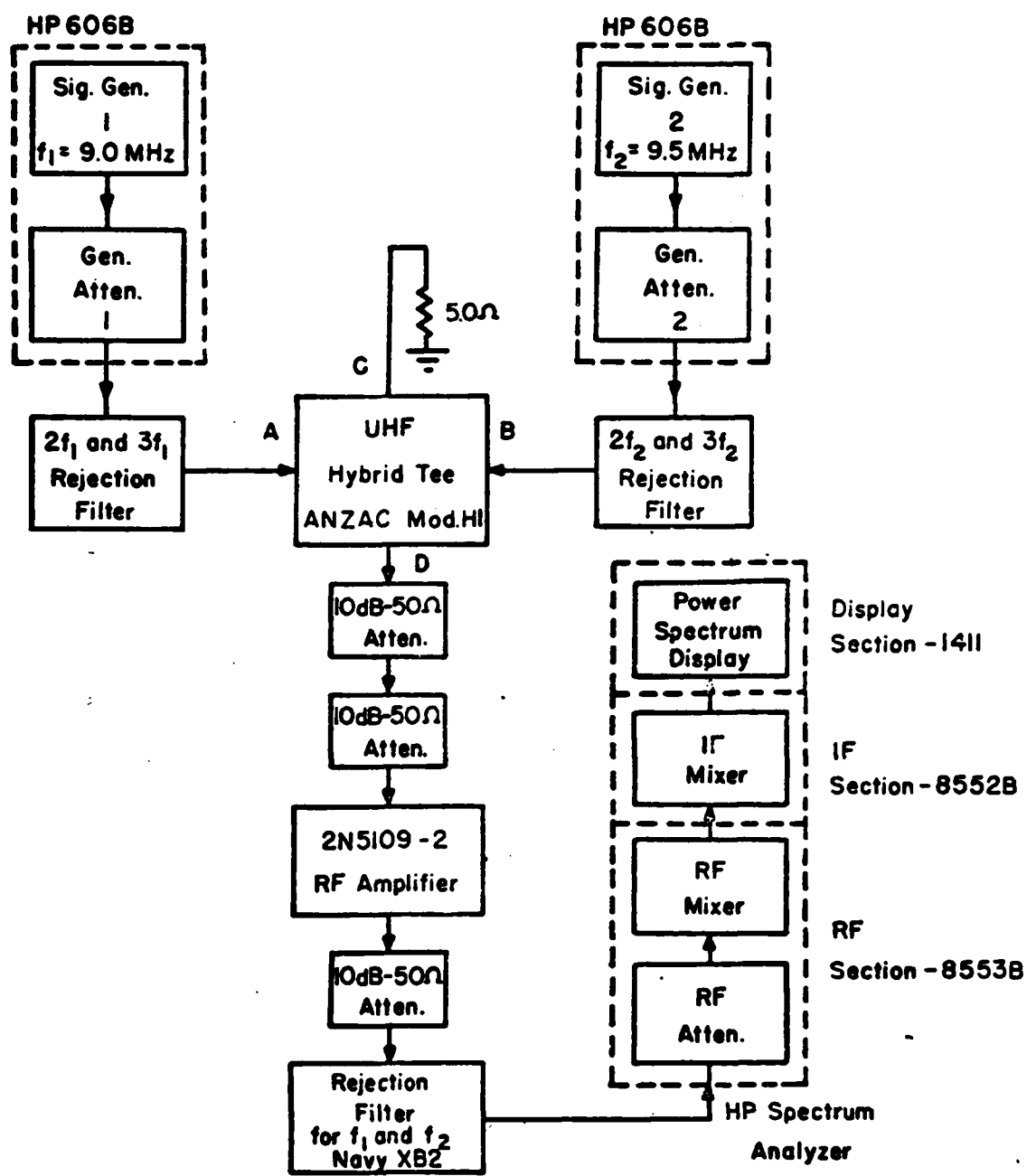


Figure 1-7. Experimental System for Measuring Third Order Transfer Functions $H_3(-f_1, f_2, f_2)$.
From Whalen, Paludi and Fang.

frequency mixes is representative of the circuit third degree nonlinearities, only the output at one such frequency $2f_2 - f_1$ will be considered as an example. The spectrum analyzer rms voltage $V(2f_2 - f_1)$ at frequency $2f_2 - f_1$ is related to the third order nonlinear transfer function $H_3(-f_1, f_2, f_2)$ by the expression^[18]

$$V(2f_2 - f_1) = (3/4) |H_3(-f_1, f_2, f_2)| A_1 A_2^2, \quad (1-15)$$

where A_1 and A_2 are the voltage amplitude of the two input signals at frequencies f_1 and f_2 .

1.2 System Nonlinearity of the Integrated BJT Operational Amplifier

The application of integrated circuits, especially the integrated BJT Op Amp, permeates modern electronic equipment design. The EMI analysis of the IC Op Amp has become an important consideration. Such an analysis poses a number of challenges. The first is the complexity of the circuitry where 20 to 30 BJT's are interconnected. The second is the need to know the nonlinear parameters of each and every individual BJT. Finally, the effects of the parasitic elements associated with the BJT's have to be accounted for. Recently the nonlinear analysis of the μ A741 Op Amp was successfully achieved by Fang.^[18] The schematic circuit diagram of this widely used IC is shown in Figure 1-8.^[23] The Nonlinear Circuit Analysis Program (NCAP) was the main analysis tool used by Fang. The NCAP input coding diagram for the 741 buffer amplifier is shown in Figure 1-9.^[18] The NCAP pre-

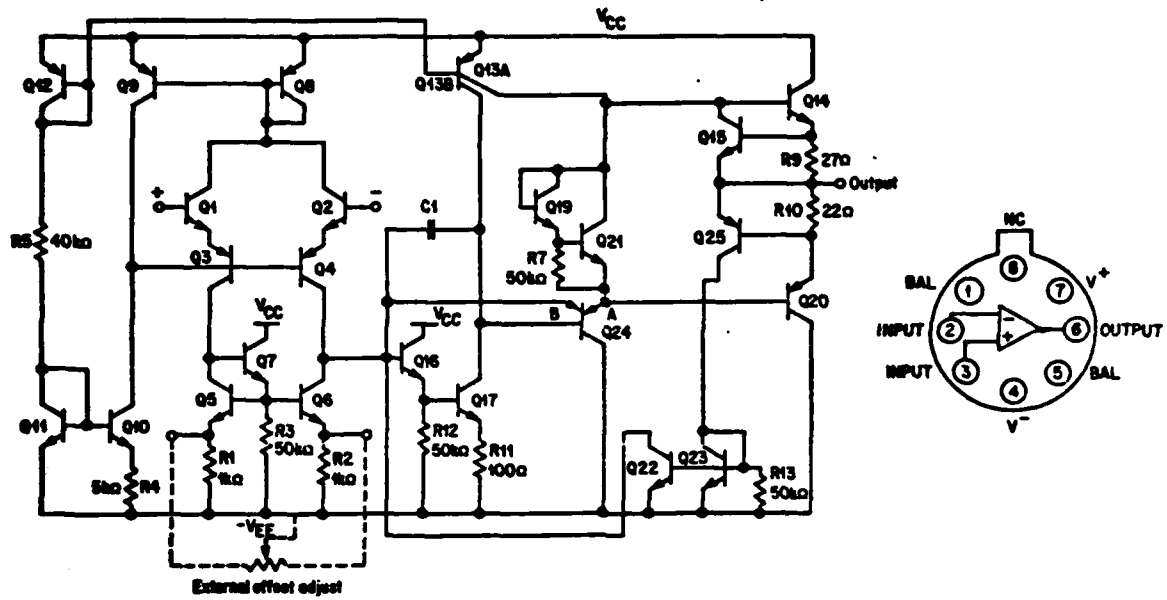


Figure 1-8. Schematic Diagram of the 741 Op Amp.²³

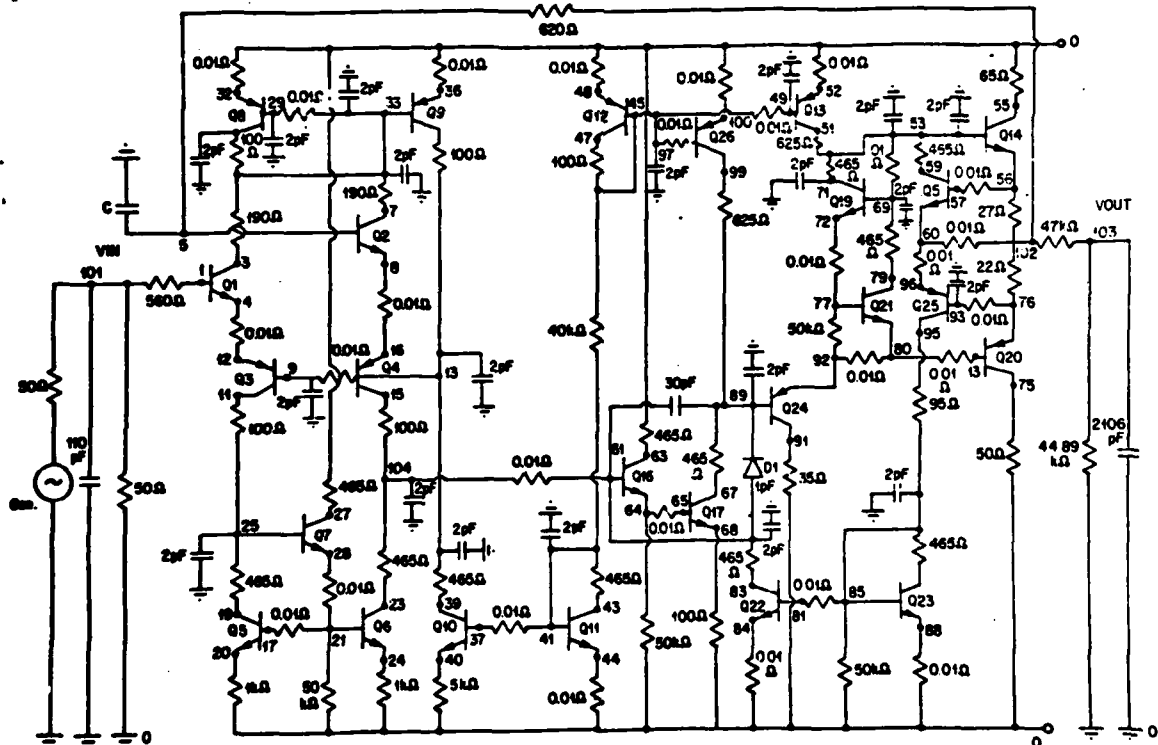


Figure 1-9. NCAP Input Coding Diagram for the 741 Op Amp in the Buffer Amplifier Configuration from Fang. ¹⁸

dition for the first order transfer function $V_{\text{OUT}}/V_{\text{IN}}$ vs frequency is compared with the experimental data in Figure 1-10. The NCAP calculation of the second order nonlinear transfer function $H_2(f_2, -f_1)$ vs RF frequency is compared with the experimental data in Figure 1-11. It can be seen that the nonlinear analysis utilizing NCAP predicts accurately the location of the most susceptible RFI RF frequency range and the general shape of the RFI frequency response. The accuracy achieved establishes the nonlinear analysis techniques as a useful tool for EMI prediction.

The NCAP input coding diagram shown in Figure 1-9 with 104 nodes creates a very large admittance matrix. The NCAP computer code employs a sparse matrix technique to reduce the in-core storage. The data are passed back and forth between the Central Processing Unit (CPU) and the peripheral accessory memories. For a five-frequency sweep, determining the 741 buffer amplifier second order transfer function requires approximately half an hour CPU time and another half hour peripheral time on a Honeywell 6180 computer. Up to 500 nodes can be handled by the present NCAP algorithm. The computational procedure used by NCAP begins with the construction of nodal equations using Kirchhoff's Voltage Law. The first order transfer function in Equation (1-7) is calculated next at each frequency f_i required. The second order nonlinear current source vector $J_d(f_i, f_k)$ is then determined at the frequency $(f_i + f_k)$ using the first order nodal voltages at frequencies f_i and f_k . The appropriate second

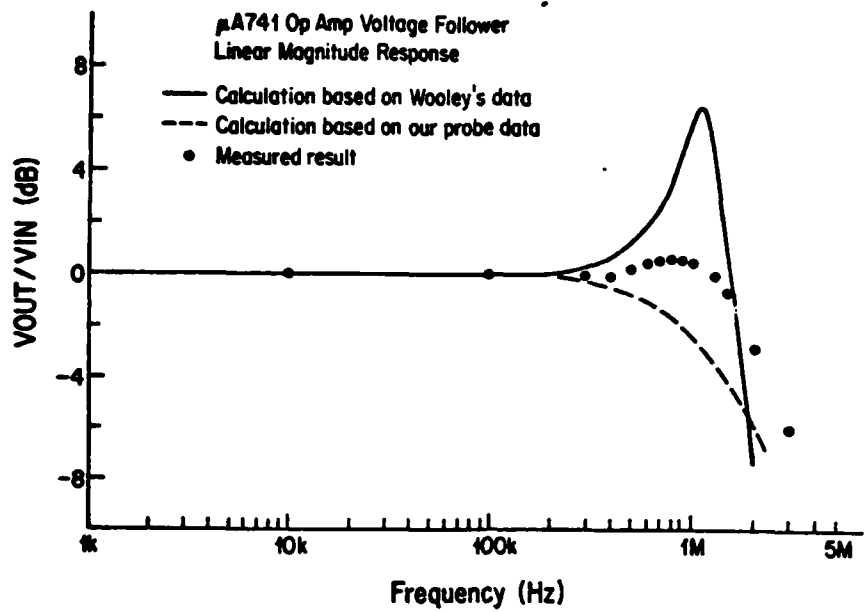


Figure 1-10. Predicted and Measured Values for a 741 Op Amp Buffer Amplifier First Order Transfer Function,
from Fang.¹⁸

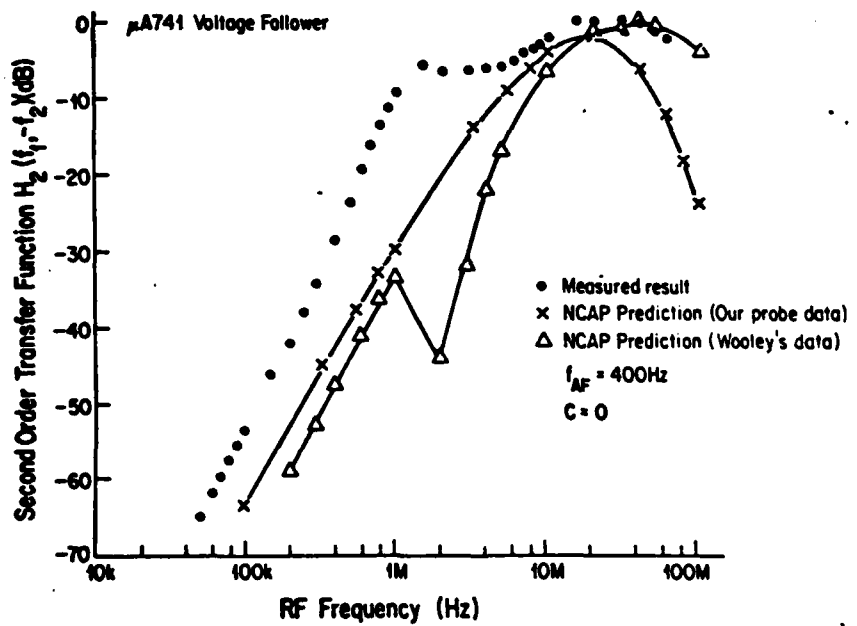


Figure 1-11. Measured and Predicted Values for a 741 Op Amp Buffer Amplifier Second Order Transfer Function,
from Fang.¹⁸

order transfer function is then calculated from Equation (1-8). The procedure is repeated for each combination of frequencies (f_i, f_j) required. Similarly, the third and higher order transfer functions are calculated. The NCAP program can calculate up to the sixth order transfer function. It is to be noted that a calculation of a third order transfer function for a two tone excitation requires that first order transfer functions at f_1 and f_2 and second order transfer functions at $f_2 - f_1$, $2f_1$, $f_1 + f_2$ and $2f_2$ be calculated first.

The NCAP model parameters for the BJTs in the μ A741 were determined by Fang [18] in two ways. Fang used the modified Ebers-Moll BJT model parameters reported by Wooley et al. [24] for the Intersil 741 type chip. Fang also measured parameters *in situ* on a Fairchild μ A741 devices using probe methods. [18] Input parameters for both the SPICE2 (Simulation Program with Integrated Circuit Emphasis) [53] Computer Program and NCAP were determined. There are six BJT types in the 741 IC: small npn, large npn, lateral pnp, large substrate pnp, dual-collector lateral pnp and dual-emitter substrate pnp. The "small" and "large" refer to the device geometry, ranging from $60 \mu\text{m} \times 100 \mu\text{m}$ to $140 \mu\text{m} \times 200 \mu\text{m}$. For the first time the NCAP BJT model parameters for integrated BJTs became available. The application of nonlinear analysis computer program NCAP for EMI analyses of bipolar ICs was made possible. This was a major achievement. Fang's NCAP input coding data are reproduced in Table 1-3. Fang reported that there is considerable uncertainty in the measurement of substrate capacitances in both his own

TABLE 1-3
NCAP μ A741 BJT PARAMETER VALUES^a

Pa De	γ	V_{CB} (V)	V_{CB0} (V)	μ	I_C (μ A)	I_{Cmax} (mA)	a	η_{FETmax} (pF-V $_{f}^{1}$)	k	Ref	C_{je} (pF)	C_{j2} (pF/m)	R_B (Ω)	R_C (M)	C_1 (pF)	C_2 (pF)
Q1 *	4	14.42	100	0.333	9.66	0.3	4.35	210	0.286	1.0	0.65	44.6	670	5.0	0.1	0.1
Q1 #	1.34	14.57	20	0.165	7.85	0.5	12	400	1.23	1.09	1.23	9.09	830	5.33	0.1	0.1
Q2 *	4	14.42	100	0.333	9.66	0.3	4.35	210	0.286	1.0	0.65	44.6	670	5.0	0.1	0.1
Q2 #	1.34	14.57	20	0.165	7.85	0.5	12	400	1.23	1.09	1.23	9.09	830	5.33	0.1	0.1
Q3 *	1.5	12.65	95	0.333	9.58	0.11	0.807	75	0.834	1.0	0.1	1060	500	0.5	0.1	0.1
Q3 #	1.48	13.05	100	0.376	7.69	0.1	1.07	35	0.77	1.34	0.23	914	520	0.575	0.1	0.1
Q4 *	1.5	12.61	95	0.333	9.58	0.11	0.807	75	0.834	1.0	0.1	1060	500	0.5	0.1	0.1
Q4 #	1.48	13.0	100	0.376	7.69	0.1	1.07	35	0.77	1.34	0.23	914	520	0.575	0.1	0.1
Q5 *	4	0.594	100	0.333	9.52	0.3	4.35	210	0.286	1.0	0.65	44.6	670	5.0	0.1	0.1
Q5 #	3.79	0.53	100	0.254	7.66	0.5	1.21	300	0.61	1.04	0.88	15.07	1040	15.3	0.1	0.1
Q6 *	4	0.641	100	0.333	9.52	0.3	4.35	210	0.286	1.0	0.65	44.6	670	5.0	0.1	0.1
Q6 #	3.79	0.585	100	0.254	7.66	0.5	1.21	300	0.61	1.04	0.88	15.07	1040	15.3	0.1	0.1
Q7 *	4	28.81	100	0.333	12.0	0.3	4.35	210	0.286	1.0	0.65	14.6	670	5.0	0.1	0.1
Q7 #	3.79	28.93	100	0.254	10.8	0.5	0.84	300	0.61	1.04	0.8	15.07	1040	15.3	0.1	0.1
Q8 *	1.5	0.1	95	0.333	18.8	0.11	0.912	75	0.834	1.0	0.1	1060	500	0.5	0.1	0.1
Q8 #	1.4	0.1	100	0.376	14.9	0.1	1.23	35	0.77	1.34	0.23	914	601	0.575	0.1	0.1
Q9 *	1.5	15.57	95	0.333	18.8	0.11	0.912	75	0.834	1.0	0.1	1060	500	0.5	0.1	0.1
Q9 #	1.48	15.45	100	0.376	19.5	0.1	1.17	35	0.77	1.34	0.23	914	631	0.575	0.1	0.1
Q10 *	4	13.14	100	0.333	19.1	0.3	1.81	210	0.286	1.0	0.65	44.6	670	5.0	0.1	0.1
Q10 #	3.79	13.46	100	0.254	19.8	0.5	0.62	300	0.61	1.04	0.88	15.07	1040	15.3	0.1	0.1
Q11 *	4	0.1	100	0.333	712	0.3	1.61	210	0.286	1.0	0.65	44.6	670	5.0	0.1	0.1
Q11 #	3.79	0.1	100	0.254	718	0.5	0	300	0.61	1.04	0.88	15.07	1040	15.3	0.1	0.1
Q12 *	1.5	0.1	95	0.133	615	0.11	1.61	7.5	0.34	1.0	0.1	1060	500	0.5	0.1	0.1
Q12 #	1.48	0.1	100	0.376	549	0.1	1.37	35	0.77	1.34	0.23	914	681	0.575	0.1	0.1

* Values based upon Wooley's data

Values based upon our probe data

^aTable 4-3 of Fang, Ref. 46.

TABLE 1-3 CONTINUED
NCAP 1A741 BJT PARAMETER VALUES^a

P _a D _e	γ	V _{CB} (V)	V _{CEO} (V)	μ	I _C (μ A)	I _{Crss} (mA)	α	$ V_{FE} _{max}$ (pF-V _t)	k	Ref	C _{je} (pF)	C _{je} (pF)	R _B (M _Ω)	R _C (M _Ω)	C ₁ (pF)	C ₂ (pF)
Q13 * #	1.5	13.68	95	0.333	22	0.03	0.6	0.3	0.24	1.0	0.1	1060	1000	1.0	0.1	
Q14 * #	1.72	13.89	130	0.32	45.3	0.2	0.48	0.6	0.38	1.22	0.36	1000	6.1	1.14	0.1	
Q15 * #	1.5	14.36	100	0.333	22.4	0.3	5.06	400	1.23	1.0	2.8	29.5	1.5	4.0	0.1	
Q16 * #	1.42	14.42	100	0.327	110	2.0	1.26	300	1.0	1.05	3.0	19.1	500	3.96	0.1	
Q17 * #	4	0.64	100	0.333	437E	0.3	10	210	0.286	1.0	0.65	44.6	670	5.0	0.1	
Q18 * #	3.79	0.573	100	0.254	2.43E	0.5	4.33	300	0.61	1.04	0.98	15.0	1040	15.3	0.1	
Q19 * #	4	28.76	100	0.333	13.1	0.3	3.54	210	0.286	1.0	0.65	44.6	670	5.0	0.1	
Q20 * #	3.79	28.88	100	0.254	11.9	0.5	0.89	300	0.61	1.04	0.88	15.07	1040	15.3	0.1	
Q21 * #	4	13.19	100	0.333	61.0	0.3	0.82	210	0.286	1.0	0.65	44.6	670	5.0	0.1	
Q22 * #	3.79	13.50	100	0.254	66.6	0.5	0.65	300	0.61	1.04	0.88	15.07	1040	15.3	0.1	
Q23 * #	4	0.1	100	0.333	11.8	0.3	1.35	210	0.286	1.0	0.65	44.6	670	5.0	0.1	
Q24 * #	3.79	0.1	100	0.254	11.4	0.5	0.87	300	0.61	1.04	0.88	15.07	1040	15.3	0.1	
Q25 * #	4	0.594	100	0.333	10.1	0.3	4.35	210	0.286	1.0	0.65	44.6	670	5.0	0.1	
Q26 * #	3.79	0.54	100	0.254	33.6	0.5	0.73	300	0.61	1.04	0.88	15.07	1040	15.3	0.1	
Q27 * #	2.5	14.46	90	0.333	22.3	0.11	2.44	117	2.22	1.0	4.05	1030	80	0.15	0.1	
Q28 * #	2.67	14.47	90	0.565	109	0.3	1.03	60	1.5	1.13	1.25	360	190	0.147	0.1	
Q29 * #	4	1.24	100	0.333	8.45	0.3	10	210	0.286	1.0	0.65	14.6	670	5.0	0.1	
Q30 * #	3.79	1.12	100	0.254	1.16	0.5	4.65	300	0.61	1.04	0.88	15.07	1040	15.3	0.1	
Q31 * #	4	0.1	100	0.333	6.4E-4	0.3	10	210	0.286	1.0	0.65	14.6	670	5.0	0.1	
Q32 * #	3.79	0.1	100	0.254	0.75E	0.5	1.85	300	0.61	1.04	0.88	15.07	1040	15.3	0.1	
Q33 * #	3.5	13.84	90	0.333	21.8	0.015	5.4	80	1.906	1.0	1.1	1030	1100	10.0	0.1	
Q34 * #	3.69	14.09	50	0.252	-6.2	0.2	7.4	80	5.08	1.45	1.75	280	195	13.1	0.1	
Q35 * #	1.5	15.0	95	0.333	2.31E	0.11	10	75	0.834	1.0	0.1	1060	500	0.5	0.1	
Q36 * #	1.48	15.0	100	0.376	5.01E	0.1	1.66	35	0.77	1.34	0.23	1307	681	0.575	0.1	
Q37 * #	1.5	15.49	95	0.333	60.8	0.07	1.0	1.5	0.715	1.0	0.1	1060	1600	1.0	0.1	
Q38 * #	1.72	15.37	130	0.32	663	0.2	0.87	6	1.14	1.22	0.36	1000	681	1.14	0.1	

* Values based upon Wooley's data

Values based upon our probe data

^aTable 4-3 of Pang, Ref. 46.

and Wooley's data. The individual substrate capacitance values may not correspond directly to the device surface geometry. The important effects of the substrate capacitance values on the nonlinear analysis of IC Op Amps are considered in detail in this research.

1.3 Macromodeling of BJT ICs

The ICs fabricated today are complex, and the ICs fabricated tomorrow will be more complex. The complexity of ICs makes computer-aided analysis of EMI in IC circuits time consuming and expensive. Furthermore, the EMI analyst's comprehension of the overall system behavior tends to be obscured when he attempts to keep track of what is happening at the device level. There is a need of a simplified and yet representative equivalent circuit for the IC. [25] This need has lead to the development of macromodels.

There are a number of approaches to macromodeling. The IC may be represented by an approximation of one or more of its transfer functions. Another method is to represent the IC by its terminal behavior. The goal of macromodeling is to simplify the internal IC circuitry. The result can be reduction of computation time required for an analysis by four to ten fold. When IC macromodels are used, a system employing many IC's becomes amenable to analysis by the circuit designer and the EMI analyst. Macromodeling efforts all share some common characteristics. The range of application is necessarily limited. Nearly all macromodels

are developed in conjunction with computer aided circuit design techniques and are intended for computer analysis. One clear distinction need be made in our definition of a macromodel. That is, a macromodel involves an approximate representation of one or more actual transistors in an IC. Therefore an idealized transfer function representation, such as a voltage gain parameter to represent an amplifier for example, is not a macromodel in the context of the present research.

Narud reported a macromodel for digital ICs in 1970. [26] This early model maintained the individual device characteristics at the inputs, up to the gate or flip-flop level. The balance of the IC is represented by an idealized black-box. This approach has proven to be widely useful. Digital IC macromodels have been developed continuously and now are widely used in the analysis and design of large scale integration (LSI) IC's. [27,28] However, the various digital macromodels used by different manufacturers are usually proprietary information and are seldom available to the EMC community.

Boyle et al. reported a macromodel for the IC Op Amp which can be used for nonlinear dc and transient analysis. [29] This macromodel provides a pin-for-pin representation as shown in Figure 1-12. The values of the elements in the macromodel are determined from the Op Amp specifications and input-output responses. The three-stage model include elements related to dc circuit quantities: I_{EE} for the dc current source in the input stage, R_E related to the Early Voltage of

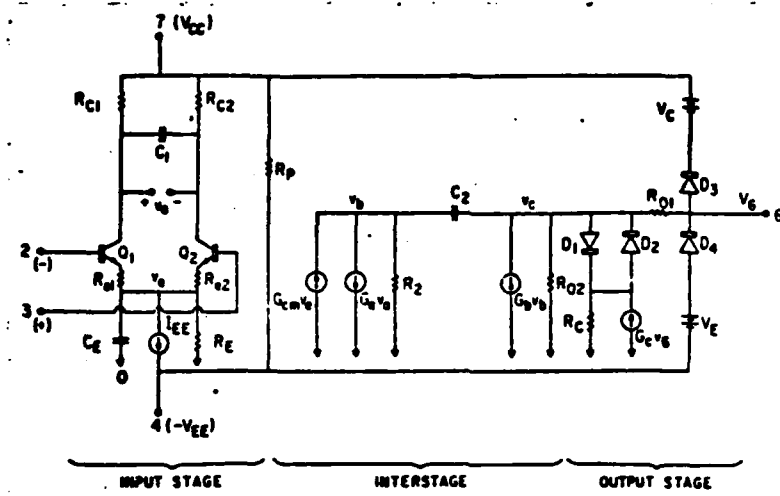


Figure 1-12. A Macromodel for the 741 Type BJT IC
Op Amp for DC, Small-Signal and Trans-
ient Analyses Developed by Boyle et al.²⁹

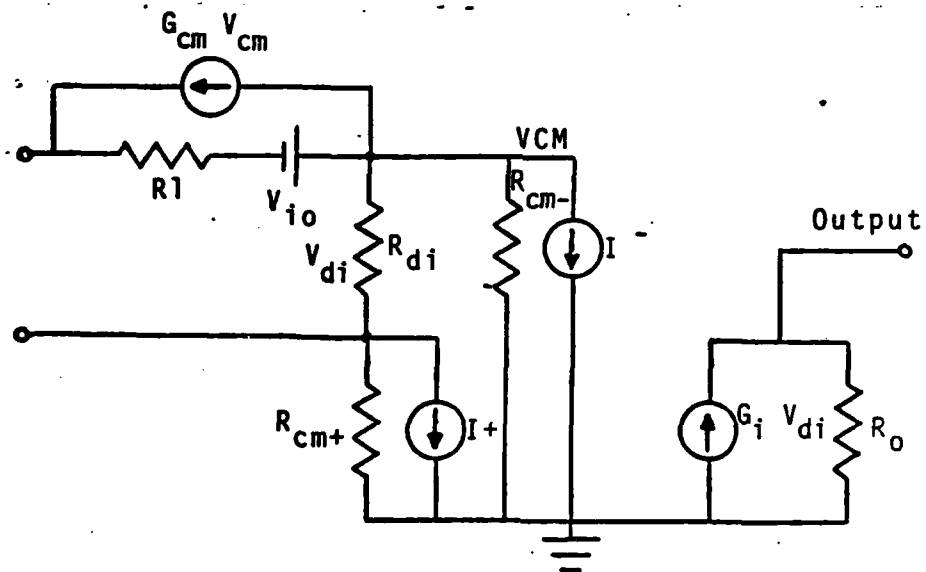


Figure 1-13. A Small-Signal Macromodel, from
Treleaven and Trofimenkoff.³⁰

the current source transistor, R_p representing the dc power dissipation, output stage current limiting parameters, G_C , R_C , D_1 , D_2 and R_{01} , and the output voltage limiting elements V_C , D_3 , V_E , and D_4 . Small-signal operation is modeled by the elements G_a for the differential gain, G_{cm} for the Common Mode Rejection Ratio (CMRR), G_b for the inter-stage gain, R_{02} for the ac output resistance, C_1 for the differential amplifier excess phase effect, and C_2 for the 3 dB cutoff frequency. The positive slew rate is related to C_1 , and the negative slew rate to C_E and C_2 .

It is significant that Boyle et al. found that four junctions at the input stage are necessary and sufficient to model the 741 IC performance. This is in agreement with the work of Narud. The Boyle macromodel employs two ideal transistors which contain four p-n junctions. An earlier model by Treleavan and Trofimenkoff, [30] shown in Figure 1-13, employs no representation of any physical junctions. Other macromodels [31-33] also eschew the direct inclusion of physical devices as shown in Figure 1-14. The necessity for physical modeling in the nonlinear application of the macromodel will be developed in this dissertation.

The macromodel developed by Boyle et al. can be used for dc, small-signal, and transient calculations. However, it was not designed for nonlinear analysis related to EMI predictions. A macromodel has also been developed for the IC Comparator. [34] Usually, about an order of

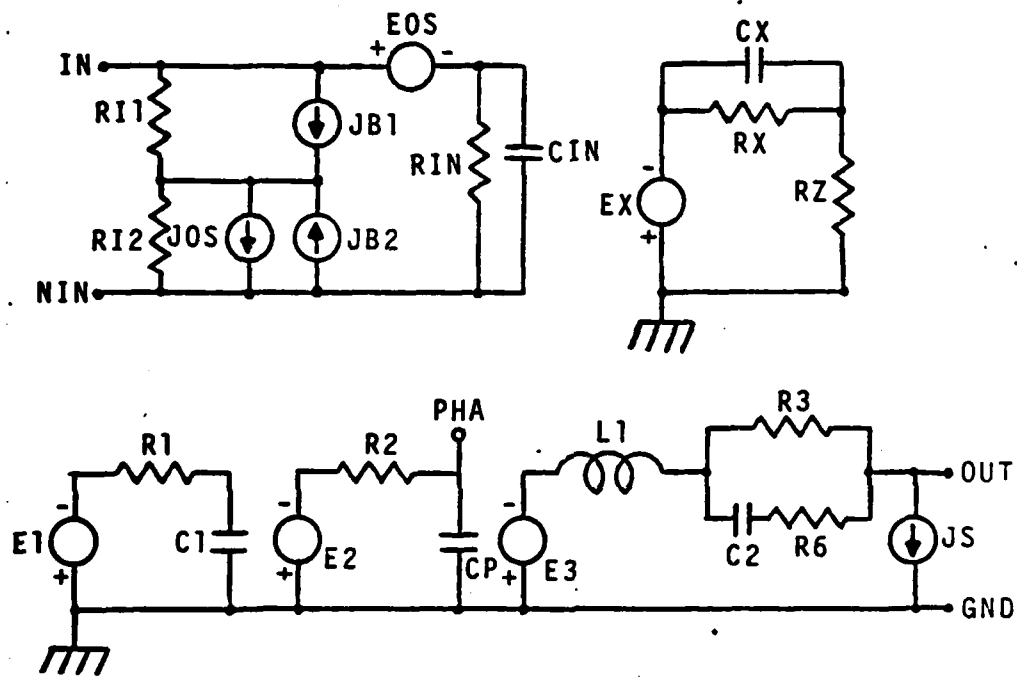


Figure 1-14. Op Amp Macromodel for AC, Transient
and Thermal Analysis.³²

magnitude reduction in matrix size and computation time is realized when these macromodels are used in place of device level or full models.

For completeness, two other nonlinear macromodels for the Op Amp should be mentioned even though no attempt has been made to use these nonlinear macromodels for EMI analysis. The Weil nonlinear macromodel^[35] represents the nonlinearities by two diodes at the input of the IC. The diode current-voltage characteristic is exponential and includes an ideality factor. The input resistance is nonlinear as a result of the diode exponential current-voltage characteristic. The nonlinear macromodel developed by Majewski and Sanchez-Sinencio^[36,37] falls in the category of transfer function modeling in the manner of piecewise linear analysis,^[39,40] as opposed to physical device modeling. In their model, the saturation or clipping of the input current versus input voltage represents the overall IC nonlinearity. Output waveform distortion under large signal operation can be predicted with the aid of Fourier analysis. Output voltage limiting is represented by a delta function type of nonlinear resistance. These nonlinear macromodels were not designed for EMI applications nor can the BJT nonlinear current generators shown in Figure 1-2 be included in these models.

Macromodels for ICs have been reported upon by several investigators.^[26-38] The macromodel for the Op Amp developed by Boyle et al. was selected for EMI analysis because it includes two transistors which

model in a physical sense the actual Op Amp input circuitry. Because the Boyle Op Amp macromodel predicts EMI in real Op Amps so well, no effort to develop or to modify the other IC macromodels for EMI analyses was made. The remainder of this dissertation is devoted to describing how well the Boyle Op Amp macromodel predicts the demodulation of AM modulated RF carriers in op amp circuits and to explaining why it works so well.

The results of the research reported in this dissertation has been summarized in a paper which was presented at the International Conference on Electromagnetic Compatibility at Southampton, England, the 16th to 18th, September, 1980. A copy of this paper is attached as Appendix A.

CHAPTER TWO

THE NONLINEAR MACROMODEL FOR EMI ANALYSIS OF THE BIPOLAR IC OPERATIONAL AMPLIFIER

As discussed in Chapter 1 the Op Amp macromodel developed by Boyle et al. was selected for EMI analysis because it includes two transistors which model in a physical sense the Op Amp input circuitry. In Section 2.1 the transformation of the original Boyle macromodel, which was developed primarily for dc and transient nonlinear analyses, into a nonlinear small-signal macromodel suitable for use with NCAP will be described. In Section 2.2, intermodulation predictions made using the nonlinear small-signal Op Amp macromodel will be compared to predictions made using a full Op Amp model and to experimental results. The specific case investigated involves the demodulation of amplitude modulated RF signals in Op Amps to produce undesired low frequency responses related to AM modulation on the RF carrier. In Section 2.3 the important effects caused by parasitic capacitances associated with the p-n junctions used to provide isolation in integrated circuit Op Amp is discussed in some detail.

2.1 The Nonlinear Macromodel Based on a Two-Transistor Physical Representation

An analog IC can be blocked into three main sections:[41,42] the input stage, the gain stage and the output stage. For the purpose of

nonlinear small-signal analysis, the output stage can be viewed as a linear stage that provides power amplification and impedance transformation. The input stage is a differential amplifier. The gain stage provides nearly all of the open-loop gain and phase compensation. A schematic representation of the IC Op Amp can be drawn as in Figure 2-1. [43] As noted previously this two-transistor configuration furnishes the means of including physical device nonlinearities because the BJT nonlinear current generators shown in Figure 1-2 can be included. The Op Amp model shown in Figure 2-1 is a simple model. It can be refined as necessary. It is interesting to note that the use of a two-transistor input configuration followed with a linear amplifier for an analog IC was used in an early computer simulation. [44]

In the nonlinear small-signal macromodel shown in Figure 2-2, the transistors Q_1 and Q_2 are the two BJTs at the inputs of the IC Op Amp being modeled. These two BJTs can be characterized by the nonlinear BJT model of Figure 1-2 and by the model parameters of Table 1-3. The nonlinear behavior of the Op Amp is caused by these two transistors. The nonlinear macromodel of Figure 2-2 can be derived directly from the Boyle macromodel [29] of Figure 1-12. When the nonlinear small-signal behavior of the Op Amp is to be modeled, several dc and limiting circuit elements in the Boyle macromodel, namely R_p , D_1 , D_2 , R_C , $G_C v_6$, V_C , D_3 , D_4 and V_E can be omitted. In the small-signal macromodel the capacitor C_1 is related to the nondominant pole of the differential gain response

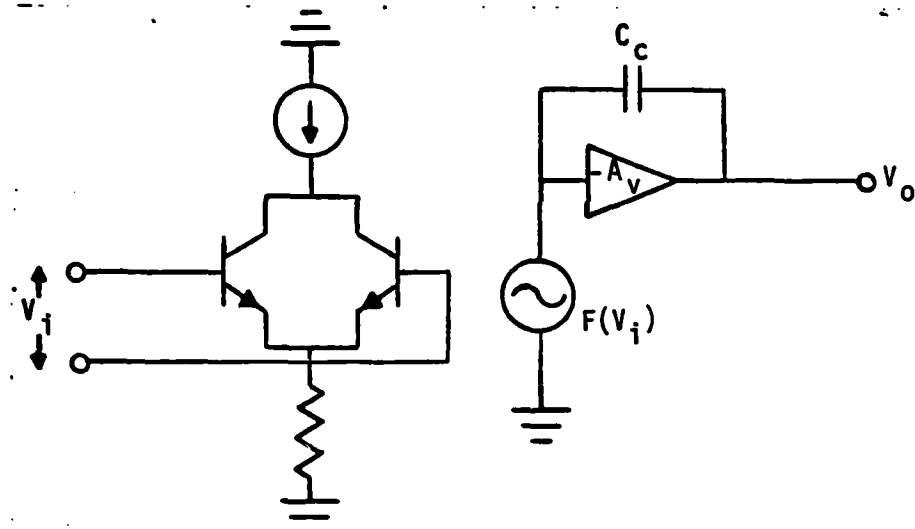


Figure 2-1. Schematic Representation of the 741 Type Op Amp.
The signal generator F is a function of the input voltage V_i .

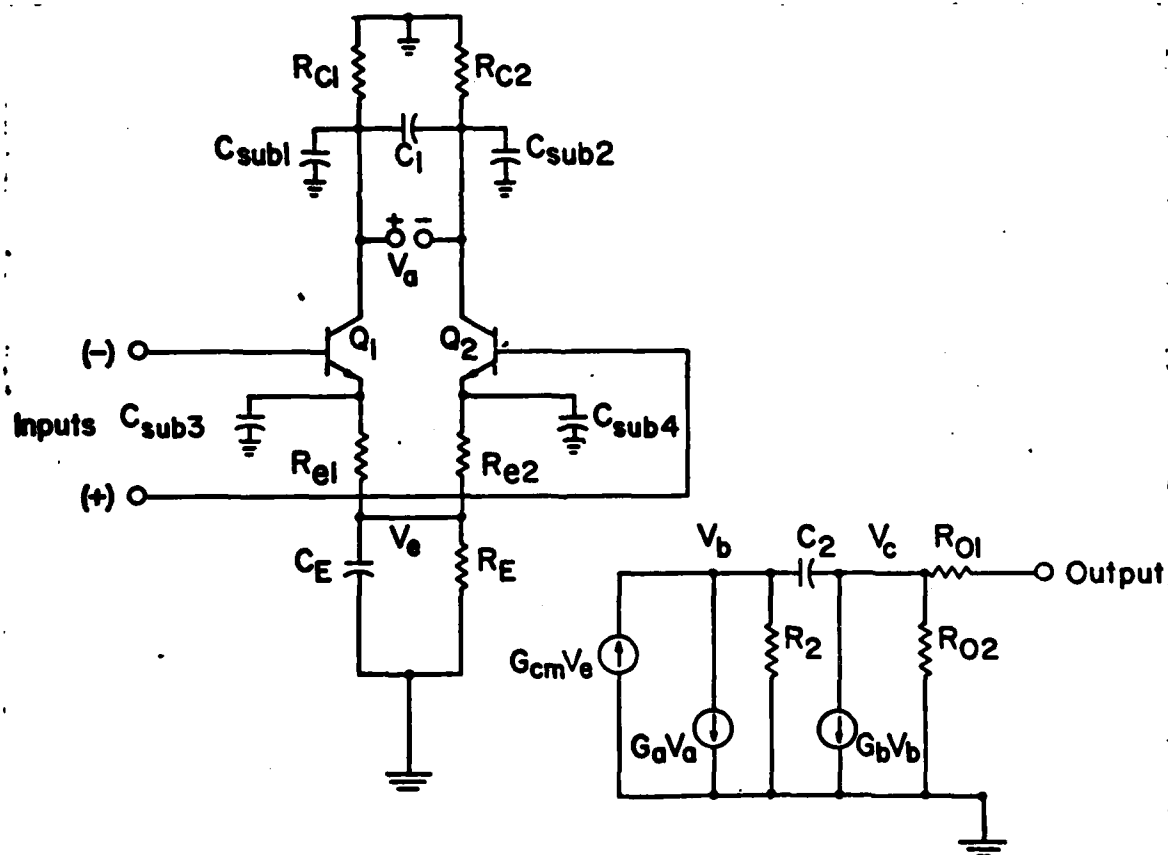


Figure 2-2. Nonlinear Macromodel for the BJT IC Op Amp in Small-Signal Operation.

and to the excess phase at the cutoff frequency f_{0dB} . The capacitor C_2 is the phase compensation capacitance in the gain stage of the actual IC. The resistors $R_{C1} = R_{C2}$ are determined by the requirement that the 0 dB frequency $f_{0dB} = 1/2\pi R_{C2} C_2$. The resistors $R_{e1} = R_{e2}$ model the emitter degeneration for slew rate enhancement. [47,48] The resistor R_E is related to the differential input resistance. The capacitor C_E models charge storage effects at the input. The transconductances G_a and G_b are related to the differential voltage gain. The value for the voltage gain of the differential input stage is not critical in either linear or nonlinear analysis and is assigned a value of unity. The input stage differential mode voltage gain equals the product $G_a \times R_2$. The product $G_b \times R_{02}$ equals the single-ended open-loop differential voltage gain of the IC. The resistor R_{01} is the dc component of the internal output resistance. The resistor R_{02} is a small-signal internal output resistance. The common-mode transconductance G_{cm} models the effect of the Common-Mode Rejection Ratio (CMRR).

The macromodel circuit parameters can be extracted from the IC manufacturer's specification sheets using procedures given by Boyle et al. The macromodel parameters for the LM741 Op Amp are given in Table 2-1.

The NCAP BJT model parameters for the input transistors Q_1 and Q_2 in the macromodel are taken directly from the published data by Fang and Whalen and are reproduced in Table 2-2. The BJT parameters used

TABLE 2-1
MACROMODEL PARAMETERS FOR LM741^a

T	300° K	G _a	188.6 μ mho
I _{SD3}	8×10^{-16} A	G _{CM}	6.28 nmho
R ₂	100 k Ω	R ₀₁	32.13 Ω
C ₂	30 pF	R ₀₂	42.87 Ω
C _E	2.41 pF	G _b	247.49 mho
I _{EE}	20.26 μ A	I _{SD1}	8×10^{-16} A
R _E	9.872 M Ω	R _C	0.02129×10^{-3} Ω
R _{C1}	5305 Ω	G _C	49964 mho
R _{e1}	2712 Ω	V _C	1.803 V
C ₁	5.460 pF	V _E	2.303 V

From Boyle et al., Ref. 29.

TABLE 2-2
NCAP INPUT PARAMETER VALUES FOR μ A741 OP AMP MACROMODEL^a

Parameter	Q1	Q2
η	4.34	4.34
V_{CB} (V)	14.57	14.57
V_{CBO} (V)	20	20
μ	0.165	0.165
I_C (A)	10 _, E-6	10 _, E-6
$I_{C \max}$ (A)	0.5 _, E-3	0.5 E-3
a	0.90	0.62
$h_{FE \max}$	400	400
$k (F - V \frac{1}{2})$	1.23 E-12	1.23 E-12
Ref.	1.091	1.091
C_{je} (F)	1.23 E-12	1.23 E-12
C_2^1 (F/A)	9.09 E-9	9.09 E-9
r_b (ohms)	830	830
r_c (ohms)	5.33 E6	5.33 E6
C_1 (F)	0.1 E-12	0.1 E-12
C_3 (F)	0.1 E-12	0.1 E-12

^aThis set of parameter values is based upon the full Op Amp BJT parameter values reported by Fang,⁴⁶ with the exceptions of I_C and a as noted on page 40.

are those for the Op Amp input transistors which are small npn transistors. As will be discussed later, the nonlinear BJT parameters of Table 2-2 can be considered applicable to BJT IC Op Amps of present day technology.

Utilizing the nonlinear small-signal macromodel described in this section, the NCAP predictions for the second order transfer function of the 741 unity gain buffer amplifier are reported upon in the next section.

2.2 NCAP Intermodulation Predictions with the Nonlinear Macromodel and Experimental Verification.

The validity of the nonlinear macromodel proposed in Figure 2-2 has to be established by determining its effectiveness in EMI analysis. The nonlinear circuit analysis program NCAP is used for the validation. Two criteria for the nonlinear macromodel are proposed:

1. Do NCAP predictions based upon the macromodel agree with the same predictions based upon the full model (device level model) of the Op Amp IC?
2. Do NCAP predictions of EMI effects based upon the macromodel agree with the experimental results?

The 741 Op Amp circuit selected for the validation is the unity gain buffer amplifier. The circuit configuration is shown in Figure 2-3. The nonlinear macromodel equivalent circuit for this amplifier is shown in Figure 2-4. The experimental system for the measurement of the second order transfer function $H_2(f_2, -f_1)$ is shown in Figure 2-5.

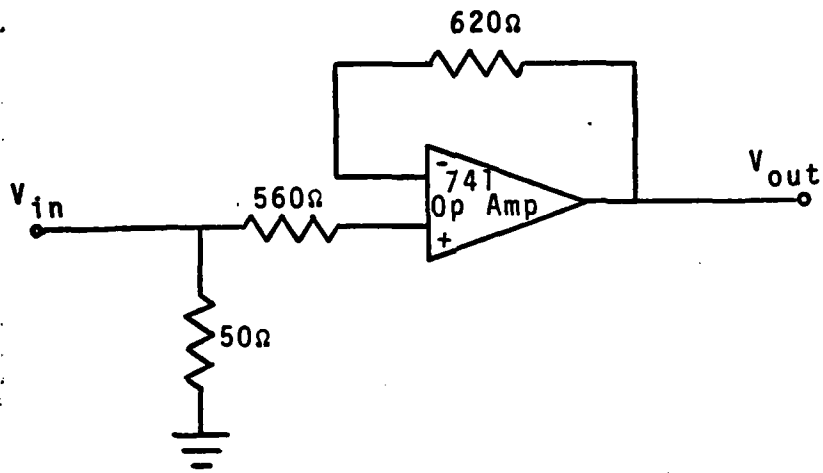


Figure 2-3. Unity Gain Buffer Amplifier with IC Op Amp as the Active Device.

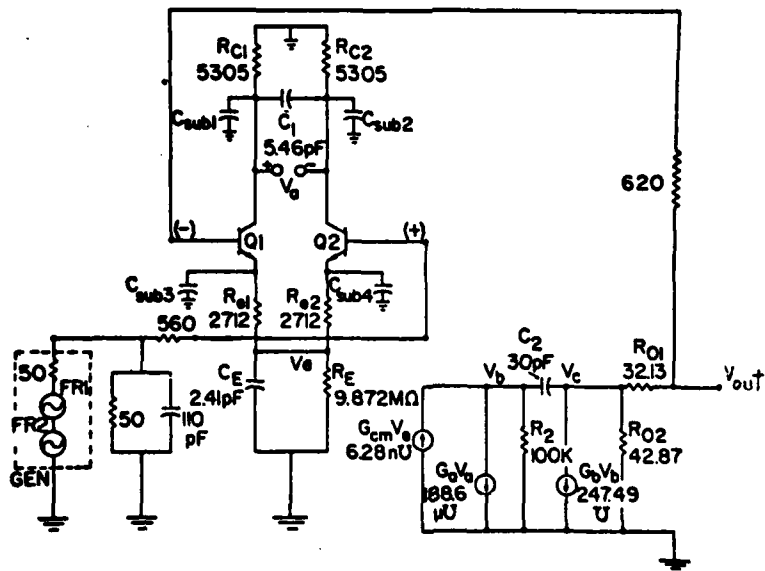


Figure 2-4. Macromodel Circuit of the 741 Buffer Amplifier.

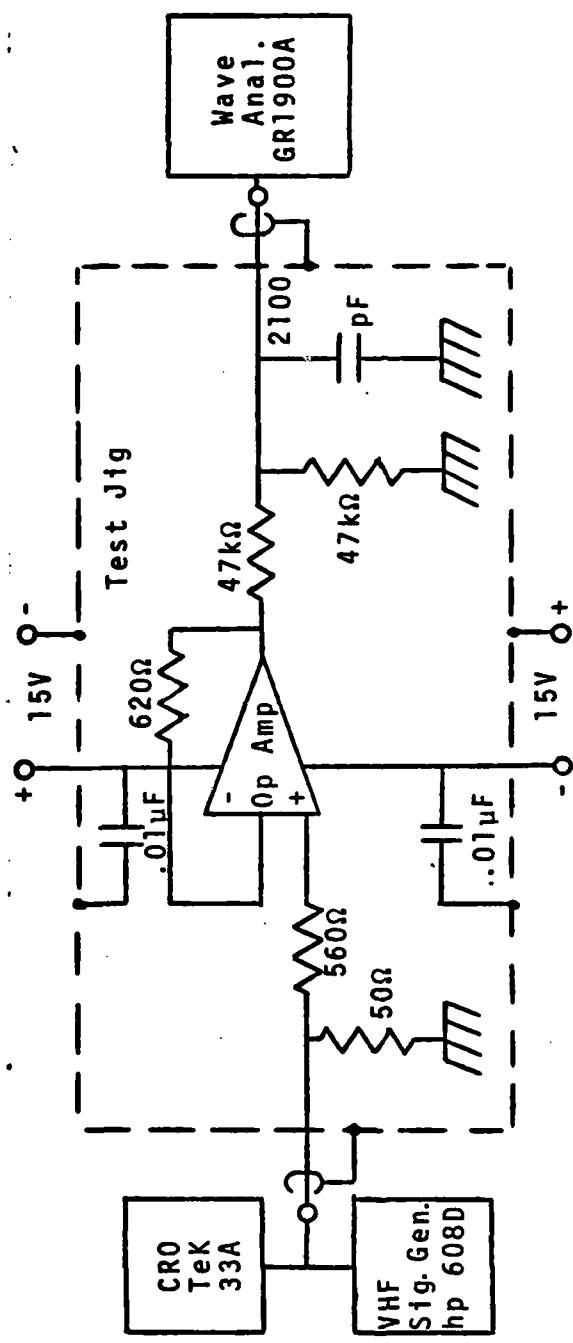


Figure 2-5. Experimental System for a Buffer Amplifier Second Order Intermodulation Measurement.

The coding diagram for an NCAP analysis with the nonlinear macromodel is shown in Figure 2-6. The circuit of Figure 2-6 represents the small-signal equivalent circuit of the experimental circuit of Figure 2-5. If nonlinear effects do not occur in the IC Op Amp, the Wave Analyzer shown in Figure 2-5 should read zero. Then the NCAP EMI predictions for Figure 2-6 should be zero also. It is noted that any EMI predicted for the macromodel circuit of Figure 2-6 results solely from the nonlinearities of the two BJT's. The NCAP input coding list for a second order intermodulation analysis [46] of the circuit of Figure 2-6 is given in Table 2-3. The circuit element parameter values used in Table 2-3 are taken from Figure 2-6. The nonlinear BJT parameter values given in Table 2-2 are taken from Table 1-3 with two exceptions. Fang [46] reports a value $I_C = 7.85 \mu A$. Boyle et al. uses a value $I_C = 10 \mu A$. The Boyle value is used in our analysis. The value of the h_{FE} Nonlinearity Coefficient "a" is adjusted using the following empirical relationship:

$$a = \frac{h_{FEmax.} - h_{FE}}{h_{FE} \left[\log \left(\frac{I_C}{I_{Cmax}} \right) \right]^2} \quad (2-1)$$

The values obtained for "a" of the macromodel transistors Q_1 and Q_2 [29] are

$$a_1 = \frac{400 - 111.67}{111.67 \left[\log \left(\frac{10.0 \times 10^{-6}}{0.5 \times 10^{-3}} \right) \right]^2} = 0.9$$

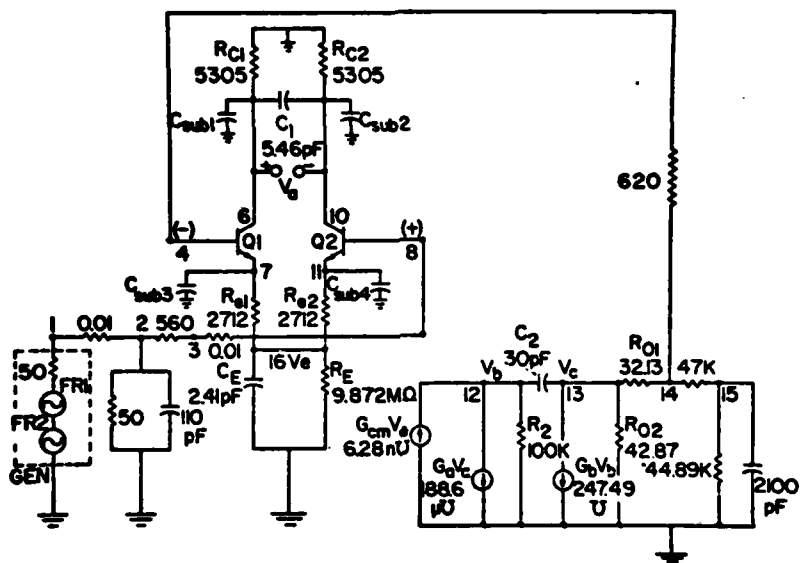


Figure 2-6. NCAP Coding Circuit Diagram for the Voltage Follower Circuit with Op Amp Macromodel.

* The 0.01 Ω resistors represent jumper wires, as 0 Ω resistors are not allowed in NCAP.

Table 2-3

NCAP INPUT CODE FOR SECOND ORDER INTERMODULATION ANALYSIS
OF THE EXPERIMENT OF FIGURE 2-5

```
** MACROMODEL OF 741 OP AMP
** ANALYSED BY NCAP FOR H2
** SUBMITTED AT SUNY BUFFALO
** GORDH OUTPUT NODE IS 15
* START CIRCUIT
* GENERATOR
NODE 1 0
FR 1 1E6 10E6 5 LIN
AMP 1.0 0.0
FR 2 -0.9996E6 -9.9996E6 5 LIN
AMP 1.0 0.0
IMP 50 0
* LINEAR COMPONENTS
R 2 1 0.01
R 2 3 560
R 3 8 0.01
R 2 0 50
R 0 6 5305
R 7 16 2712
R 0 10 5305
R 11 16 2712
R 16 0 9.872E6
R 12 0 1.0E5
R 13 0 42.87
R 13 14 32.13
R 14 15 4.7E4
R 15 0 4.489E4
R 14 4 620
C 2 0 1.1E-10
C 6 10 5.460E-12
C 16 0 2.41E-12

C 12 13 3.0E-11
C 15 0 2.106E-9
** SUBSTRATE CAPACITANCE
C 6 0 4.0E-15†
C 10 0 4.0E-15
C 7 0 4.0E-15
C 11 0 4.0E-15

* TRANSISTOR
NODE 4
4.34 14.57 20 0.165 10.05E-6
0.5E-3 0.90 400 1.23E-12 1.091
1.23E-12 9.09E-9 830 5.33E6
0.1E-12 0.1E-12

* TRANSISTOR
NODE 8
4.34 14.57 20 0.165 10.05E-6
0.5E-3 0.62 400 1.23E-12
1.091 1.23E-12 9.09E-9 830
5.33E6 0.1E-12 0.1E-12

* LINEAR DEPENDENT SOURCE
NODE 6 10 0 12
VC 1.886E-4 0.0

* LINEAR DEPENDENT SOURCE
NODE 16 0 12 0
VC 6.28E-9 0.0

* LINEAR DEPENDENT SOURCE
NODE 12 0 0 13
VC 247.49 0.0

* END CIRCUIT
* END
```

† For ease of adding and eliminating substrate capacitances in NCAP runs, a 0 pF substrate capacitance is represented by a reduction of three orders of magnitude.

$$a_2 = \frac{400 - 143.57}{143.57 \left[\log \left(\frac{10.0 \times 10^{-6}}{0.5 \times 10^{-3}} \right) \right]^2} = 0.62$$

The values for the second order transfer function $H_2(f_1, -f_2)$ calculated by NCAP as a function of RF frequency are plotted in Figure 2-7. In order to generate the transfer function spectrum plotted, the frequency sweeping feature of the NCAP program was used. The experimental results* obtained using the system shown in Figure 2-5 were converted to experimental values for the second order nonlinear transfer function using Equation 1-14 and are plotted in Figure 2-7.**

The results shown in Figure 2-7, while not satisfactory, are encouraging. The macromodel does predict the frequency range at which maximum second order intermodulation occurs. Although the predicted second order transfer function is in error by 15 dB, there is qualitative agreement between macromodel predictions and experimental results. Plotted on the same figure are the NCAP predictions for the same buffer amplifier based on a full model for the Op Amp. It is seen that the full model predicted results are higher than the macromodel by 5 dB in the critical frequency range of maximum second order intermodulation

* The experimental results were obtained using the Fairchild μ A741 IC which is essentially the same as the LM741.

** Values for a third order nonlinear transfer function were also calculated and determined to be less than -100 dB. An experimental verification of such a low intermodulation signal strength would be very difficult if not impossible and was not attempted.

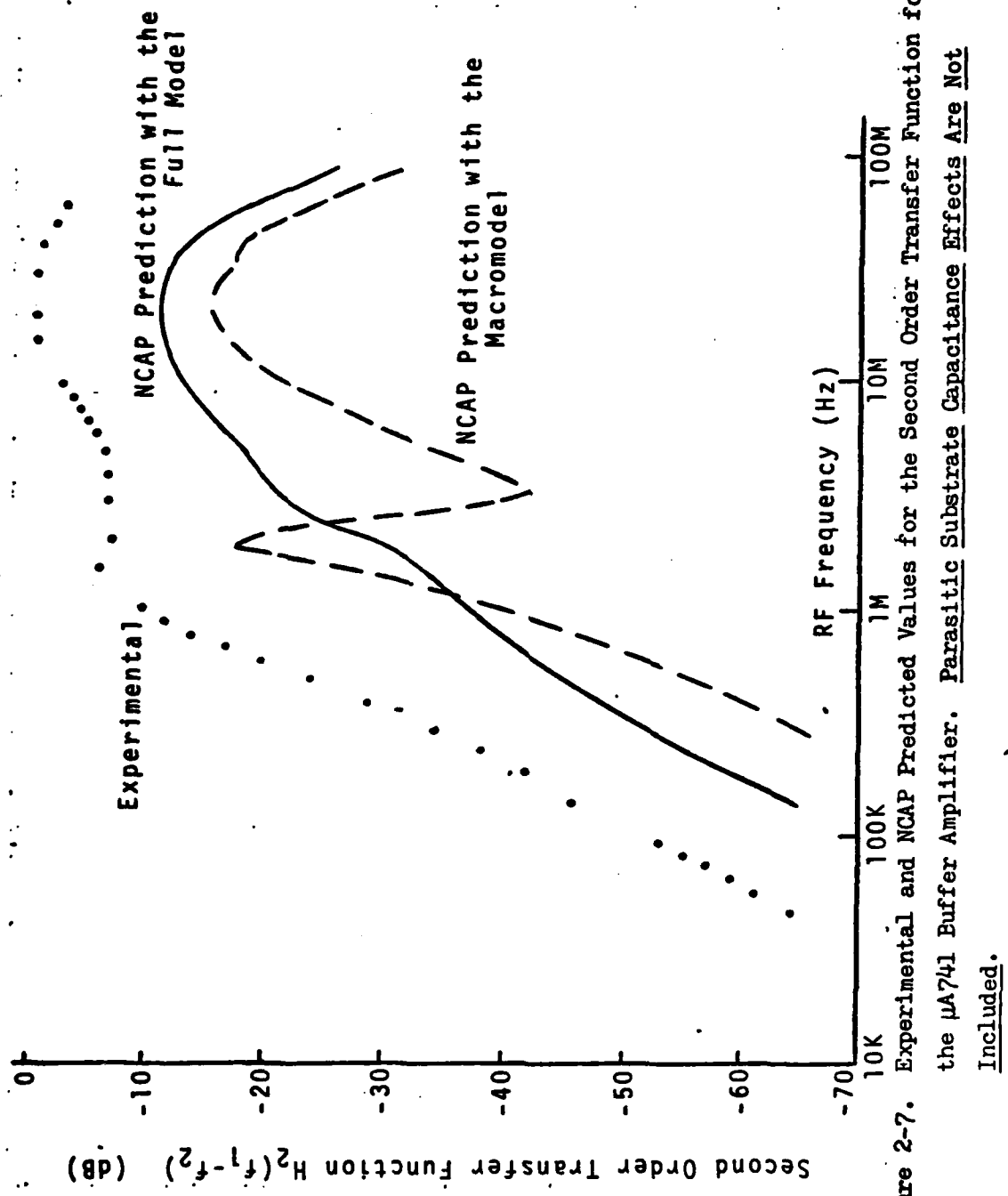


Figure 2-7. Experimental and NCAP Predicted Values for the Second Order Transfer Function for the μ A741 Buffer Amplifier. Parasitic Substrate Capacitance Effects Are Not Included.

effects, but are still 10 dB lower than the experimental results. Similar NCAP predictions by Fang et al. [46] using the full model for the Op Amp matches the experimental results more closely. The Fang NCAP simulation accounted for the parasitic effects of the substrate capacitances (See Figure 1-9). These parasitic effects are not accounted for in the NCAP predictions of Figure 2-7. The need to account for the parasitic effects of the substrate capacitances in nonlinear IC Op Amp modeling is evident. Substrate capacitance effects are discussed in the next section.

2.3 Substrate Capacitances in Nonlinear Macromodeling

In the EMI modeling of electronic circuits, Whalen and Paludi [49] showed that the parasitic elements strongly influence the accuracy of computer-aided analysis. This is the case even for circuits containing only one active device which is the sole source of circuit nonlinearity. Fang [18] in his computer simulation of Op Amps using a full model included substrate capacitances as parts of his IC circuit model. The substrate capacitances of the 741 measured by Wooley et al. [24] were used. Also, a lower typical value of 2 pF was used. Consequently, Fang was able to make predictions of intermodulation effects closely matching experimental results. Although Wooley found that the substrate capacitances limits the first order response significantly, none of the macromodels referenced in Section 1.3 include these parasitic elements. Since those macromodels were not designed for EMI nonlinear analysis, the

effects of neglecting substrate capacitances were not appreciated.

The npn transistors in a bipolar IC Op Amp have substrate capacitances occurring at the collector. These capacitors are shown in the 741 full model NCAP coding diagram, Figure 1-9. According to Wooley, [24] the small npn transistor of the 741 has a collector substrate capacitance of 3.2 pF. The lateral pnp transistor has a base substrate capacitance of 5.1 pF. Taking these values as a starting point, a nonlinear macromodel for the 741 which includes substrate capacitances, is shown in Figure 2-8. The true value of the individual device substrate capacitance in situ on the IC is uncertain due to the complexity of the IC structure. Fang has found that for the purpose of numerical prediction, the exact value of substrate capacitance is unnecessary. A typical capacitance value can be used to obtain good EMI predictions. The same situation also is true for the nonlinear macromodel. Consequently, one substrate capacitance value is used at both the collector and the emitter for both BJTs in the nonlinear macromodel. It will be shown later that a structural justification for the substrate capacitance values (which cannot be given) is not essential. What is essential is a methodology for accounting for the effects of substrate capacitance upon the internal RF interaction which produces the intermodulation. At the present time no procedure exists by which the values for the parasitic capacitors C_{sub} shown in Figure 2-8 can be determined independently. Instead a parametric fitting procedure is used. Values such as 0, 2 pF, or 4 pF are assigned to the four capacitors C_{sub} and the NCAP

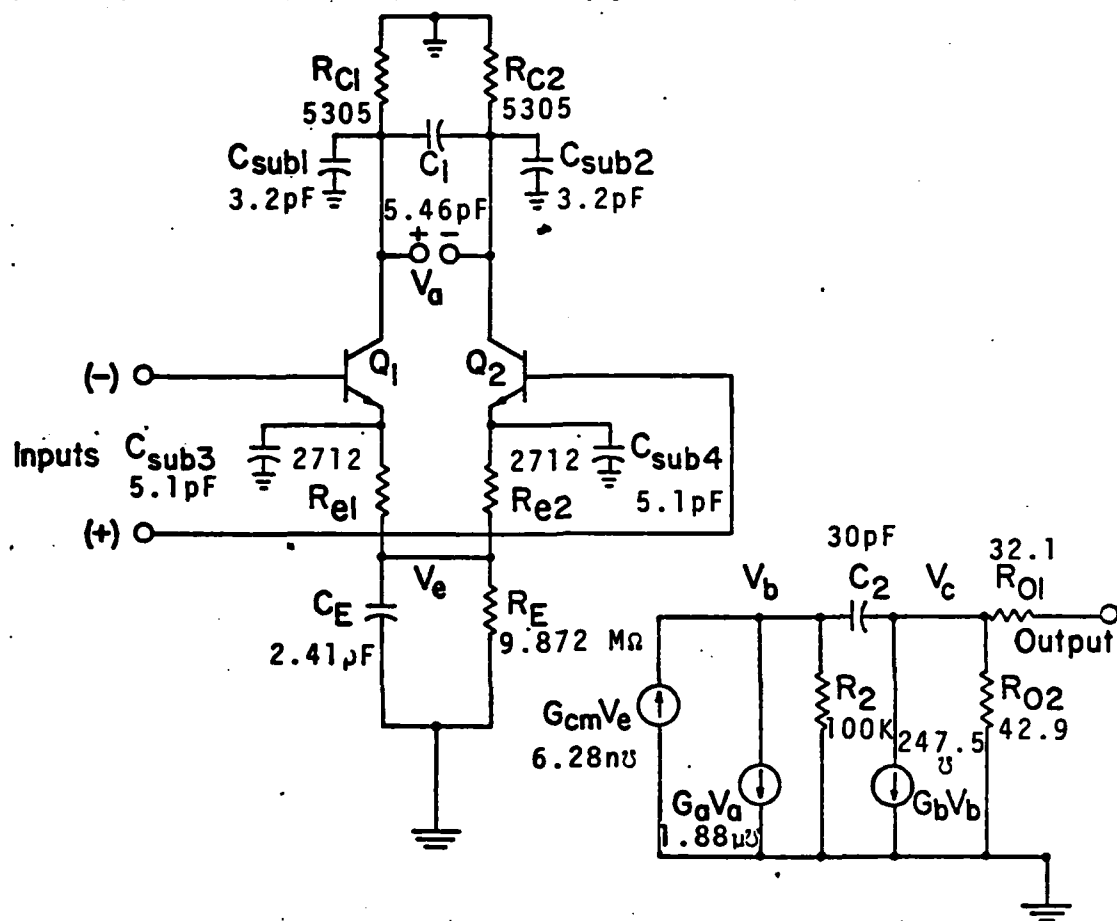


Figure 2-8. A Nonlinear Macromodel for the 741 IC
Op Amp Which Includes Substrate Capacities.

calculations are made.

The results of the NCAP predictions for the 741 buffer amplifier second order transfer function using substrate capacitance values of 0 pF, 2 pF and 4 pF are shown in Figure 2-9. It is noted that the inclusion of substrate capacitance in the nonlinear macromodel improves the numerical accuracy of prediction and also gives better qualitative agreement with the experimental results over a wider frequency range. A substrate capacitance of 4 pF produces the best fit between NCAP predictions and experimental results. Furthermore, NCAP predictions made using a Op Amp macromodel with $C_{sub} = 4$ pF compare favorably with Fang's NCAP predictions made using the Op Amp full model with $C_{sub} = 2$ pF or Wooley's C_{sub} values. See Figure 8 in Appendix A. When the macromodel substrate capacitance value is increased above 4 pF, the second order transfer function values predicted change less rapidly and tend to exceed the experimental values.

The computer time for an NCAP analysis is greatly reduced by the use of the nonlinear macromodel. On the Honeywell 6180 computer, an NCAP five-frequency sweep analysis of the 741 Buffer Amplifier second order transfer function based on the nonlinear macromodel requires 34 seconds of CPU time. In addition 30 seconds for peripheral transferring of data is required. Not only does the nonlinear macromodel reduce computer time and costs, it is also much easier for the EMC engineer

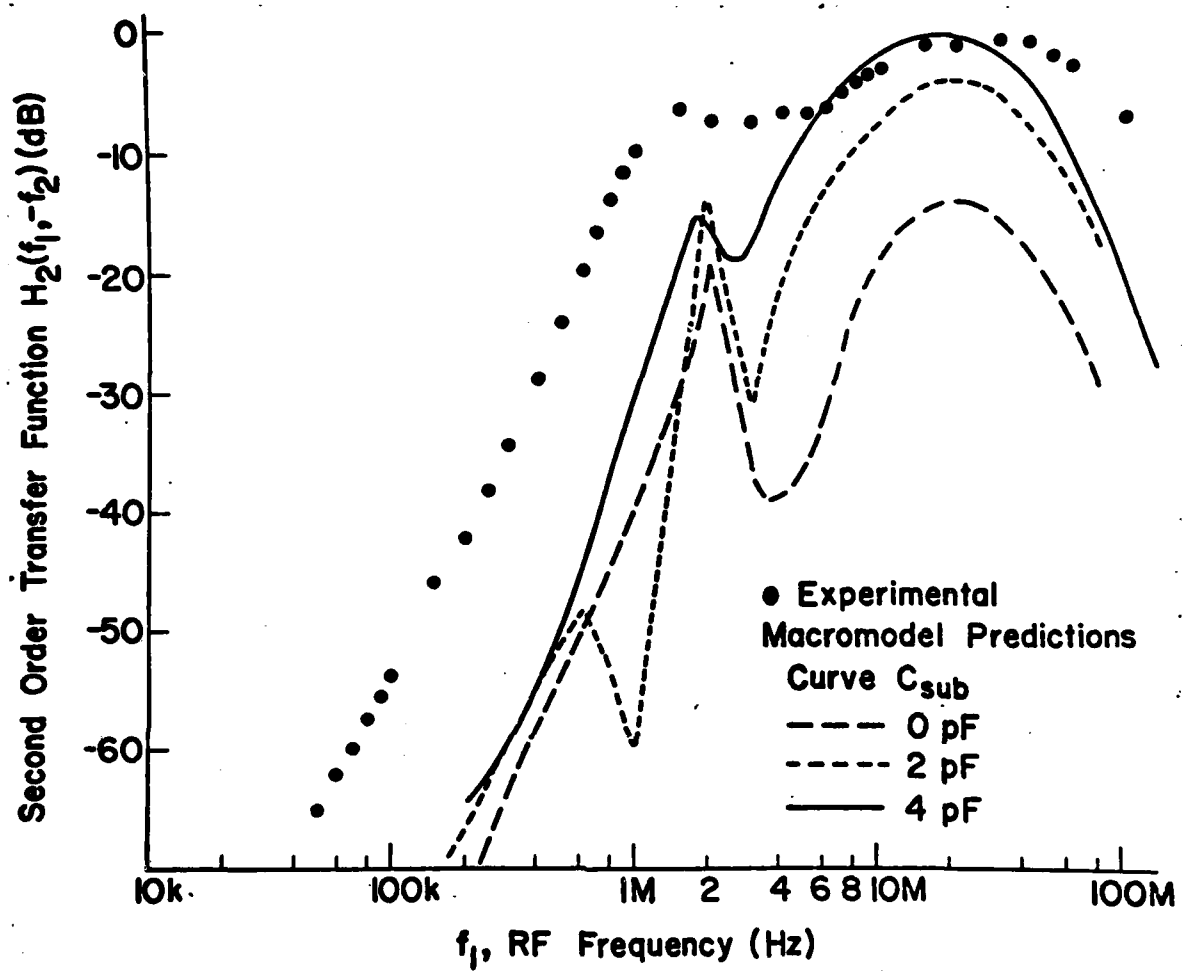


Figure 2-9. Effect of the BJT Substrate Capacitance Value on NCAP Prediction of the Second Order Transfer Function Based on the Nonlinear Macromodel of the 741 Buffer Amplifier.

CHAPTER THREE

MACROMODELING PROCEDURE AND APPLICATION

In the previous chapter an Op Amp nonlinear small-signal macro-model based upon the Op Amp nonlinear large-signal macromodel of Boyle et al. [29] was used to predict EMI in a 741 Op Amp. One obvious question is can the Op Amp small-signal macromodel be used for other Op Amp types. If the answer is yes, a second question is: What adjustments are needed for other Op Amp types? It is believed that the Op Amp nonlinear small-signal macromodel shown in Figure 2-8 is global in the same sense as the BJT nonlinear T-model shown in Figure 1-2 is global. The Op Amp nonlinear small-signal macromodel can be used for any integrated Op Amp (including JFET-bipolar, MOSFET-bipolar, and MOSFET types) when three types of adjustments are made:

1. The input transistors Q_1 and Q_2 in Figure 2-8 must correspond to the input transistor types in the actual Op Amp. Appropriate NCAP transistor model parameters for the transistors Q_1 and Q_2 must be used.
2. Appropriate values for the resistors, capacitors and transconductances in the original Boyle Op Amp macromodel must be determined using the techniques described by Boyle et al. [29] for bipolar Op Amps and by Krajewska et al. [63] for FET-bipolar Op Amps.

3. Values for the four substrate capacitances C_{sub1} , C_{sub2} , C_{sub3} , and C_{sub4} shown in Figure 2-8 must be determined using the procedures described in this chapter.

In this chapter the basic macromodeling procedures will be outlined in more detail in Section 3.1. In Sections 3.2 and 3.3 the procedures will be applied to a new Op Amp—the LM10. The LM10 Op Amp is a bipolar Op Amp, but one that is very different from the 741 Op Amp discussed in Chapter 2. In Section 3.4 NCAP EMI predictions and experimental results will be compared in order to show how to determine appropriate values for the substrate capacitances shown in Figure 2-8.

3.1 The Macromodeling Procedure

In this section the basic macromodeling procedure for Op Amps is described. The specific case for BJT input transistors is considered. A similar procedure can be used for JFET or MOSFET input transistors.

- (1) A BJT IC Op Amp is represented by the model of Figure 2-8. Note that substrate capacitances are included.
- (2) The NCAP BJT model parameters for the input BJT pair are taken from sources such as the work of Fang. [18] When device fabrication data are available, it may be possible to extract the model parameters using computer-aid analysis techniques. [54,55]
- (3) The remaining Boyle macromodel parameters are extracted from the Op Amp performance specifications using procedures described by Boyle et al. [29]

- (4) The IC is tested in the experimental system of Figure 1-3 in the unity gain buffer amplifier configuration. The data are converted into values for the second order transfer function $H_2(f_2, -f_1)$ using Equation (1-14). The second order transfer function is plotted vs frequency as shown in Figure 1-6. The second order nonlinear transfer function $H_2(f_2, -f_1)$ represents well the experimental manifestation of EMI effects related to the demodulation of AM modulated RF signals in the Op Amp.
- (5) A NCAP computer simulation is performed to obtain predicted values for $H_2(f_2, -f_1)$.^[56] The substrate capacitance values are then adjusted to obtain the best fit between predicted and experimental results.

The macromodeling procedure just described will be applied to the LM10 Op Amp.

3.2 Macromodeling of the LM10 Bipolar IC Op Amp

The LM10 Op Amp^[57] has on one monolithic chip an Op Amp, a precision voltage reference, and an adjustable reference buffer amplifier. The pin configuration and functional diagram is shown in Figure 3-1. The independent Op Amp portion has pin to pin equivalency with the 741 Op Amp. Upon examining the National LM10 data sheets (Appendix B),^[57] it is noted that the LM10 Op Amp performance is similar to that of the 741 Op Amp. However, the similarity stops here. The LM10 Op Amp has been designed so that it can be operated from a single supply voltage as low as 1.1 V. The LM10 Op Amp IC schematic circuit diagram is shown in Figure 3-2.

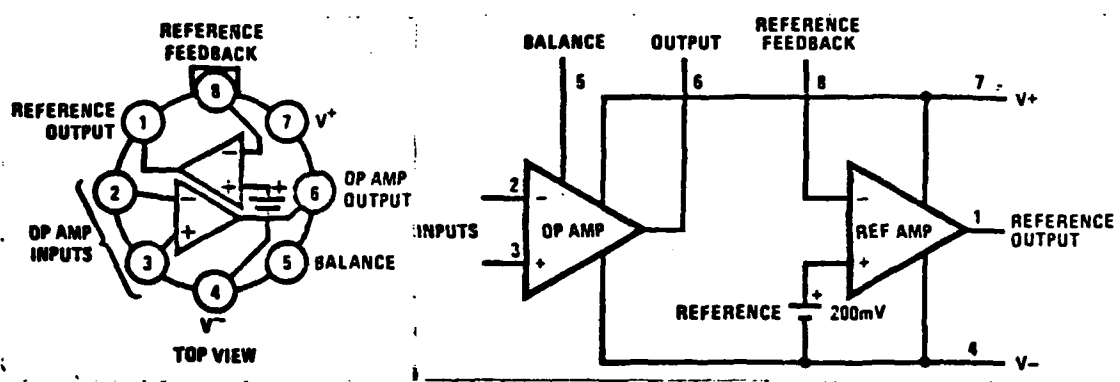


Figure 3-1. LM10 Pin Configuration and Functional Diagram. 65.

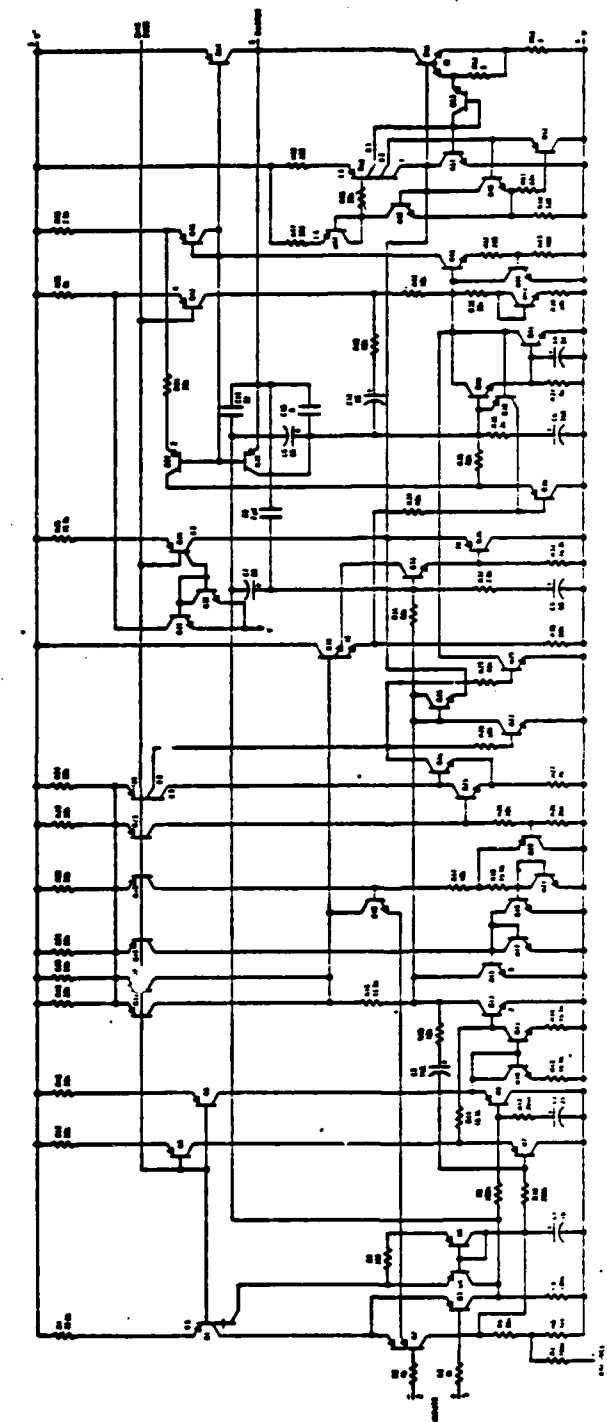


Figure 3-2. LM10 Op Amp IC Schematic. 58

The Op Amp input section of the LM10 is different from the 741 Op Amp in major design respects. The essential details of the LM10 Op Amp input section are shown in Figure 3-3. [59] Of particular significance is that the LM10 input transistors are pnp devices. Thus, the LM10 Op Amp constitutes, to a considerable degree, a new test on the effectiveness of the nonlinear macromodel for EMI analysis. The macromodel for the LM10 is shown in Figure 3-4. The macromodel equations and parameter value extraction methods are presented in the next section.

3.3 Calculation of the Macromodel Parameters

The LM10 macromodel parameter model parameters refer to the equivalent circuit of Figure 3-4. In this section values for the parameters are determined using the procedures given by Boyle et al. [29] and data from National Semiconductor data sheets for the LM10 which are included as Appendix B. For a complete understanding of the procedures used, a reading of Boyle's paper is essential. For the input pnp BJTs, the dc collector current I_C is $1.25 \mu\text{A}$ according to Wildar et al. [59]. The transconductance g_{m1} of the input differential stage is given by [47]

$$g_{m1} = \frac{qI_C}{2kT} = \frac{1.25 \times 10^{-6}}{2 \times 0.0258} = 2.42 \times 10^{-5} \text{ A/V} . \quad (3-1)$$

The compensation capacitance C_2 is given by

$$C_2 = \frac{g_{m1}}{2\pi f_{0\text{dB}}} = \frac{2.42 \times 10^{-5}}{2\pi \times 60 \times 10^3} = 6.4 \times 10^{-11} \text{ F} . \quad (3-2)$$

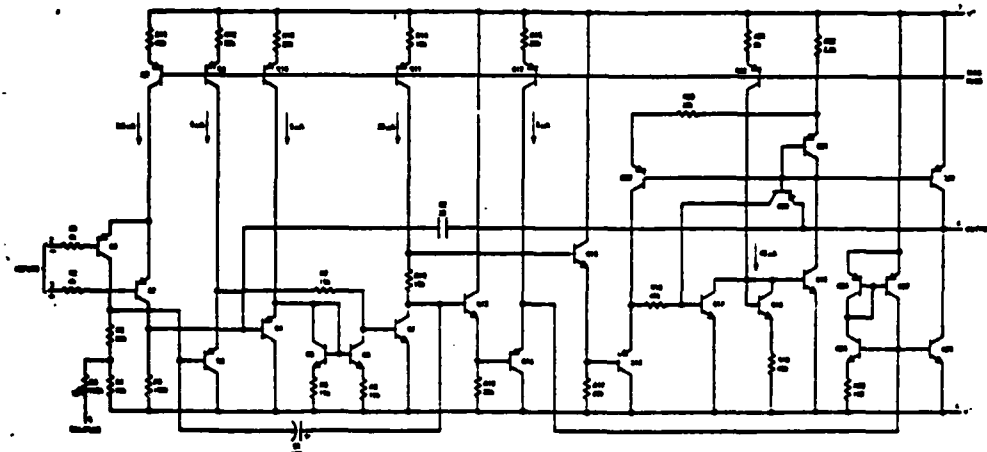


Figure 3-3. Essential Details of the LM10 Op Amp
Section. 59

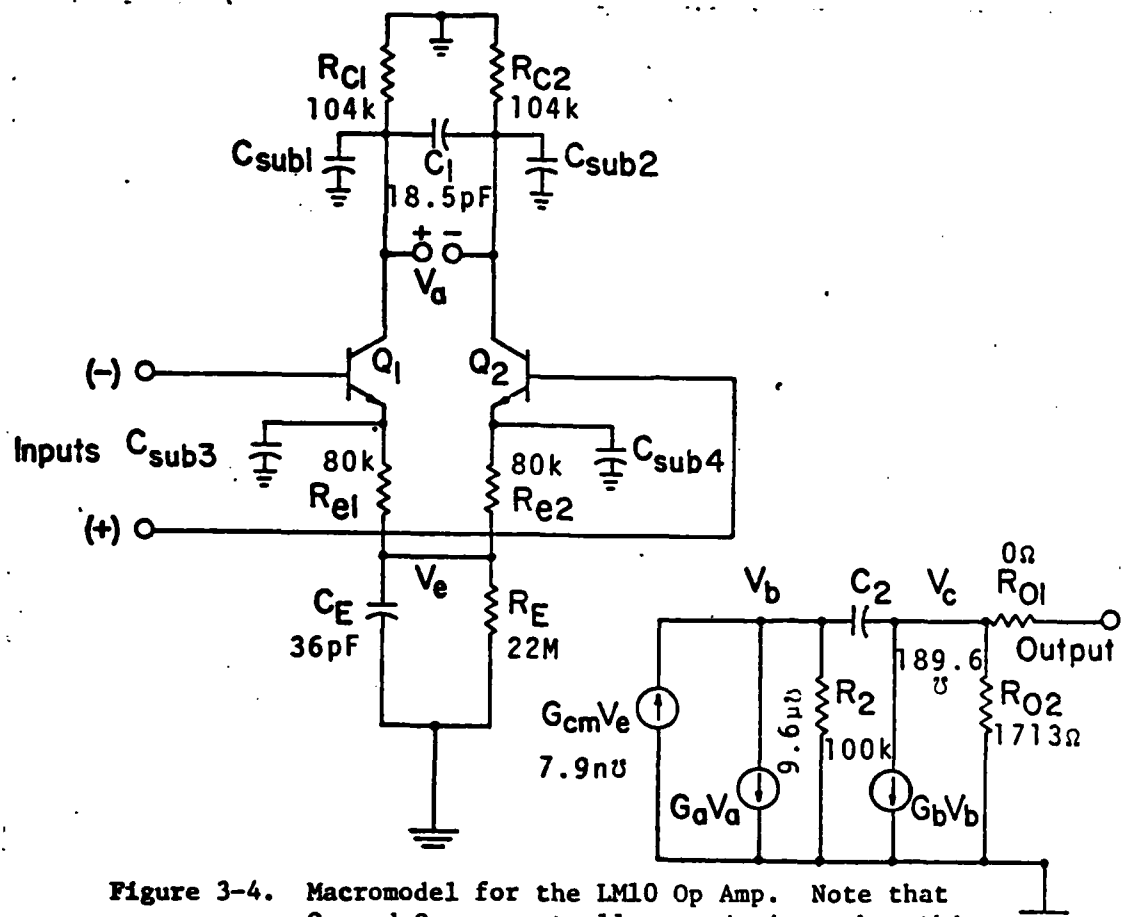


Figure 3-4. Macromodel for the LM10 Op Amp. Note that Q₁ and Q₂ are actually pnp devices, but this distinction is not recognized by NCAP small-signal analysis.

The frequency f_{0dB} at which the LM10 Op Amp open-loop gain is 0 dB is 60 kHz. The resistor $R_C = R_5 + R_6 = R_8 = 104 \text{ k}\Omega$ is taken from Figure 3-2. The conductance G_a is the reciprocal of R_C .

$$G_a = \frac{1}{R_C} = \frac{1}{104 \times 10^3} = 9.6 \times 10^{-6} \text{ A/V} \quad (3-3)$$

Next the output resistances R_{01} and R_{02} are calculated. The data sheets (Appendix B) show an output impedance varying with frequency as a function of load current over four orders of magnitude for closed-loop gains of 1 and 100. It is possible to use these curves to determine the Op Amp open-loop output resistance. The output resistance $R_{int} = R_{01} + R_{02}$ can also be determined from the open-loop dc voltage gain (A_{vD}) vs load resistance (R_L) graph shown in Appendix B using the relationship

$$A_{vD} = A_{vD} (R_L = \infty) \times R_L / (R_L + R_{int}) \quad (3-4)$$

where $A_{vD} (R_L = \infty)$ is the open-circuit value for A_{vD} . Choosing points $R_L = 2 \text{ k}\Omega$ where $A_{vD} = 110 \text{ dB}$ (3.16×10^5) and $R_L = 10 \text{ k}\Omega$ where $A_{vD} = 114 \text{ dB}$ (5.01×10^5) and using Equation (3-4), the value determined for R_{int} is 1713Ω . The macromodel dc output resistance parameter R_{01} is arbitrarily set at 0Ω . The macromodel ac output resistance parameter R_{02} is set equal to $R_{int} = 1713 \Omega$.

Wooley's [24] value for the dc current gain β_F for a lateral pnp is $\beta_F = 75$ which is close to the value $\beta_F = 100$ given by Widlar. [58] The Wooley value is used. The value for the Early Voltage V_A given by Fang

in Table 4-2 of Reference 18 for the lateral pnp transistors Q_3 and Q_4 is $V_A = 55$ V. This value is used. Using $I_{EE} \geq 2 I_C$, the resistance R_E is given by

$$R_E = V_A/I_{EE} = 55/(2.5 \times 10^{-6}) = 2.2 \times 10^7 \Omega \quad (3-5)$$

The capacitance C_1 is calculated from the frequency response curves for the gain and the phase. From the frequency response curves in the specifications (Appendix B), the phase margin ϕ_m of the open-loop response is obtained at the frequency where the gain becomes 0 dB. The ϕ_m value obtained is

$$\phi_m = 180^\circ - 120^\circ = 60^\circ$$

The excess phase shift at f_{0dB} as defined by Boyle^[29] is then,

$$\Delta\phi = 90^\circ - 60^\circ = 30^\circ$$

The excess phase shift is related to C_1 by

$$C_1 = (C_2/2)\tan\Delta\phi = (64/2)\tan30^\circ = 18.5 \text{ pF} \quad (3-6)$$

The value for h_{FE} is calculated by taking

$$h_{FEmax} = 100, \text{ and}$$

$$\begin{aligned} h_{FE} &= h_{FEmax}/\{1 + a\log^2(I_C/I_{Cmax})\} \\ &= 100/\{1 + 0.807\log^2(1.25/110)\} = 24.7 \end{aligned} \quad (3-7)$$

where the value $a = 0.807$ is the value given by Fang for the lateral pnp transistors Q_3 and Q_4 in Table 4-3 of Reference 18. The emitter resistance R_e is selected to make the gain of the input differential amplifier stage $v_d/v_{in} = 1$.^[29] Setting $v_d/v_{in} = 1$, Boyle obtained the expression

$$R_e = [R_C - 1/g_m][h_{FE}/(h_{FE} + 1)] \quad (3-8)$$

Using Equation (3-8) and the values $R_C = 104 \text{ k}\Omega$, $g_m = qI_C/kT = 48.4 \mu\text{A/V}$, and $h_{FE} = 24.7$, the value $R_e = 80 \text{ k}\Omega$ is obtained.

The transconductance G_b is calculated using the expression for the low frequency open-loop gain a_{vD} given by Boyle^[29]

$$a_{vD} = (v_d/v_{in})(G_a R_2)(G_b R_{02}) \quad (3-9)$$

The value $R_2 = 100 \text{ k}\Omega$ used by Boyle^[29] for the 741 Op Amp is also used for the LM10. Using Equation (3-9) with a typical value $a_{vD} = 300,000$, $v_d/v_{in} = 1$, $R_2 = 100 \text{ k}\Omega$, $G_a = 9.6 \mu\text{A/V}$, and $R_{02} = 1713 \Omega$, the value $G_b = 182.4 \text{ A/V}$ is calculated.

The capacitance C_E is related to the negative going slew rate by the formula

$$S_R^- = (2I_C)/(C_2 + C_E) \quad (3-10)$$

Using the graphs shown in Appendix B for the comparator response time for various input drives, it is observed that the output voltage changes

by 5 V in 0.2 ms which corresponds to a slew rate $S_R^- = 5 \text{ V}/0.2 \text{ ms} = 2.5 \times 10^4 \text{ V/s}$. Using Equation (3-10) with $S_R^- = 2.5 \times 10^4 \text{ V/s}$ and $C_2 = 64 \text{ pF}$, the value 36 pF is obtained for C_E .

The lateral pnp transistor NCAP parameter values determined using Wooley's data^[24] are used for the transistors Q_1 and Q_2 in the macro-model. These values are those for transistor Q3# in Table 1-3.

3.4 NCAP Predictions for the Second Order Transfer Function $H_2(f_2, -f_1)$ Based on the Nonlinear Macromodel

The NCAP coding diagram, using the parameters given in the previous section, is shown in Figure 3-5. The input code for an NCAP calculation of the second order nonlinear transfer function $H_2(f_2, -f_1)$ is listed in Table 3-1. The NCAP predicted results presented in Figure 3-6 do not agree well with the experimental results because substrate capacitance effects are not accounted for.

The actual location for the lateral pnp transistor parasitic substrate capacitance is from the base terminal to ground (substrate) as shown in Figure 3-7.^[24] The lateral pnp transistor in the Op Amp investigated by Wooley has a base area approximately 4.5 mil x 3 mil and a substrate capacitance of 1 pF. A measurement of the LM10 die area for the base of Q2 yields a value approximately 3 mil x 6 mil. This area is nearly equal to that of the lateral pnp transistors Q3 and Q4 listed in Table 1-3. Notwithstanding the difference in the actual physical place-

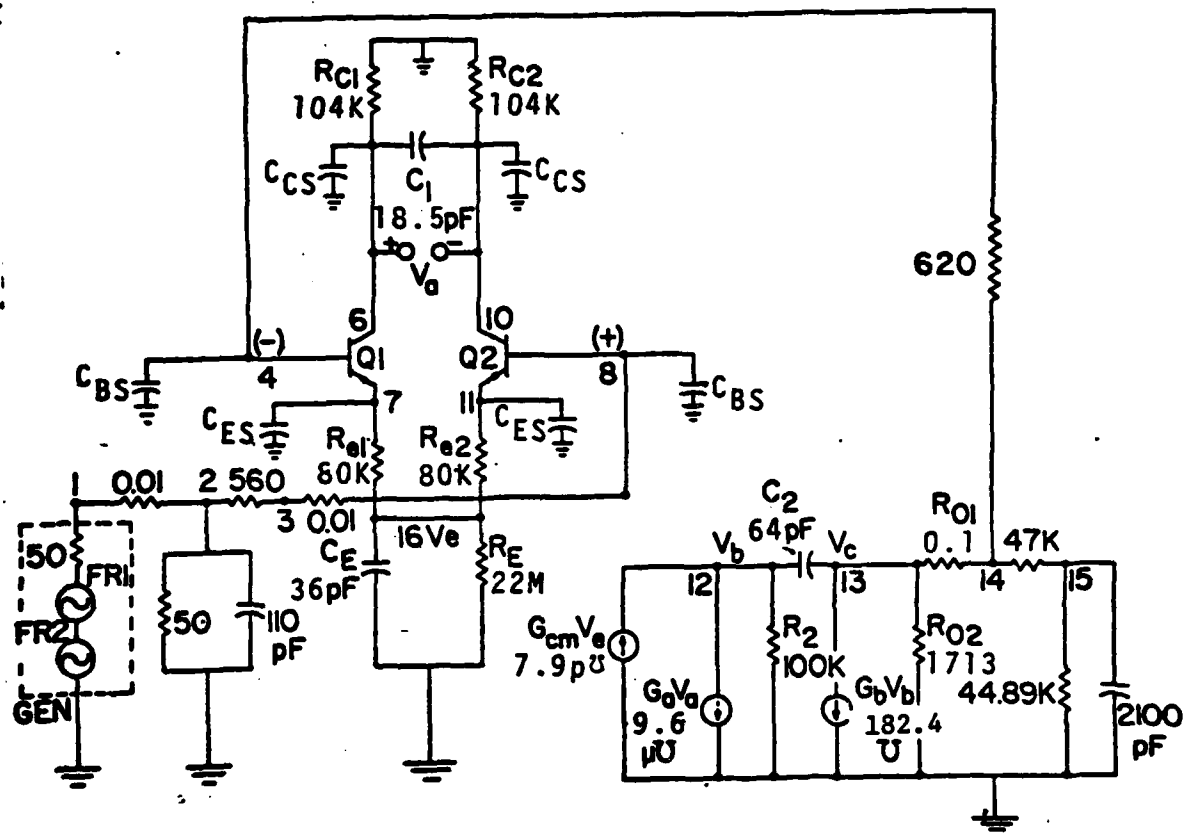


Figure 3-5. LM10 Buffer Amp NCAP Coding Diagram.

TABLE 3-1
NCAP INPUT CODE FOR THE MACROMODEL LM10 VOLTAGE FOLLOWER

```

** MACROMODEL FOR LM10 OP AMP
** ANALYSED BY NCAP FOR H2
** FOR STANDARD SUPPLY
** VOLTAGE OPERATION
** IN BUFFER AMPLIFIER
** UNITY GAIN CONFIGURATION
** SUBMITTED AT SUNY BUFFALO
** CCS=0 . CES=0 . CBS=0
** OUTPUT NODE IS 15 PIN 6 IS NODE 14
* START CIRCUIT
* GENERATOR
NODE 1 0
FR 1 1E7 8E7 5 LIN
AMP 1 0.0
FR 2 -0.99996E7 -7.99996E7 5 LIN
AMP 1 0.0
IMP 50 0
*LINEAR COMPONENTS
R 2 1 0.01
R 2 3 560
R 3 8 4E3
R 2 0 50
R 0 6 104E3
R 7 16 80E3
R 0 10 104E3
R 11 16 80E3
R 16 0 22E6
R 12 0 1.0E5
R 13 0 1713
R 13 14 0.1
R 14 15 4.7E4
R 15 0 4.489E4
R 14 17 620
R 17 4 4E3
C 2 0 1.1E-10

C 6 10 18.5E-12
C 16 0 36E-12
C 12 13 64E-12
C 15 0 2.106E-9
** SUBSTRATE CAPACITANCES CES = 0 PF,
** CBS = 0 PF, CCS = 0 PF
C 4 0 5.1E-15†
C 8 0 5.1E-15
C 6 0 4E-15
C 10 0 4E-15
C 7 0 0.5E-15
C 11 0 0.5E-15
*TRANSISTOR
NODE 4
1.5 12.6 95 0.333 1.25E-6
0.11E-3 0.808 100 0.834E-12
1.0 0.1E-12 1.06E-6 500
0.5E6 0.1E-12 0.1E-12
*TRANSISTOR
NODE 8
1.5 12.6 95 0.333 1.25E-6
0.11E-3 0.807 100 0.834E-12
1.0 0.1E-12 1.06E-6 500
0.5E6 0.1E-12 0.1E-12
*LINEAR DEPENDENT SOURCE
NODE 6 10 0 12
VC 9.6E-6 0.0
*LINEAR DEPENDENT SOURCE
NODE 16 0 12 0
VC 0.79E-11 0.0
*LINEAR DEPENDENT SOURCE
NODE 12 0 0 13
VC 182.4 0.0
*END CIRCUIT
*END

```

† For ease of adding and eliminating substrate capacitances in NCAP runs, a 0 pF capacitance is represented by a reduction of three orders of magnitude.

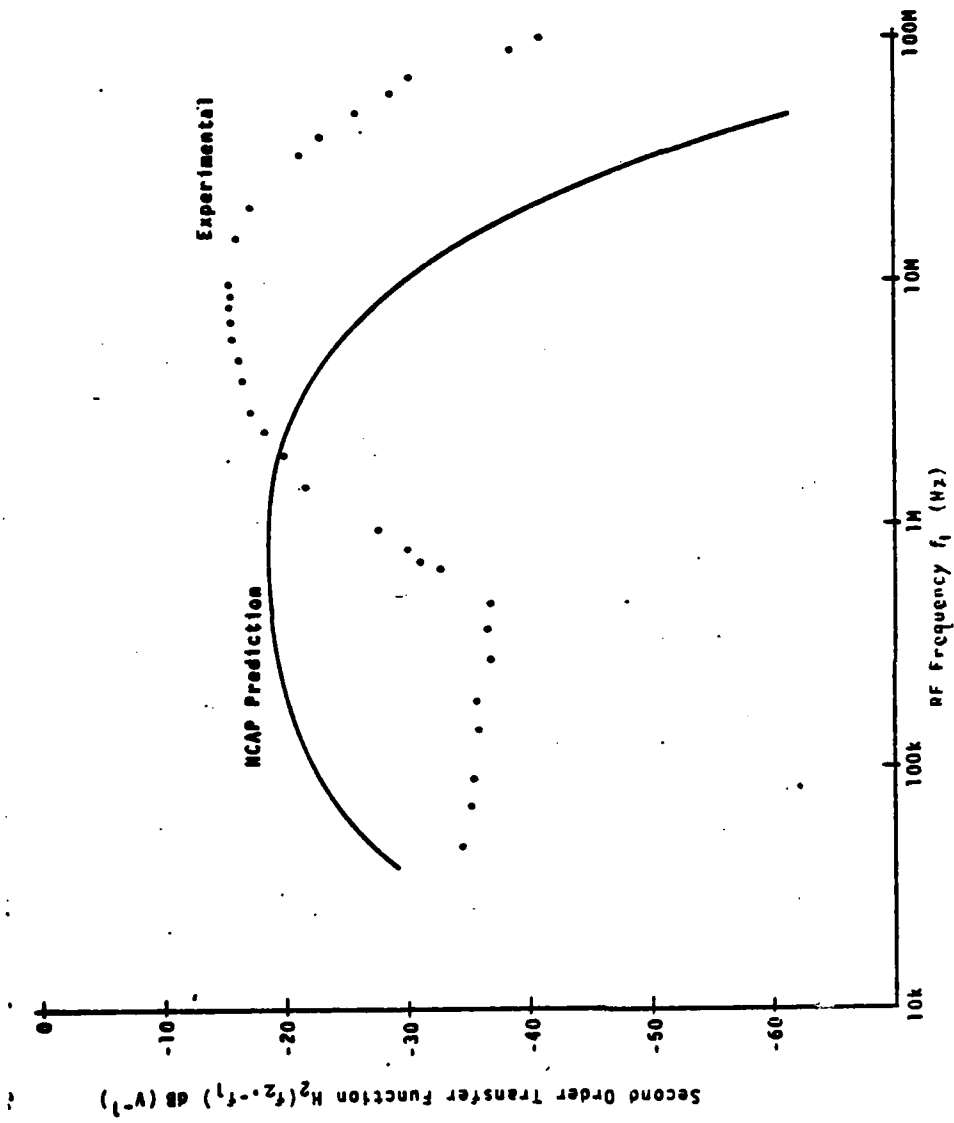


Figure 3-6. Comparison of Experimental Results and NCAP Predictions Made Using the LM10 Op Amp Macromodel in a Buffer Amplifier Configuration. Substrate Capacitance Effects are Not Accounted For.

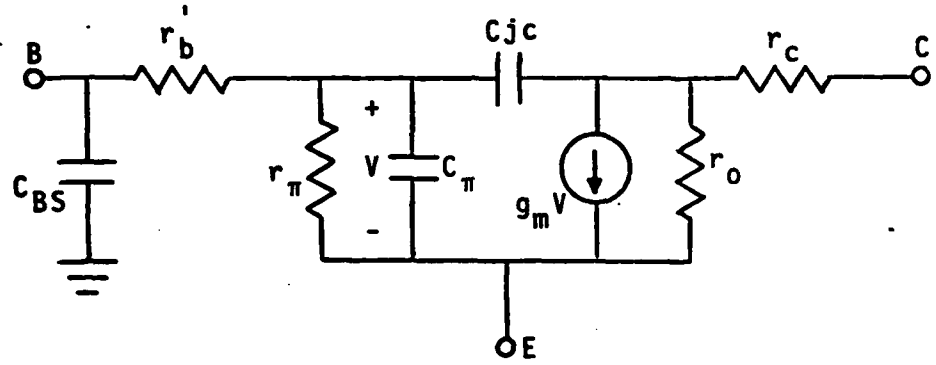


Figure 3-7. Small-Signal Equivalent Circuit of the Lateral PNP Transistor with Base-Substrate Capacitance C_{BS} . [24]

ment of the substrate capacitance from base to ground as shown in Figure 3-7, the second order transfer function fitting procedure outlined in Section 3.1 requires that an emitter to ground substrate capacitance be used. That this substrate capacitance location does not correspond to a physical location in the LM10 Op Amp implies that the emitter substrate capacitance is an equivalent parameter. The second order transfer function $H_2(f_2, -f_1)$ is very sensitive to any change in this capacitance, as illustrated in Figure 3-8. On the other hand a non-zero base-substrate capacitance C_{BS} which has more physical significance reduces the accuracy of the nonlinear macromodel predictions as illustrated in Figure 3-9. This apparent contradiction may be a result of simulating the many distributed substrate parasitic capacitances^[58] with a few discrete capacitors placed at the input transistor terminals.

The final choice for the LM10 nonlinear macromodel substrate capacitances obtained by comparing NCAP predicted and experimental values for the second order transfer function $H_2(f_2, -f_1)$ are $C_{BS} = 0$ pF, $C_{CS} = 0$ pF and $C_{ES} = 0.5$ pF. The NCAP calculated values for the first order transfer function $H_1(f)$ for the LM10 unity gain buffer amplifier are compared to experimental results in Figure 3-10. The NCAP predictions and experimental results for the second order transfer function $H_2(f_2, -f_1)$ are shown in Figure 3-11.

As shown in Figure 3-11 by properly adjusting the macromodel substrate capacitance values excellent agreement has been obtained between

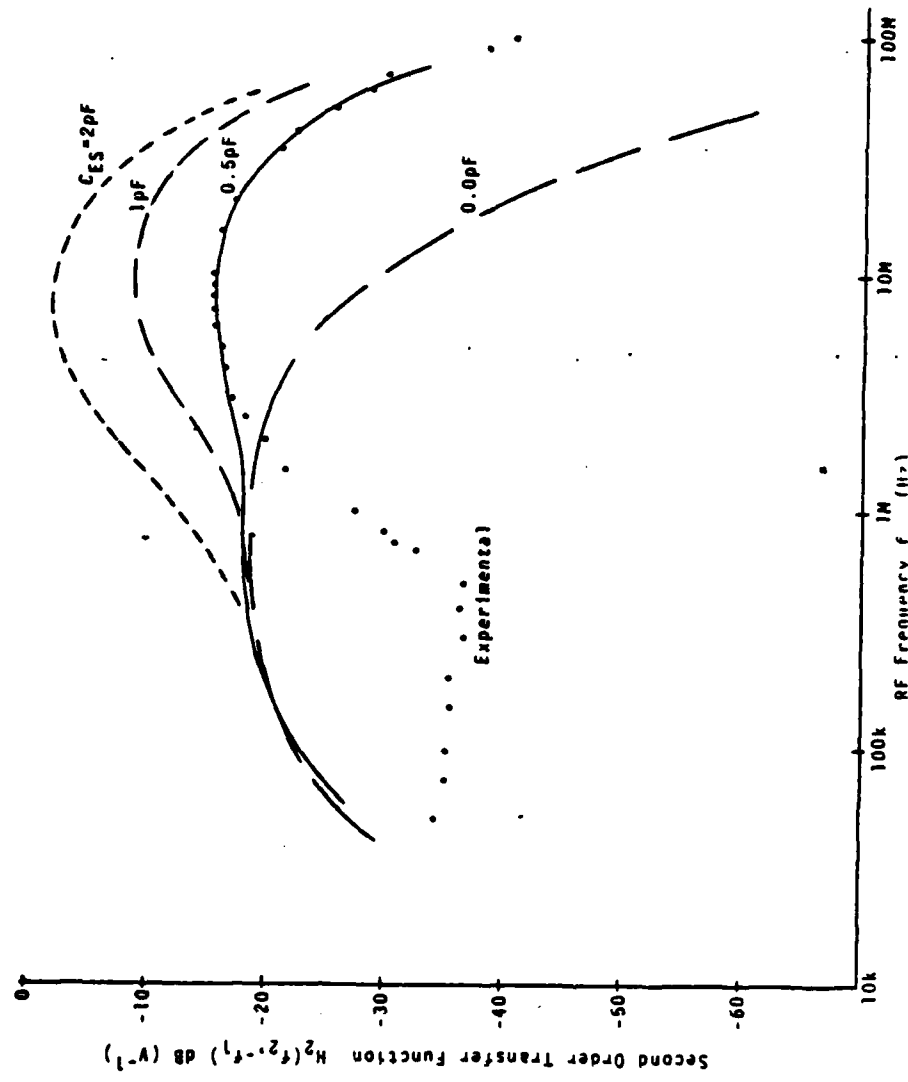


Figure 3-8. Effect of Emitter to Substrate Capacitance on the Second Order Nonlinear Transfer Function of the LM10 Voltage Follower. The NCAP Predictions Are Made Using the LM10 Macromodel. The Collector to Substrate and Base to Substrate Capacitances Are Both Zero.

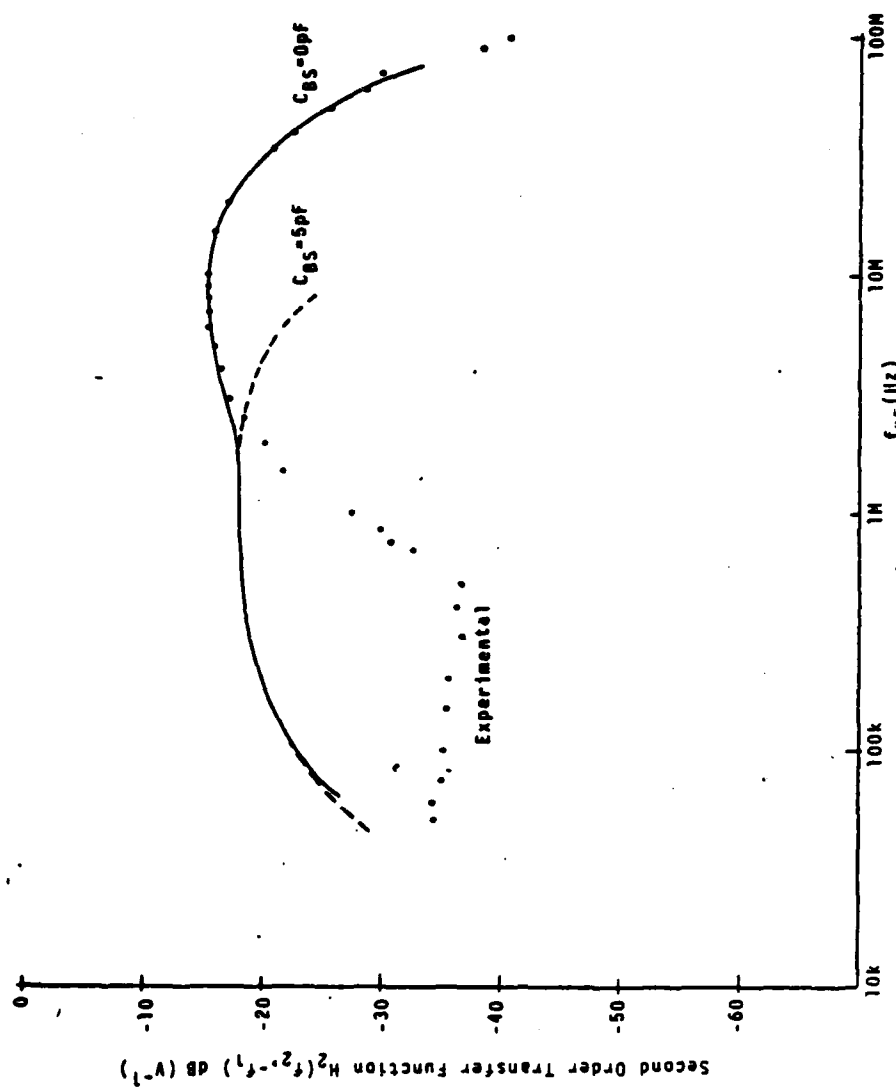


Figure 3-9. Effect of Base to Substrate Capacitance on the Second Order Nonlinear Transfer Function of the LM10 Voltage Follower. The NCAP Predictions are Made Using the LM10 Macromodel. The Emitter to Substrate Capacitance is 0.5pF. The Collector to Substrate Capacitance is 0.0pF.

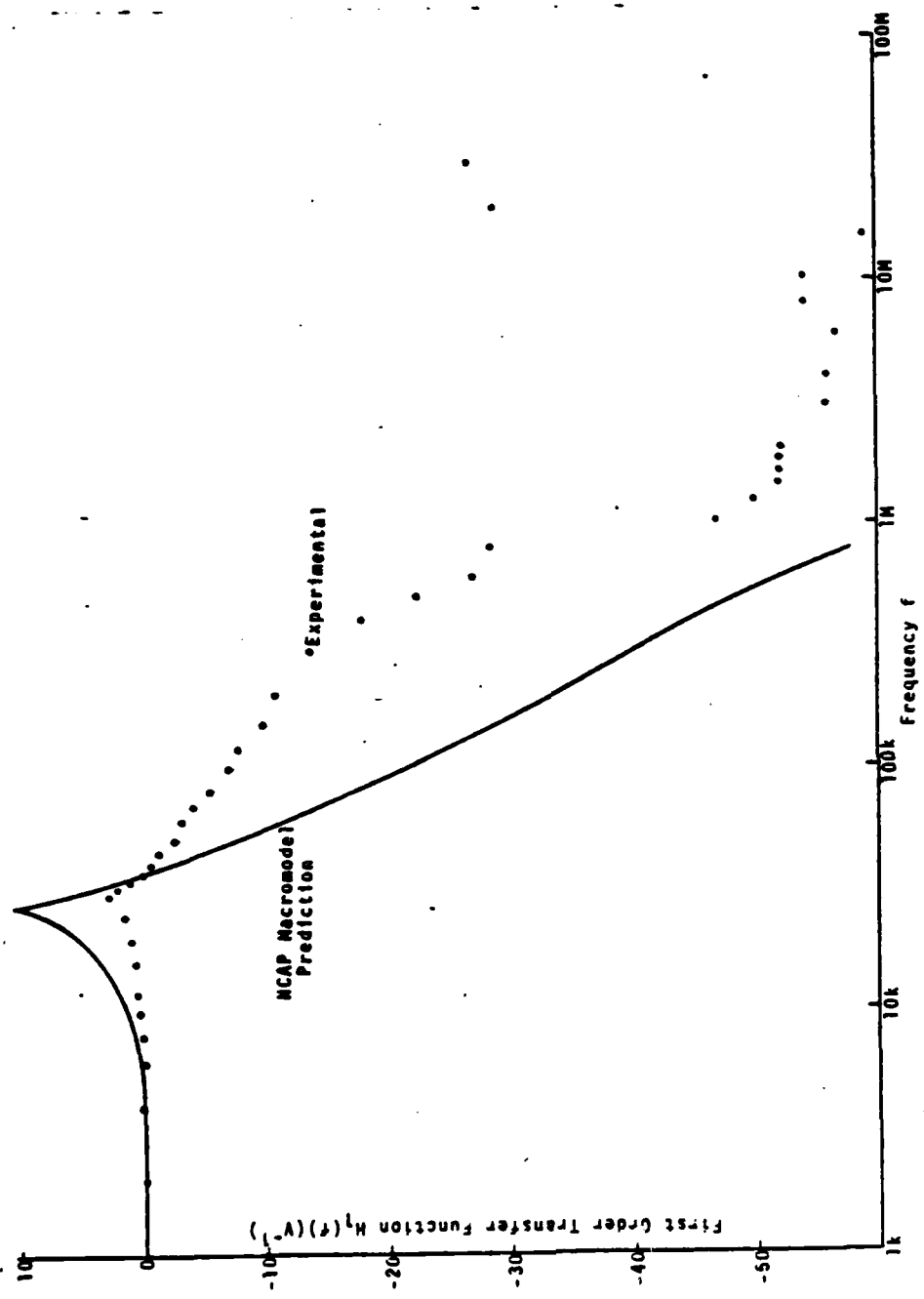


Figure 3-10. NCAP Macromodel Prediction and Experimental Results for the First Order Transfer Function of LM10 Buffer Amplifier.

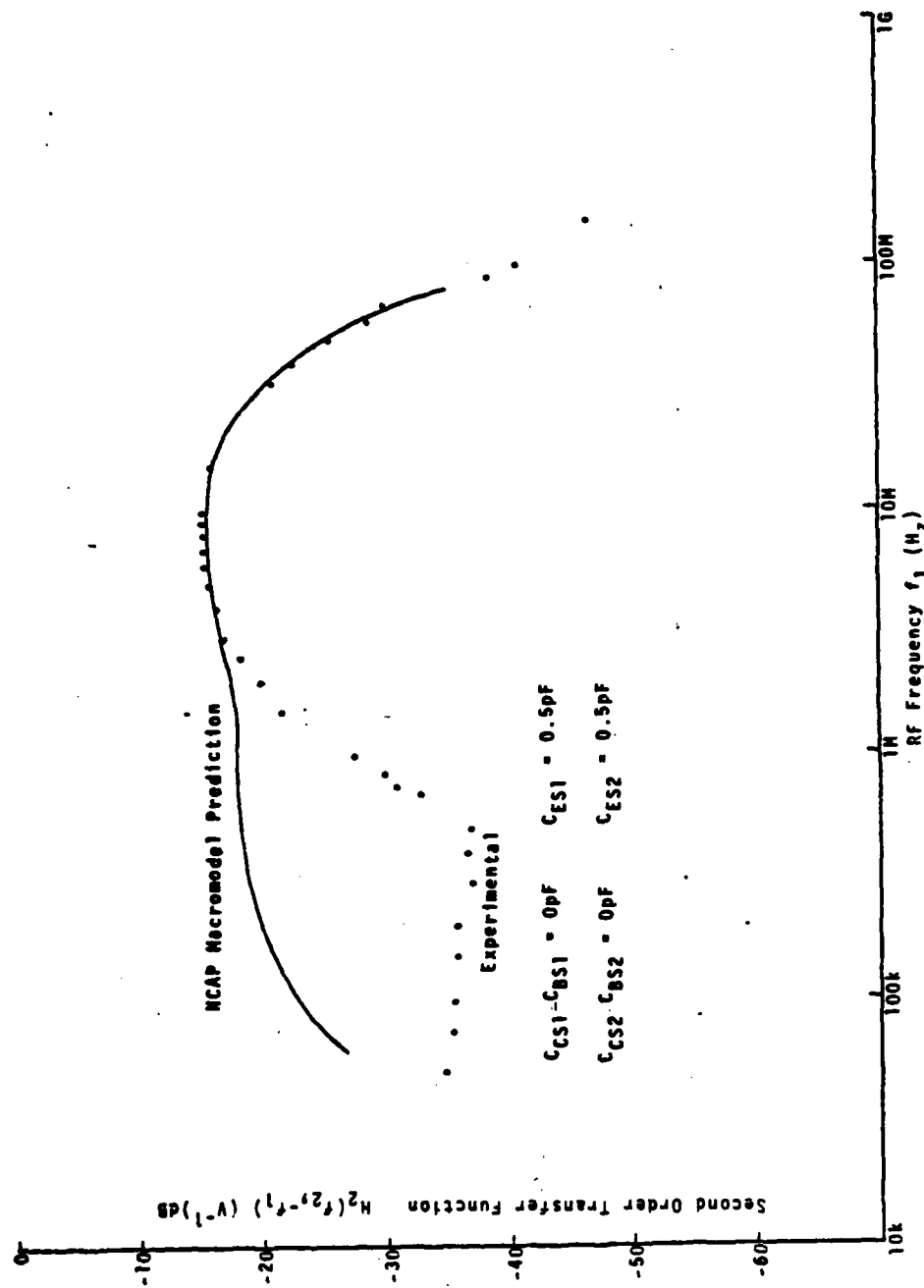


Figure 3-11. NCAP Macromodel Prediction and Experimental Results for the Second Order Transfer Function of LM10 Buffer Amplifier.

NCAP predicted values and experimental values for $H_2(f_2, -f_1)$ for frequencies above 3 MHz. For frequencies below 1 MHz the predicted values exceed the measured values by as much as 18 dB (at 300 kHz). Much of the difficulty in achieving good agreement at frequencies less than 1 MHz may be a result of the low $H_2(f_2, -f_1)$ values (-35 dB) measured below 1 MHz. A similar difficulty was encountered using a full model for the μ A741 Op Amp. (See Figure 1-11.)

It is interesting to compare μ A741 and LM10 Op Amp experimental values for $H_2(f_2, -f_1)$. As shown in Figure 3-12 at frequencies above 1 MHz the $H_2(f_2, -f_1)$ experimental values for the LM10 Op Amp are at least 15 dB below those for the μ A741 Op Amp. This means that the LM10 Op Amp is less susceptible to EMI at frequencies above 1 MHz than the μ A741 Op Amp. The lower LM10 Op Amp susceptibility to EMI above 1 MHz manifests itself in the lower C_{sub} values used in the LM10 Op Amp macromodel. Lowering the C_{sub} values lowers the predicted $H_2(f_2, -f_1)$ values.

The reason for the lower LM10 Op Amp susceptibility to EMI may be its total compensation capacitance value of 1,000 pF. [58] This large capacitance is achieved by the use of emitter isolation junction capacitances of 1 pF/mil². Also the intermediate stage has a phase compensation capacitance of 100 pF (C1 of Figure 3-3) and an overall compensation capacitance from the output to the positive input transistor of 22 pF, (C2 of Figure 3-3). By performing a full-model NCAP

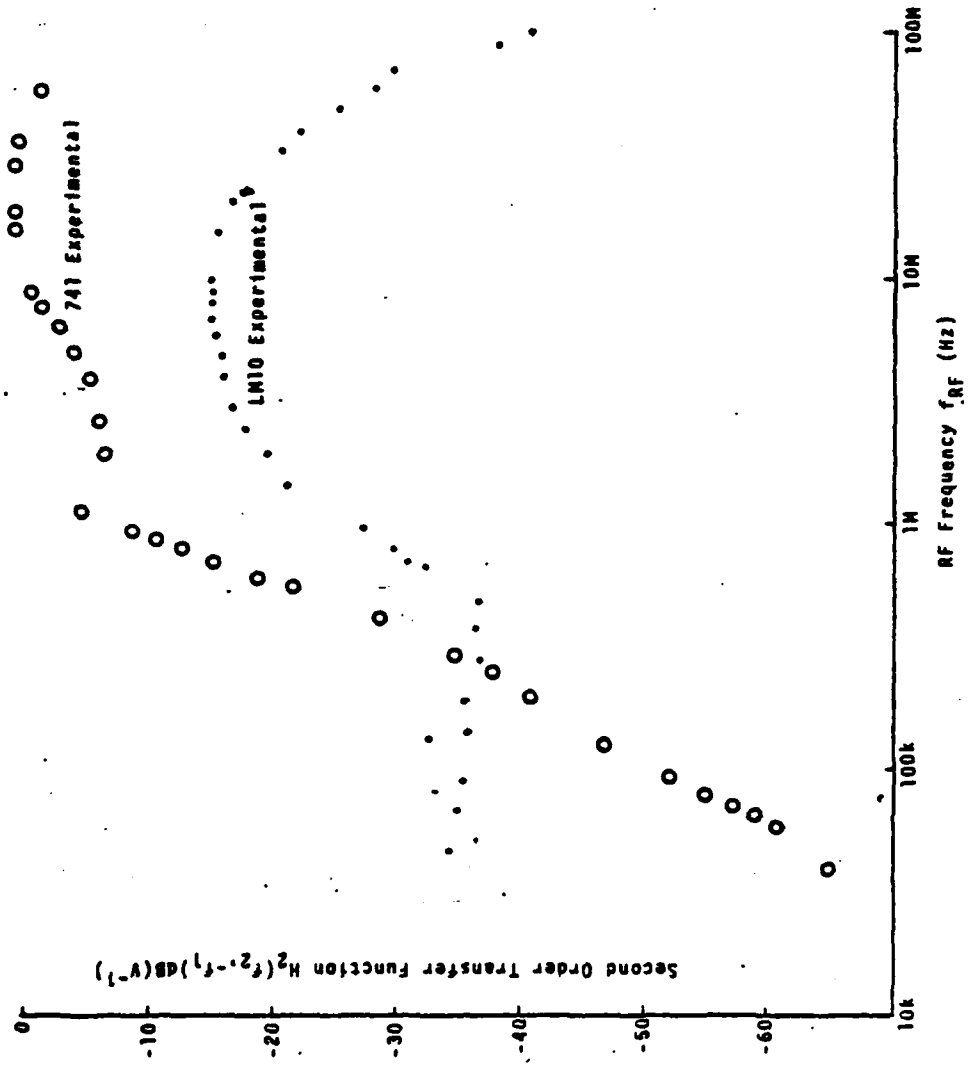


Figure 3-12. Experimental Values for the Second Order Transfer Function $H_2(f_2, -f_1)$ vs Frequency for the 741 and LM10 Op Amps.

analysis of the LM10 Op Amp, it would be possible to do a parameter sensitivity analysis to determine the importance of the various capacitors in the LM10 Op Amp. This has not been attempted because the goal of the present effort is not to evaluate Op Amp full models but to evaluate Op Amp macromodels. The ability of the Op Amp macromodel to account for EMI in the fairly complex integrated LM10 Op Amp without resorting to a full model analysis is the important point.

CHAPTER FOUR

NETWORK THEORY FOR THE NONLINEAR MACROMODEL

In the two previous chapters, it has been demonstrated that a nonlinear small-signal Op Amp macromodel which contains only two BJTs is effective and accurate for EMI analysis. Furthermore, it is believed that the nonlinear macromodel shown in Figure 2-2 is global and can be applied to all bipolar Op Amps of present technology and design. An actual bipolar Op Amp, such as the one illustrated in Figure 1-8, is of course made of many identifiable (and some unidentifiable) components. All the BJTs in the Op Amp have nonlinear parameter values which are comparable, as shown by the work of Fang. [18] How then is it that the RFI contributions of the large number of nonlinear components in the Op Amp can be represented by just two nonlinear transistors in the macromodel? This question is addressed in the present chapter.

4.1 Cascade Configuration for the IC Operational Amplifier

A common IC Op Amp design is the three stage configuration utilized in the μ A741. [42] This configuration consists of an input stage, an intermediate gain stage with compensation, and a unity gain output stage. For small-signal analysis purposes, the IC schematic diagram can be simplified to that of Figure 4-1. A small-signal linear equivalent circuit shown in Figure 4-2 illustrates the three stage cascade more clearly.

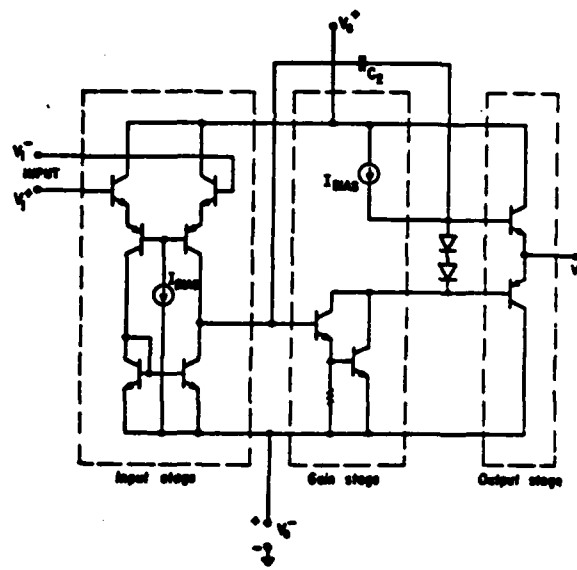


Figure 4-1. 741 Op Amp Simplified Schematic Diagram.⁴²

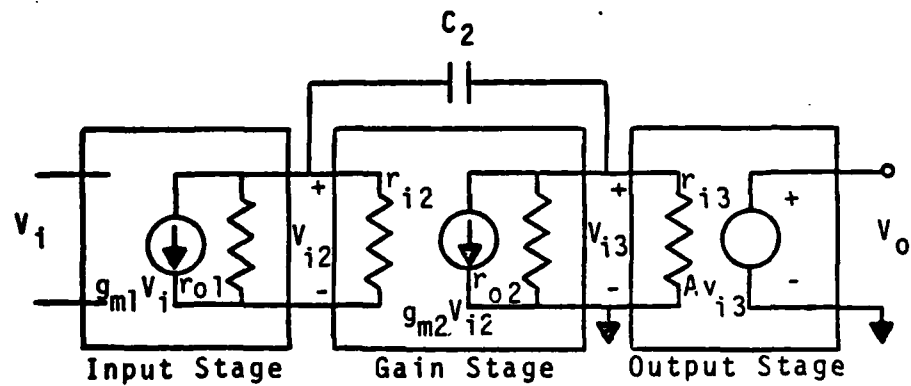


Figure 4-2. Small-Signal Equivalent Circuit of the IC Op Amp.

For small-signal nonlinear analysis, each section in Figure 4-2 is replaced by an appropriate small-signal nonlinear representation. One such representation is shown in Figure 4-3 in which $A_1(f)$ is the first order, or linear, transfer function, $A_2(f_1, f_2)$ is the second order transfer function and $A_3(f_1, f_2, f_3)$ is the third order transfer function. When needed, higher order transfer functions can also be included. The summing node indicates that all transfer functions operate on the input signal frequency spectrum $U(f)$ to produce the total output response spectrum $V(f)$.

A condensed block diagram for the Op Amp three stages is shown in Figure 4-4(a) as a three-stage cascade*. The three-stage cascade can be viewed as two two-stage cascades as illustrated in Figures 4-4(b) and (c). Therefore only the cascading relationship for two stages need be considered. The block diagram shown in Figure 4-3 can be substituted into each stage of the two-stage cascade shown in Figure 4-4(b) to obtain the block diagram shown in Figure 4-5. The two-stage cascade shown in Figure 4-5 has transfer functions $D_1(f_1)$, $D_2(f_1, f_2)$, and $D_3(f_1, f_2, f_3)$ which can be written in terms of the single-stage transfer functions using the cascade relationships given by Weiner and Spina**.

* This first order approximation of the 2-port cascading system assumes the loading effect of the stages to be negligible. [64]

** A derivation of the cascade relationships according to Weiner and Spina is given in Chapter 4 of Reference 15.

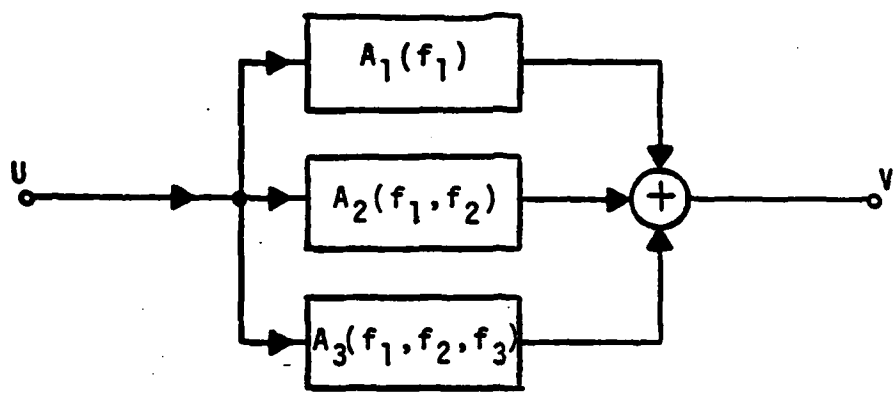


Figure 4-3. Small-Signal Nonlinear Transfer Function Representation of an Amplifier Stage.

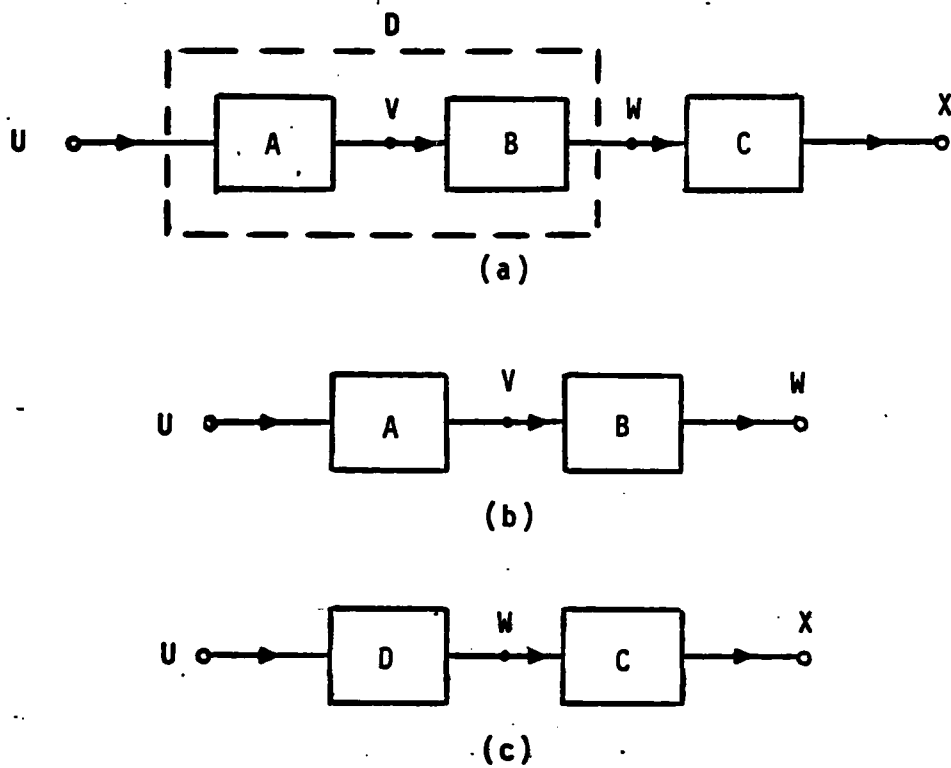


Figure 4-4. Diagrammatic Representation of Cascaded Stages Making Up an Op Amp.

- (a) Three-Stage Representation of the Op Amp Equivalent Circuit.
- (b) Two-Stage Cascade for Transfer Function Derivation.
- (c) Conversion of the Three-Stage System into a Two-Stage System.

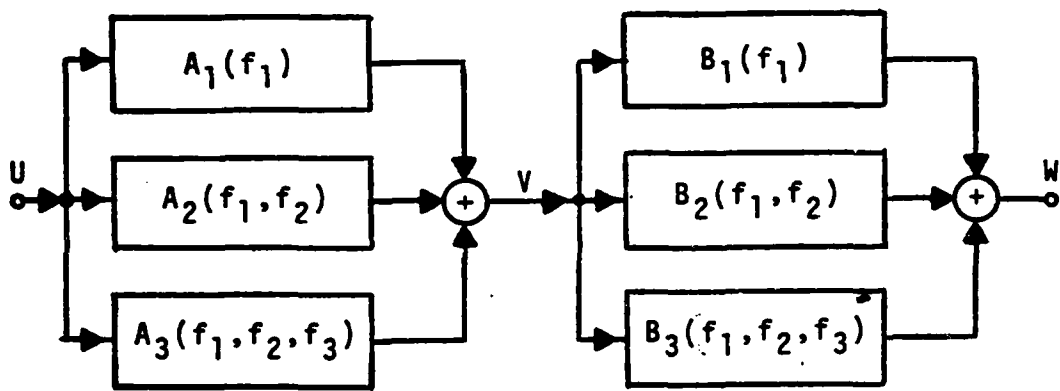


Figure 4-5. A Two-Stage Cascade Nonlinear Transfer Function Representation.

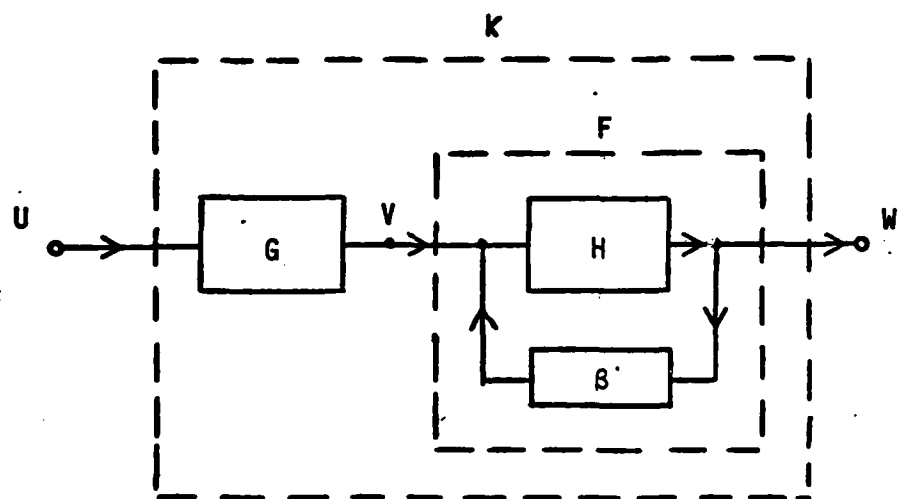


Figure 4-6. Block Diagram Illustrating Nonlinear Transfer Functions of Op Amp Input Stage and Second Stage Cascade With Feedback in the Second Stage.

The results are:

$$D_1(f_1) = B_1(f_1)A_1(f_1) \quad (4-1)$$

$$D_2(f_1, f_2) = B_1(f_1 + f_2)A_2(f_1, f_2) + B_2(f_1, f_2) \overline{\sum_{i=1}^2 A_i(f_i)} \quad (4-2)$$

$$D_3(f_1, f_2, f_3) = B_1(f_1 + f_2 + f_3)A_3(f_1, f_2, f_3) + \overline{2B_2(f_1, f_2 + f_3)A_1(f_1)A_2(f_2, f_3)} + B_3(f_1, f_2, f_3) \overline{\sum_{i=1}^3 A_i(f_i)} \quad (4-3)^*$$

Consider the second order transfer function of two cascaded stages which each have comparable nonlinearities. Equation (4-2) implies that the contributions of both the first and the second stage to the two-stage cascade second order transfer function need to be considered. Similarly, Equation (4-3) implies that the contributions of each stage to the two-stage cascade third order transfer function need to be considered. This observation is supported by the experiments of Narayanan^[7] and Weiner and Spina^[15] involving discrete BJT cascades. However, the feedback internal to the IC Op Amp strongly affects the two-stage cascade second order transfer function $D_2(f_1, f_2)$ when the sum frequency $f_1 + f_2$ is low enough. This point will be discussed in the next section.

* See Reference 15, Chapter 4 for the procedure of averaging which makes up the overbar term in Equation 4-3.

4.2 The Effect of Internal Feedback on A Cascade Nonlinear Transfer Function

The internal feedback capacitor C_2 shown in the small-signal equivalent circuit of Figure 4-2 has a major effect at RF frequencies. To emphasize the important role played by the internal feedback capacitor C_2 the input-stage-gain-stage cascade for the Op Amp is drawn as shown in the block diagram of Figure 4-6, where G represents the input stage transfer functions, H represents the gain stage transfer functions, and β represents the feedback of the internal compensation capacitor C_2 . Employing Narayanan's algorithm (see Equations 8 and 11 of Reference 8), the first order transfer function $F_1(f)$ of the second stage with the linear feedback β is:

$$F_1(f) = \frac{H_1(f)}{1 + \beta(f)H_1(f)} \quad (4-4)$$

and the second order transfer function $F_2(f_1, f_2)$ of the second stage with the feedback is:

$$F_2(f_1, f_2) = \frac{H_2(f_1, f_2) \prod_{i=1}^2 [1 - \beta(f_i)F_1(f_i)]}{1 + \beta(f_1 + f_2)H_1(f_1 + f_2)} \quad (4-5)$$

Substituting Equation (4-4) into Equation (4-5) leads to the result

$$F_2(f_1, f_2) = \frac{H_2(f_1, f_2)}{[1 + H_1(f_1)\beta(f_1)][1 + H_1(f_2)\beta(f_2)][1 + H_1(f_1 + f_2)\beta(f_1 + f_2)]} \quad (4-6)$$

Note that Equation (4-6) for the second order transfer function $F_2(f_1, f_2)$ has been written in terms of the first order transfer function $H_1(f)$.

The gain stage of the μ A741 Op Amp which is now considered as a specific case has the small-signal equivalent circuit shown in Figure 4-7. The feedback factor β is given by

$$\beta = 1/[1 - j/2\pi fRC_2]. \quad (4-7)$$

For $R = 100 \text{ k}\Omega$ and $C_2 = 30 \text{ pF}$, Equation (4-7) can be written as

$$\beta = 1/[1 - j \cdot 05/f(\text{MHz})] \quad (4-8)$$

since the cutoff frequency $1/2\pi RC_2 \approx .05 \text{ MHz}$. The feedback factor β has a magnitude 0.008 at 400 Hz, 0.7 at 0.050 MHz and 1.0 at frequencies greater than 0.2 MHz. Typical values for the open-loop second-stage first order voltage gain $H_1(f)$ are estimated to be 30,000 at 400 Hz, 250 at .050 MHz and less than 0.1 at 9 MHz. The denominator of Equation (4-6) varies over a wide range of values. Let us consider the specific case corresponding to the demodulation of AM modulated RF signals by the second stage. The frequency $f_1 + f_2$ is kept constant at 400 Hz. The frequency f_2 is varied over the range .05 to 100 MHz. The frequency f_1 is negative and must track the frequency f_2 so that the condition $f_1 + f_2 = 400 \text{ Hz}$ is satisfied. The factor $[1 + H_1(f_1+f_2)\beta(f_1+f_2)]$ has a value given by

$$[1 + H_1(f_1+f_2)\beta(f_1+f_2)] = [1 + (30,000)(0.008)] = 240 \quad (4-9)$$

which does not vary as the frequency f_2 is varied because $f_1 + f_2$ is kept constant at 400 Hz. At a low RF frequency such as $f_2 = .050 \text{ MHz}$,

RD-A141 369

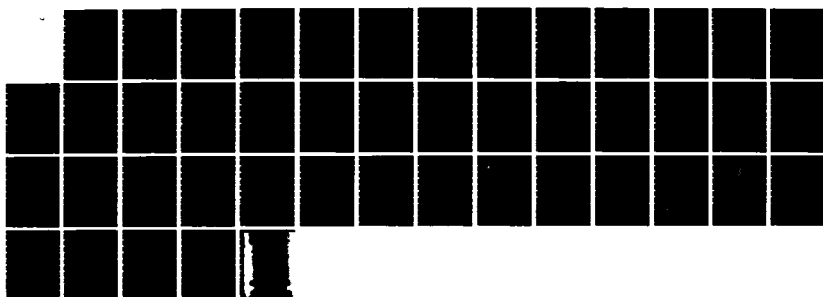
BASIC EMC (ELECTROMAGNETIC COMPATIBILITY) TECHNOLOGY
ADVANCEMENT FOR C3 S. (U) SOUTHERN CENTER FOR
ELECTRICAL ENGINEERING EDUCATION INC S.

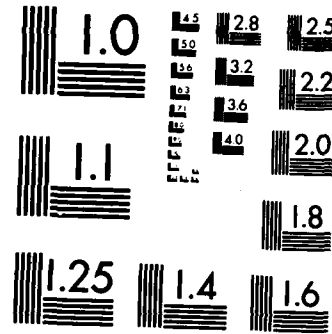
2/2

UNCLASSIFIED

G K CHEN ET AL. DEC 83 RADC-TR-82-286-VOL-1 F/G 9/5

NL





MICROCOPY RESOLUTION TEST CHART
NATIONAL BUREAU OF STANDARDS-1963-A

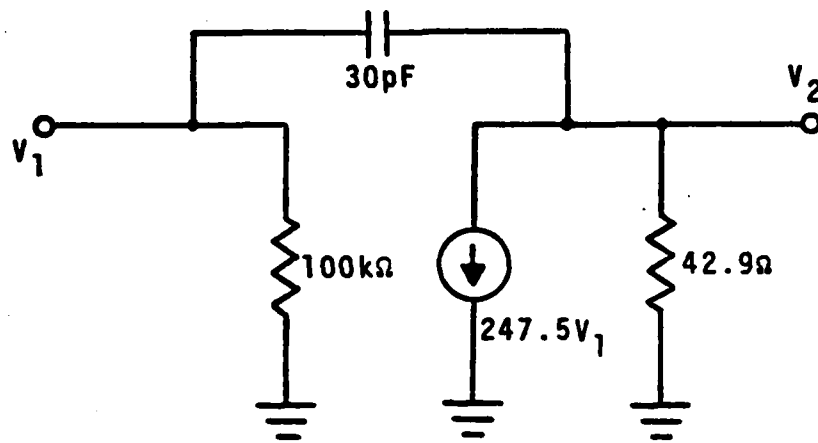


Figure 4-7. The Small-Signal Equivalent Circuit of the Gain Stage of the 741 IC Op Amp.

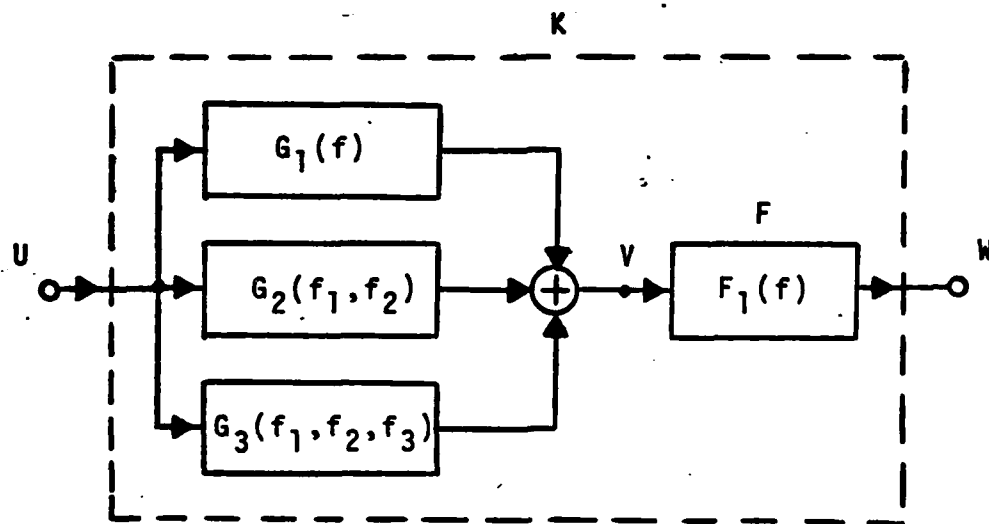


Figure 4-8. The Nonlinear Cascaded Transfer Function of Figure 4-6 with Second and Higher Orders of the Second-Stage Neglected.

the factors $[1 + H_1(f_1)\beta(f_1)]$ and $[1 + H_1(f_2)\beta(f_2)]$ are of the order $[1 + (250)(0.7)] \approx 200$ and the denominator of Equation (4-6) is of the order of $(200)(200)(250) \approx 10^7$. Clearly at an RF frequency $f_2 = 0.050$ MHz the second-stage second order transfer function $F_2(f_1, f_2)$ is reduced essentially to zero by the feedback internal to that stage. For an RF frequency f_2 above 1 MHz, the factors $[1 + H_1(f_1)\beta(f_1)]$ and $[1 + H_1(f_2)\beta(f_2)]$ have a value near unity and the denominator of Equation (4-6) has a constant value 240 given by Equation (4-9). For an RF frequency $f_2 > 1$ MHz, the open-loop second-stage second order transfer function $H_2(f_1, f_2)$ is reduced by a factor 240 by the feedback internal to that stage. Thus the contribution of the second-stage to the Op Amp total second-order transfer function is suppressed significantly by the internal feedback capacitor C_2 of that stage. This suggests (but does not prove absolutely) that the nonlinear effects associated with the second stage can be neglected. It is believed that similar analysis would show that the third order transfer function $F_3(f_1, f_2, f_3)$ of the second stage is also reduced by the internal feedback capacitor C_2 . Thus it seems reasonable to simplify the Op Amp first-stage and second-stage cascade representation from that shown in Figures 4-5 and 4-6 to that shown in Figure 4-8. In Figure 4-8 the second-stage second and third order transfer functions are omitted.

Now the Op Amp output stage needs to be considered. As shown in Figure 4-1, the output stage is a unity gain stage consisting of com-

plementary emitter followers. Emitter followers may be viewed as feedback amplifiers having internal unity feedback and a high loop gain which causes the closed-loop gain to be one. The analysis and arguments presented for the second stage with its internal feedback should apply completely to the output stage with its internal feedback. Thus the output stage second and third order transfer functions can be ignored, and the output stage can be represented by a linear gain stage.

A numerical evaluation of the second-stage and third-stage contributions to the Op Amp second order transfer function could be carried out by using a complete Op Amp model NCAP analysis. The first and second order transfer function for the input stage, the gain stage with $C_2 = 0$ and $C_2 = 30 \text{ pF}$, and output stage could be determined separately. Then the cascade relationship expressed by Equation (4-2) could be used to determine how important the second-stage contribution is relative to the first-stage contribution. A similar expression to Equation (4-2) could also be used to compare the third-stage contribution relative to the combined input-stage gain-stage contribution. To date such a numerical evaluation has not been performed. The estimates made using analytical expressions provide the sole basis for claiming that the Op Amp overall nonlinearity can be represented by the nonlinearity of the input stage alone and that the gain stage and the output stages can be represented by linear transfer functions. It now remains to be shown that the input stage nonlinearity can be adequately modeled by two transistors.

4.3 Nonlinear Modeling of the Input Stage.

The input stage of the 741 is repeated in Figure 4-9. It is seen that some 12 BJTs are involved each having nonlinearities of comparable value. The fact that the first stage can be effectively modeled with a differential pair of transistors in common-emitter (CE) configuration will now be discussed.

The operation of an IC Op Amp such as the μ A741 has been treated in a number of references. [50,51,52] The transistors Q8 through Q12 are used for dc biasing. In a small-signal equivalent circuit, they can be represented by linear resistors. The transistors Q1 through Q7 are involved in active small-signal processing, and therefore contribute to the nonlinear transfer functions. The small-signal equivalent circuit is a differential amplifier. Each branch of the differential pair is a composite BJT amplifier. On the positive input side the transistors Q1 and Q3 form a common-collector (CC) to common-base (CB) cascode. The transistors Q5 and Q7 form the active load for this cascode amplifier. Similarly the transistors Q2 and Q4 form a CC to CB cascode with transistor Q6 the active load. For the purpose of nonlinear small signal modeling, only the cascode amplifiers need be considered. Modeling the BJTs with the nonlinear T-model of Figure 1-2, the cascode amplifier formed by transistors Q1 and Q3 or by the transistors Q2 and Q4

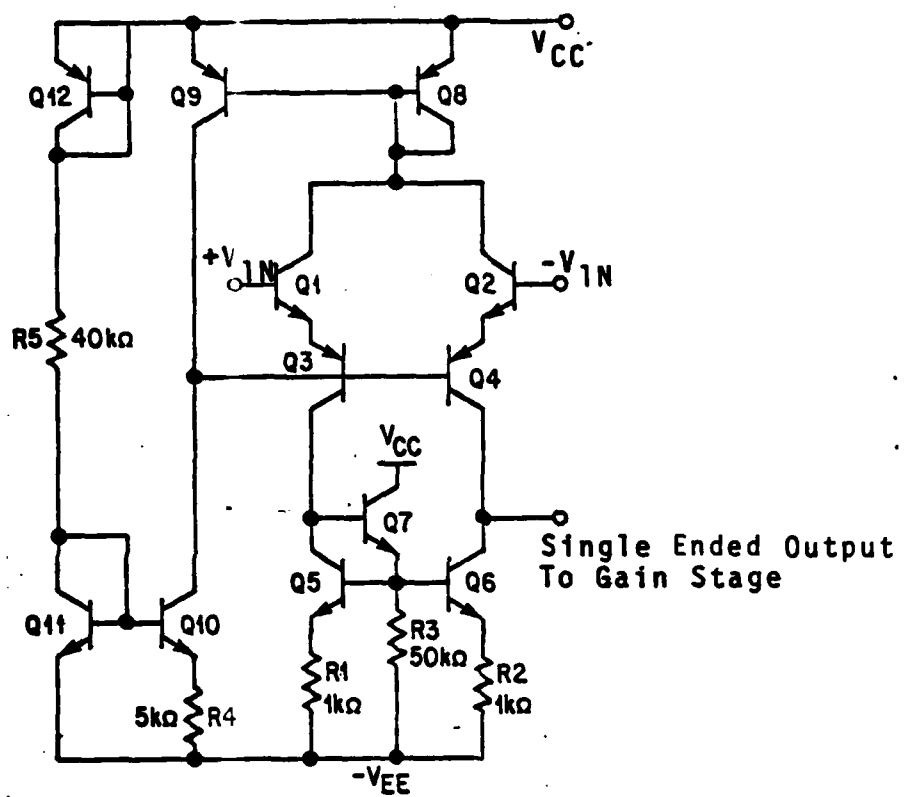


Figure 4-9. Full Model of the 741 Input Stage.

is represented by the small-signal nonlinear equivalent circuit of Figure 4-10. An examination of this circuit shows that a three-terminal representation of the cascode is possible. With terminal C3 being the composite collector, C1 the emitter and B1 the base, a common-emitter stage results for each cascode pair. Thus the input stage of the IC Op Amp can be represented by a differential amplifier formed by two CE stages. Note that for the cascode pair shown in Figure 4-10, Kirchhoff's Law applied to node E1(E3) yields

$$k_1(V_2 - V_3) + \gamma_{e1}(V_2 - V_3) = k_3(V_4 - V_3) + \gamma_{e3}(V_4 - V_3) \quad (4-10)$$

For the purpose of converting the CC - CB cascode shown in Figure 4-10 to a single CE amplifier, it is not necessary to solve Equation (4-10). Instead, the cascading relationship of Equation (4-2) can be applied. It may be noted that the first order gain of the CC stage is unity. The first order gain of the CB stage is much greater than unity. It also was reported that the CB connected transistor has a second order transfer function considerably lower than that of the CC connected BJT.^[7,12] Therefore, in applying Equation (4-2) to Figure 4-10, we have B_1 high and A_1 low and $B_2(f_1, f_2) < A_2(f_1, f_2)$. Equation 4-2 then can be written as

$$D_2(f_1, f_2) \approx B_1(f_1 + f_2) A_2(f_1, f_2) \quad (4-11)$$

which may be viewed as second order transfer function of a single stage amplifier.

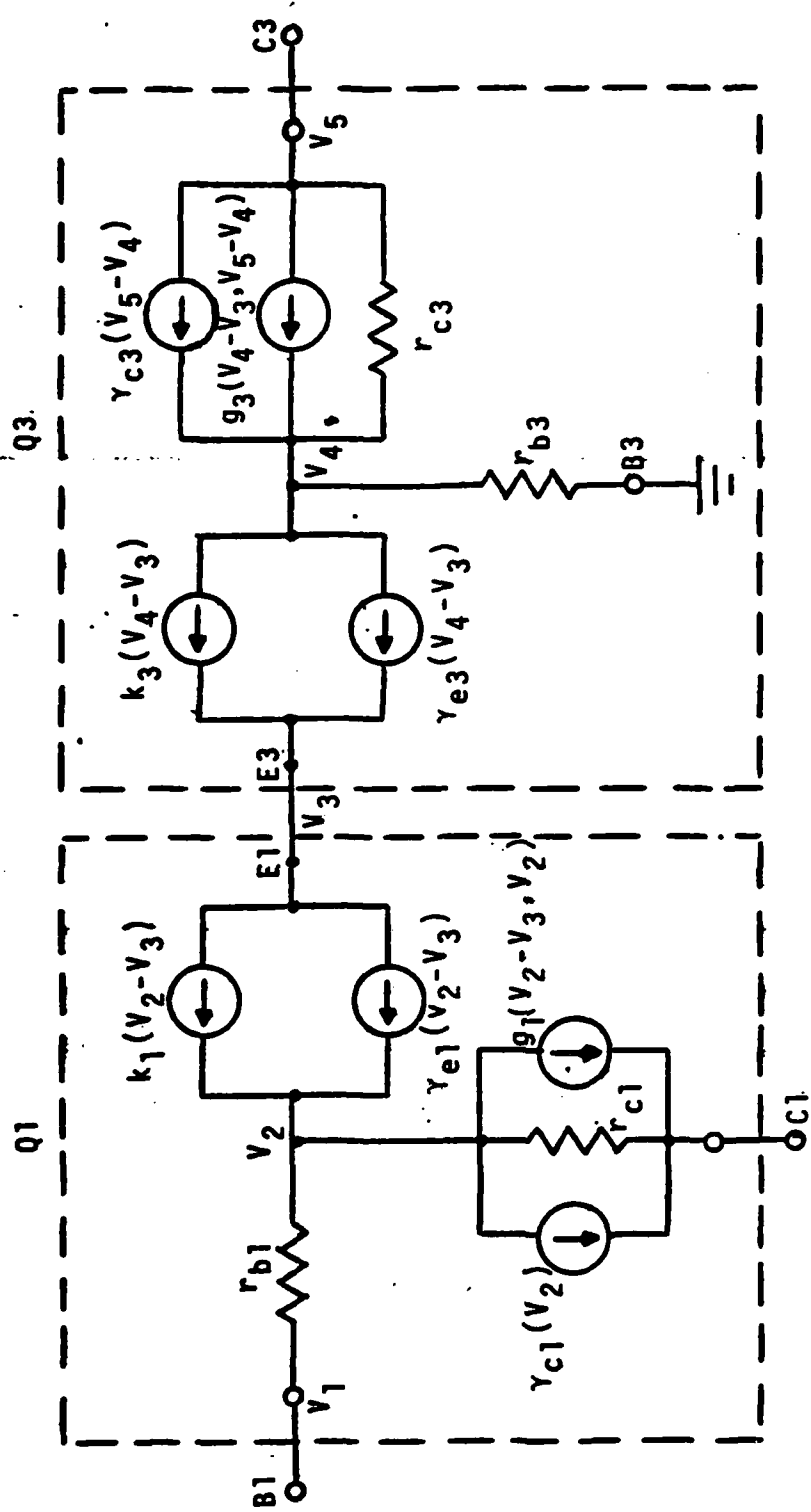


Figure 4-10. Nonlinear Equivalent Circuit for the CC-CB Cascode Formed by the Transistor Pair Q1-Q3 (or Q2-Q4).

In summary, it has been argued effectively in this chapter that the three-stage amplifier design that makes up the 741 type of IC Op-Amp has its overall nonlinear transfer function dominated by the input stage. The gain stage and output stage that follow can be represented by a linear transfer function. In the input stage, the nonlinear transfer function of CC-CB cascode with active load can be represented by a single CE stage. These arguments provide considerable justification that the nonlinear macromodel of Figure 2-2 can be used for Op-Amp second order transfer function calculations.

CHAPTER FIVE

CONCLUSIONS AND RECOMMENDATIONS

5.1 Conclusions

This dissertation describes a small-signal nonlinear macromodel for the bipolar IC Op Amp which can be used successfully for RFI analysis. Two BJT's are adequate to characterize the complete IC. The small-signal nonlinear macromodel can be obtained directly from the large-signal macromodel developed by Boyle et al. [29]. The effectiveness of the small-signal nonlinear macromodel is verified by the agreement between NCAP predictions and experimental results for the second order transfer function of the 741 Op Amp unity gain buffer amplifier. Good agreement is also obtained between NCAP calculations based on the macromodel and the full model. By using the Op Amp macromodel, a saving of nearly an order of magnitude in computer costs is achieved. Not only does the macromodel conserve computer resources, it makes possible for the EMC engineer to analyse electronic systems involving many Op Amps.

Another important aspect of the small-signal nonlinear macromodel is that it is a global model which can be used for all Op Amp types. The two macromodel transistors should be the same type as those at the input of the IC Op Amp being modeled. The need for laboratory

characterization of the individual transistors in each new bipolar Op Amp appears not to be required. A combination of manufacturer's specifications and Fang's [18] IC BJT results can be used. This was demonstrated by the successful application of the nonlinear macromodel to the new LM10 IC Op Amp for RFI analysis by NCAP, without resorting to full model analysis, nor experimental device characterization.

However, the accuracy of the nonlinear macromodel relies on the inclusion of capacitors to represent the effects of substrate parasitic capacitances. The proper selection of substrate capacitors does not necessarily follow the structural IC parasitic capacitances. The effects caused by these capacitances are simulated by four capacitors in the macromodel. The best values for these capacitors were found by comparing NCAP predicted values with experimental values for a second order transfer function of the Op Amp in an unity gain buffer amplifier. Thus a parametric fitting is involved when a new Op Amp is modeled.

That the combined nonlinearities of tens of BJTs in a linear IC Op Amp can be represented quite well by a pair of BJTs in a macromodel is explained by the cascading theory of nonlinear transfer functions. The essential point appears to be that the second stage (gain-stage) contribution to the Op Amp second order transfer function is reduced greatly by the internal feedback capacitor of the second stage. Also it was argued that the input stage which consists of two cascode stages

in a differential pair arrangement can be represented by two common emitter stages in a differential pair configuration used in the Op Amp macromodel. The validity of the nonlinear macromodel is therefore supported both by experimental verification and by network theory.

5.2 Recommendations

The following topics are suggested for future efforts.

(1) Nonlinear macromodels for FET-Bipolar IC Op Amp

Large-signal macromodels for JFET-Bipolar and MOSFET-Bipolar Op Amps have been achieved recently. [63] A small-signal nonlinear macromodel for the JFET-Bipolar Op Amp can be developed using the NCAP JFET small-signal nonlinear model now available. [61] A small-signal nonlinear macromodel for a MOSFET-Bipolar Op Amp can be developed with a four-terminal MOS transistor nonlinear model which is expected to become available shortly. [62]

(2) Study of the EMI Internal to IC Op Amps

The program NCAP calculates the nonlinear transfer function $H_n(f_1, \dots, f_n)$ by first calculating the circuit admittance matrix $Y(f_1 + \dots + f_n)$ and the n-th order source vector $I_n(f_1, \dots, f_n)$ [61] and solving the equation

$$[Y(f_1 + \dots + f_n)]H_n(f_1, \dots, f_n) = I_n(f_1, \dots, f_n) . \quad (5-1)$$

It may be possible to study the behavior of EMI generation inside an integrated circuit by examining the admittance matrix and

current source vector. [68] An alternate method was suggested in Section 4.2. (See p. 85.)

(3) Op Amp Modeling Below 1 MHz

All efforts to predict EMI in IC Op Amps have not been very accurate at frequencies below 1 MHz. This includes predictions for the second order nonlinear transfer functions using the 741 full model and macromodel and the LM10 macromodel. Part of the problem is a result of the very low EMI observed at RF frequencies below 1 MHz. While EMI at low RF frequencies may be of less practical concern, research into low frequency modeling of EMI in Op Amps may contribute to a better understanding of Op Amp full models and macromodels.

(4) Macromodels For Linear Electronic Systems.

Electronic systems designed to be linear usually contain nonlinear devices such as BJTs and FETs in which EMI effects may occur. These systems often contain a cascade of linear stages and a variety of feedback paths. It would appear that a general nonlinear macromodeling procedure could be developed for such systems. The simplest procedure would be one based upon the approach used by Boyle et al.. The input stages could be modeled in a physical manner; interior gain stages and output stages could be modeled as linear systems. A more systematic approach would be to use the cascading relationships given in Chapter 4, especially when internal feedback is used, to estimate what stages make important

contributions to different nonlinear transfer functions. Stages that can make an important contribution to the nonlinear transfer function of interest should be represented by an appropriate small-signal nonlinear model. Other stages can be represented by small-signal linear models.

(5) Nonlinear Macromodels For Digital IC's.

Macromodeling of digital ICs preceded that for IC Op Amps and is widely used by the semiconductor industry. Unfortunately, the digital IC macromodels developed appear to be proprietary. This may mean that EMC analysts will have to develop their own digital IC macromodels. It is anticipated that small-signal nonlinear macromodels and the computer program NCAP cannot be used to predict EMI in digital ICs. Large-signal macromodels and time domain analysis routines such as the transient analysis routine of SPICE2^[53] will be required.

REFERENCES

1. AKGUN, M. and M. J. O. STRUTT: Cross Modulation and Nonlinear Distortion in RF Transistor Amplifiers, IRE Transactions on Electron Devices, vol. ED-6, pp. 457-467, October 1959.
2. LOTSCH H.: Third-Order Distortion and Cross Modulation in a Grounded Emitter Transistor Amplifier, IRE Transactions on Audio, vol. AU-9, pp. 49-58, March-April 1961.
3. RIVA G. M., P. J. BENETEAU, and E. DALLA VOLTA: Amplitude Distortion in Transistor Amplifiers, Proc. IEE, vol. 111, pp. 481-490, March 1964.
4. REYNOLDS J.: Nonlinear Distortion and Their Cancellation in Transistors, IEEE Transactions on Electron Devices, vol. ED-12, pp. 595-600, November 1965.
5. NARAYANAN S.: Transistor Distortion Analysis Using Volterra Series Representation, Bell System Technical Journal, vol. 46, pp. 991-1024, May-June 1967.
6. THOMAS L. C.: Eliminating Broadband Distortion in Transistor Amplifiers, Bell System Technical Journal, vol. 47, pp. 315-342, March 1968.
7. NARAYANAN S.: Intermodulation Distortion of Cascaded Transistors, IEEE Journal of Solid-State Circuits, vol. SC-4, pp. 97-106, June 1969.
8. NARAYANAN S.: Application of Volterra Series to Intermodulation Distortion Analysis of Transistor Feedback Amplifiers, IEEE Transactions on Circuit Theory, vol. CT-17, pp. 518-527, November 1970.

9. MEYER R. G., M. J. SHENSA and R. ESCHENBACH: Cross Modulation and Intermodulation in Amplifiers at High Frequencies, IEEE Journal of Solid-State Circuits, vol. SC-7, pp. 16-23, February 1972.
10. DROBISH W. E.: Higher Order Models for Computer-Aided Circuit Design, IEEE Journal of Solid-State Circuits, vol. SC-7, pp. 208-211, April 1972.
11. POON H. C.: Modeling of Bipolar Transistor Using Integral Charge Control Model with Application to Third-Order Distortion Studies, IEEE Transactions on Electron Devices, vol. ED-19, pp. 719-731, June 1972.
12. NARAYANAN S. and H. C. POON: An Analysis of Distortion in Bipolar Transistors Using Integral Charge Control Model and Volterra Series, IEEE Transactions on Circuit Theory, vol. CT-20, pp. 341-351, July 1973.
13. EACHUS J.: Distortion in Ultralinear Solid-State Devices, IEEE Journal of Solid-State Circuits, vol. SC-10, pp. 485-497, December 1975.
14. FANG, T. F. and J. J. WHALEN: Application of the Nonlinear Circuit Analysis Program NCAP to Predict RFI Effects in Linear Bipolar Integrated Circuits, Proceedings of the Third Symposium and Technical Exhibition on Electromagnetic Compatibility, pp. 263-268, Rotterdam, The Netherlands, May 1-3, 1979.
15. WEINER, D. D. and J. F. SPINA: "Sinusoidal Analysis and Modeling of Weakly Nonlinear Circuits with Applications to Nonlinear Interference Effects," Van Nostrand Reinhold Co., New York, 1980 (ISBN 0-442-26093-8)
16. TERMAN, F. E.: "Electronic and Radio Engineering," McGraw-Hill, 1955.

17. GRAHAM, J. W. and L. EHRMAN: "Nonlinear System Modeling and Analysis with Application to Communications Receivers," Technical Report RADC-TR-73-178, Rome Air Development Center, Griffiss Air Force Base, New York, June 1973.
18. FANG T. F.: "Nonlinear System Analysis in Bipolar Integrated Circuits," Ph.D. Dissertation, State University of New York at Buffalo, February 1979. Also published as Technical Report RADC-TR-79-324, Rome Air Development Center, Griffiss Air Force Base, NY 13441, January 1980.
19. VALENTE, J. B.: The Nonlinear Circuit Analysis Program, 1977 IEEE International Electromagnetic Compatibility Symposium Record, pp. 461-466, Seattle, Washington, August 2-4, 1977.
20. WHALEN J. J., C. A. PALUDI and T. F. FANG: Application of the Nonlinear Circuit Analysis Program NCAP, 1977 IEEE International Electromagnetic Compatibility Symposium Record, pp. 467-474, Seattle, Washington, August 2-4, 1977.
21. VOLTERRA, V.: "Theory of Functionals and of Integral and Integro-Differential Equations," Dover Publications, New York, 1959.
22. PALUDI C. A. and WHALEN J. J.: The NCAP Nonlinear T Model for Bipolar Junction Transistors at UHF Frequencies, 1979 IEEE International Electromagnetic Compatibility Symposium Record, pp. 96-103, San Diego, California, October 9-11, 1979.
23. "Linear Integrated Circuits Data Book," Fairchild Semiconductor, Mountain View, California, 1976.
24. WOOLEY, B. A., S. Y. J. WONG, and D. O. PEDERSON, A Computer-Aided Evaluation of the 741 Amplifier, IEEE Journal of Solid-State Circuits, vol. SC-6, pp. 357-366, December 1971.
25. BOWERS, J. C.: Terminal Modeling of Linear and Digital Integrated Circuits for CAD Applications, Proc. 15th Midwest Symposium on Circuit Theory, pp. IV.4.1-10, Rolla, Mo. May 1972.

26. NARUD, J. A.: Computer Aided Analysis and Artwork Generation for Integrated Circuits, 1970 IEEE International Convention Digest, pp. 82-83, New York, N.Y., March 1970.
27. KOZEMCHAK, E. B.: Computer Analysis of Digital Integrated Circuits by Macromodeling, IEEE Proceedings of the International Symposium on Circuit Theory, p. 379, North Hollywood, Calif., April 1972.
28. RABBAT, N. B. and H. Y. HSIEH: A Latent Macromodular Approach to Large-Scale Sparse Networks, IEEE Transactions on Circuits and Systems, vol. CAS-23, pp. 745-752, December 1976.
29. BOYLE, G. R., B. M. COHEN, D. O. PEDERSON and J. E. SOLOMON: Macromodeling of Integrated Circuit Operational Amplifiers, IEEE Journal of Solid-State Circuits, vol. SC-9, pp. 353-363, December 1974.
30. TRELEAVEN, D. H., and F. N. TROFIMENKOFF: Modeling Operational Amplifiers for Computer-Aided Circuit Analysis, IEEE Transactions on Circuit Theory, correspondence, vol. CT-18, pp. 206-207, January 1971.
31. TANENHAUS, M. E. and R. L. MARTIN: Linear Integrated Circuit Models and Applications for Computer Aided Circuit and System Analysis and Design, Proc. 8th Asilomar Conference on Circuits, Systems and Computer, Western Periodicals, pp. 339-344, Pacific Grove, Calif., December 1974.
32. GLESNER M. and C. WEISANG: Computer Aided Macromodeling of Integrated Circuit Operational Amplifiers, Proc. IEEE International Symposium on Circuits and Systems, pp. 255-258, Munich, Germany, April 1976.
33. GLESNER M. and C. WEISANG: Computer Aided Macromodeling of Integrated Circuit Operational Amplifiers, Archiv der Elektronik und Uebertragungetechnik, vol. 31, pp. 289-295, 1977.

34. GETREU, I. E., A. D. HADIWIDJAJA and J. M. BRINCH: An Integrated-Circuit Comparator Macromodel, IEEE Journal of Solid-State Circuits, vol. SC-11, pp. 826-833, December 1976.
35. WEIL, P. and L. P. MCNAMEE: A Nonlinear Macromodel for Operational Amplifiers, Proc. 8th Asilomar Conference on Circuits, Systems and Computers, Western Periodicals, pp. 345-350, Pacific Grove, Calif., December 1974.
36. MAJEWSKI, M. L. and E. SANCHEZ-SINENCIO: A Nonlinear Large Signal Macromodel of Operational Amplifiers, Proc. IEEE International Symposium on Circuits and Systems, pp. 364-368, New York, May 1978.
37. SANCHEZ-SINENCIO and M. L. MAJESSKI: A Nonlinear Macromodel of Operational Amplifiers in the Frequency Domain, IEEE Transactions on Circuits and Systems, vol. CAS-26, pp. 395-402, June 1979.
38. RUEHLI, A. E., R. B. RABBAT and H. Y. HSIEH: Macromodelling - An Approach for Analyzing Large-Scale Circuits, Computer Aided Design, vol. 10, pp. 122-129, March 1978.
39. STERN, T. E." Piecewise-Linear Network Analysis and Synthesis, Symposium on Nonlinear Circuit Analysis, Polytechnic Institute of Brooklyn, Symposium Proceedings, vol. VI, pp. 315-345, April 1956.
40. HAJJ, I., K. SINGHAL, J. VLACH and P. BRYANT: WATAND-A Program for the Analysis and Design of Linear and Piecewise-Linear Networks, Proceedings 16th Midwest Symposium on Circuit Theory, pp. VI.4.1-VI.4.9, Waterloo, Ontario, Canada, April 1973.
41. WIDLAR, R. J.: Design Techniques for Monolithic Operational Amplifiers, IEEE Journal of Solid-State Circuits, vol. SC-4, pp. 184-191, August 1969.
42. GRAY, P. R. and R. G. MEYER: Recent Advances in Monolithic Operational Amplifier Design, IEEE Transactions on Circuits and Systems, vol. CAS-21, pp. 317-327, May 1974.

43. ROBERGE, J. K.: "Operational Amplifiers, Theory and Practice," Wiley, New York, 1975.
44. HERBERT, D. B.: Simulate ICs with Black Boxes by Using ECAP Digital Computer Program and Basic Circuit Building Blocks, Electronic Design, vol. 15, pp. 75-79, November 1967.
45. GETREU, I.: "Modeling the Bipolar Transistor," Part No. 062-2841-00, Tektronix, Inc., Beaverton, Oregon 97077, 1976.
46. FANG, T. F., J. J. WHALEN and G. K. C. CHEN, Using NCAP to Predict RFI Effects in Operational Amplifiers, 1979 IEEE International Electromagnetic Compatibility Symposium Record, pp. 96-103, October 9-11, 1979, San Diego, California.
47. SOLOMON, J. E.: The Monolithic Op Amp: A Tutorial Study, IEEE Journal of Solid-State Circuits, vol. SC-9, pp. 314-332, December 1974.
48. SOLOMON, J. E., W. R. DAVIS and P. L. LEE: A Self Compensated Monolithic Operational Amplifier with Low Input Current and High Slew Rate, ISSCC Digest Technical Papers, pp. 14-15, 1969.
49. WHALEN, J. J. and C. Paludi: Computer-Aided Analysis of Electronic Circuits - the Need to Include Parasitic Elements, International Journal of Electronics, vol. 43, pp. 501-511, November 1977.
50. FULLAGAR, D.: A New High Performance Monolithic Operational Amplifier, Fairchild Semiconductor Tech. Paper, 1968.
51. HAMILTON, D. J. and W. G. HOWARD: Basic Integrated Circuit Engineering, McGraw Hill, 1975.
52. GRAY, P. and R. MEYER: "Analysis and Design of Analog ICs," Wiley, New York, 1976.

53. NAGEL, W. L. and D. O. PEDERSON: SPICE-Simulation Program with Integrated Circuit Emphasis, Technical Memorandum No. ERL-M382, Electronic Research Laboratory, University of California, Berkeley, Calif., 94720, April 12, 1973.
54. HAJJ, I. N., D. J. ROULSTON and P. R. BRYANT: Generation of Transient Response of Nonlinear Bipolar Transistor Circuits from Device Fabrication Data, IEEE Journal of Solid-State Circuits, vol. SC-12, pp. 29-38, February 1977.
55. ROULSTON, D. J., S. G. CHAMBERLAIN and J. SEHGAL: Simplified Computer-Aided Analysis of Double-Diffused Transistors Including Two-Dimensional High-Level Effects, IEEE Transaction on Electron Devices, vol. ED-19, pp. 809-820, June 1972.
56. VALENTE, J. B., S. STRATAKOS: Nonlinear Circuit Analysis Program (NCAP) Documentation User's Manual, RADC-TR-79-245, Vol. II, Rome Air Development Center, Air Force Systems Command, Griffiss Air Force Base, New York 13441.
57. NATIONAL SEMICONDUCTOR: LM10/LM10B (L)/LM10C(L) Op Amp and Voltage Reference, National Semiconductor Corporation, 2900 Semiconductor drive, Santa Clara, Calif., 95051, December 1978.
58. WIDLAR, R. J.: Low Voltage Techniques, TP-14, National Semiconductor Corporation, 2900 Semiconductor Drive, Santa Clara, California 95051, December 1978.
59. WIDLAR, R. J., R. C. DOBKIN and M. YAMATAKE: New Op Amp Idea, AN 211, National Semiconductor Corporation, 2900 Semiconductor Drive, Santa Clara, California 95051, December 1978.
60. VALENTE, J. B. and S. STRATAKOS: Nonlinear Circuit Analysis Program (NCAP) Documentation Programmer's Manual, RADC-TR-79-245, Vol. III, Rome Air Development Center, Air Force Systems Command, Griffiss Air Force Base, New York 13441, September 1979.

61. SPINA, J. F., C. A. PALUDI, D. D. WEINER and J. J. WHALEN: *Nonlinear Circuit Analysis Program (NCAP) Documentation Engineering Manual*, RADC-TR-79-245, Vol. 1, Rome Air Development Center, Air Force Systems Command, Griffiss Air Force Base, New York 13441, September 1979.
62. WHALEN, J. J.: Private communication, State University of New York at Buffalo, Amherst, N.Y. 14226.
63. KRAJEWSKA, G. and F. E. HOLMES: Macromodeling of FET/Bipolar Operational Amplifiers, *IEEE Journal of Solid-State Circuits*, vol. SC-14, pp. 1083-1087, December 1979.
64. WEINER, D. D. and NADITCH, G. H.: A Scattering Variable Approach to the Volterra Analysis of Nonlinear Systems, *IEEE Trans. Microwave Theory Tech.*, vol. MTT-24, pp. 422-433, July 1976.

Appendix A

Reprint of Paper

Preprint of paper to be presented at International Conference on Electromagnetic Compatibility, University of Southampton, Great Britain, September 16-18, 1980.

MACROMODEL PREDICTIONS FOR EMI IN BIPOLAR OPERATIONAL AMPLIFIERS

Gordon K. C. Chen and James J. Whalen*

SUMMARY

A macromodel containing two transistors can accurately predict how amplitude modulated RF signals with RF carrier frequencies in the .05 to 100 MHz range are demodulated in a bipolar operational amplifier (uA741 op amp) to cause undesired low frequency responses related to the modulation envelope of the RF signals. The original op amp macromodel which was developed by Boyle et al. was modified by adding four capacitors (each 4 pF) to account for parasitic capacitance effects in the integrated circuit op amp. The macromodel can be used when the RFI signals are incident upon the op amp input terminals. The use of the macromodel leads to a substantial reduction in computer time and expense.

1. Introduction

The Nonlinear Circuit Analysis Program NCAP provides the EMC community with a usable procedure for analysis of electronic circuits which must operate in an EMI environment (ref.1-6). Among the nonlinear effects that NCAP can predict is demodulation. The use of NCAP to predict demodulation RFI effects in linear bipolar integrated circuits (ICs) such as broadband cascode amplifiers and operational amplifiers (op amps) has been demonstrated recently (ref.7-8). Up to now all NCAP simulations reported upon have used an approach in which every transistor is modeled. For example the 25 transistors shown in the op amp circuit in Fig. 1 were each modeled in ref.8. The objective of this paper is to demonstrate that the op amp macromodel shown in Fig. 2 which contains just two transistors can predict accurately how amplitude modulated (AM) RF signals with RF carrier frequencies in the .05 to 100 MHz range are demodulated in 741 op amps to cause undesired low frequency responses. An important point is that the computer time required for op amp macromodel calculations is approximately one-tenth the time required for op amp complete model calculations.

This paper is organized in the following manner. In Section 2 the op amp macromodel used with NCAP is shown. In Section 3 the unity voltage gain op amp circuit (voltage follower) used in the investigation is described. Also described are equivalent circuits using the op amp complete model in which 25 transistors are modeled and the op amp macromodel in which 2 transistors are modeled. NCAP predicted RFI effects are compared to experimental RFI effects in Section 4. The comparison will show that demodulation RFI effects predicted using the op amp macromodel are in good agreement both with those predicted using the op-amp complete model and with those determined experimentally.

* Department of Electrical Engineering, State University of New York at Buffalo, Amherst, New York 14226, U.S.A.

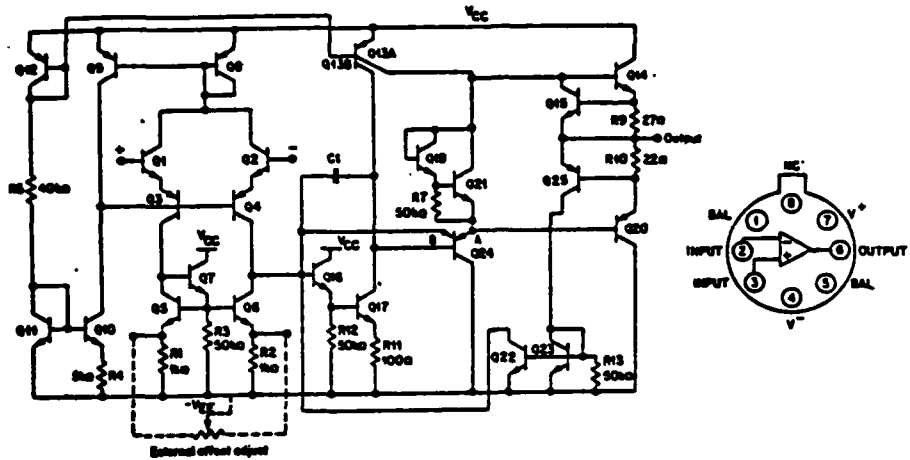


Fig. 1 Schematic of uA741 operational amplifier (op amp).

2. Op Amp Models

The computer program NCAP contains models for passive components such as resistors, capacitors, and inductors and for semiconductor devices such as pn-junction diodes, bipolar junction transistors, (BJTs) and field-effect transistors. To use NCAP, an equivalent circuit for the electronic circuit to be analysed must be developed using the available models. Then values for the model parameters must be specified. A schematic of the uA741 op amp used in this investigation is shown in Fig. 1. The uA741 op amp contains 25 BJTs. The direct approach is to model the op amp completely. Each of the 25 BJTs in the op amp is replaced by an appropriate BJT model. Predictions obtained using the direct approach on how amplitude modulated RF signals are demodulated in op amps to cause undesired low frequency responses have been reported upon recently (ref. 8). When every transistor in the op amp is modeled, computer simulations of op amp circuit performance can require long computation times and can be expensive. An alternative approach is to use the integrated circuit op amp macromodel developed by Boyle et al. which can accurately predict op amp input voltage - output voltage relationships for large-signal nonlinear transient operation (ref.9).

Shown in Fig. 2 is a circuit diagram for the op amp macromodel reported upon by Boyle et al. Since the macromodel is to be used with the computer program NCAP which performs nonlinear incremental analyses, several modifications have been made. The power supply terminals have been grounded. Four diodes used to provide current limiting and voltage saturation have been omitted because they are normally reverse-biased. The last modification involves adding capacitors C_{sub} from collector to ground and from emitter to ground for both macromodel transistors. The capacitors C_{sub} are added to account for parasitic capacitances associated with the pn-junctions used to provide isolation between transistors

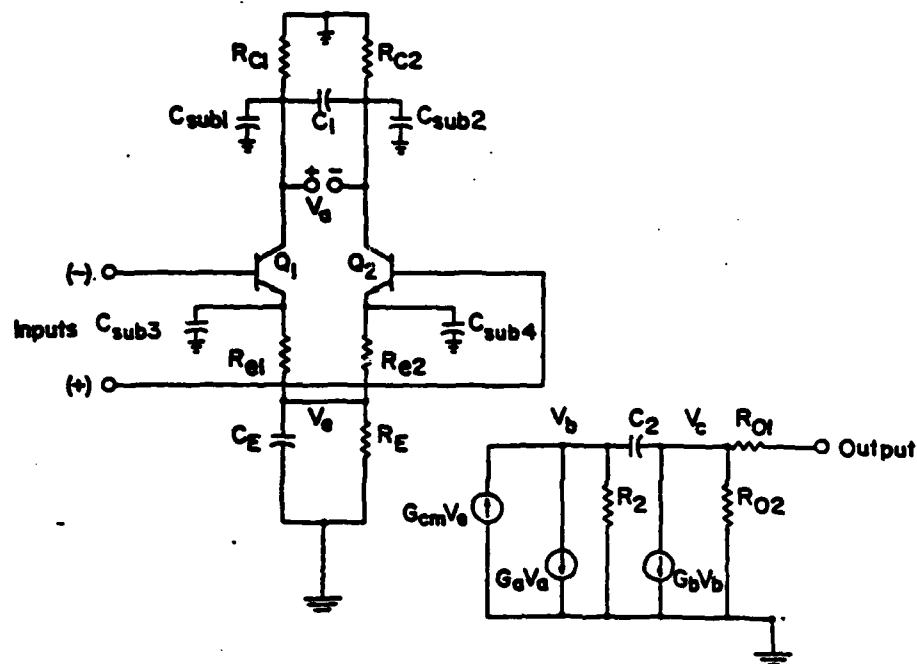


Fig. 2 Circuit diagram of op amp macromodel as modified for use with Nonlinear Circuit Analysis Program NCAP. Note the inclusion of four parasitic substrate capacitances C_{sub} .

in integrated circuit op amps. The importance of accounting accurately for parasitic junction capacitances in integrated circuit op amps was discussed previously when the op amp complete model was used to make RFI predictions (ref.8). It will be demonstrated in Section 4 that it is also important to account for the effects of parasitic junction capacitances when the op amp macromodel is used to make RFI predictions.

The op amp macromodel shown in Fig. 2 contains two BJTs. The NCAP model for the BJT is the nonlinear T model (ref.1-6). The nonlinear T model parameter values for the two BJTs in the op amp macromodel are given in Table 1. It is appropriate to comment briefly upon these values. The two transistors Q1 and Q2 in the op amp macromodel are in a differential pair configuration that corresponds to the differential pair formed by Q1 and Q2 in the op amp schematic shown in Fig. 1. The NCAP model parameter values for all 25 BJTs in the op amp are given in Table 1 of ref.8. The NCAP parameter values for transistors Q1 and Q2 in the op amp complete model are also used for transistors Q1 and Q2 in the op amp macromodel. These are two exceptions: (1) a dc collector current $I_C = 10 \mu A$ for Q1 and Q2 in the op amp macromodel is used because that value is specified by Boyle et al.; (2) the values for the parameter a were adjusted to obtain the values for the dc common-emitter short-circuit current-gain h_{FE1} and h_{FE2} specified by Boyle et al. (ref.9).

TABLE 1
NCAP INPUT PARAMETERS FOR uA741
OP AMP MACROMODEL

Parameter	'1	'2
n	4.34	4.34
V_{CB} (V)	14.57	14.57
V_{CBO} (V)	20	20
n	0.165	0.165
I_C (A)	10.E-6	10.E-6
I_{Cmax} (A)	0.5E-3	0.5E-3
a	0.90	0.62
I_{PEmax}	400	400
$k(F-V^{-5})$	1.23E-12	1.23E-12
Ref.	1.091	1.091
C_{je} (F)	1.23E-12	1.23E-12
C_2^l (F/A)	9.09E-9	9.09E-9
r_b (ohms)	830	830
r_c (ohms)	5.33E6	5.33E6
C_1 (F)	0.1E-12	0.1E-12
C_3 (F)	0.1E-12	0.1E-12

3. Op Amp Circuits

The situation of interest involves electromagnetic radiation (EMR) incident upon a system outer enclosure being coupled through apertures in the skin to the system interior. The interior EM fields induce RF voltages on the system cables. The RF voltages are conducted to semiconductor devices such as integrated circuits (ICs) located inside electronic equipment. The RF voltages can cause RFI effects in ICs. The specific case discussed in this paper is illustrated in Fig. 3. The RF voltage induced on a system cable is represented by an RF signal source with a 50 Ω impedance. The bipolar IC is an operational amplifier (op amp) which is being used in a unity voltage gain circuit called a voltage follower. The RF signal which is an amplitude modulated (AM) sinusoidal signal is being injected into the noninverting input terminal. Previous investigations have indicated that this case exhibits EM susceptibility at lower RF power levels than other cases (ref.10). The RFI effect investigated in this paper is caused by amplitude modulated RF signals being demodulated in the op amp to produce undesired low frequency responses related to the modulation envelope on the RF signals.

The computer program NCAP uses an iterative procedure to calculate non-linear responses. The first-order (linear) responses are calculated first. Then the first-order node voltages are used to calculate second-order current generators which may be viewed as the cause of the demodulation being investigated. In general discrepancies between predicted and measured first-order node voltages lead to larger discrep-

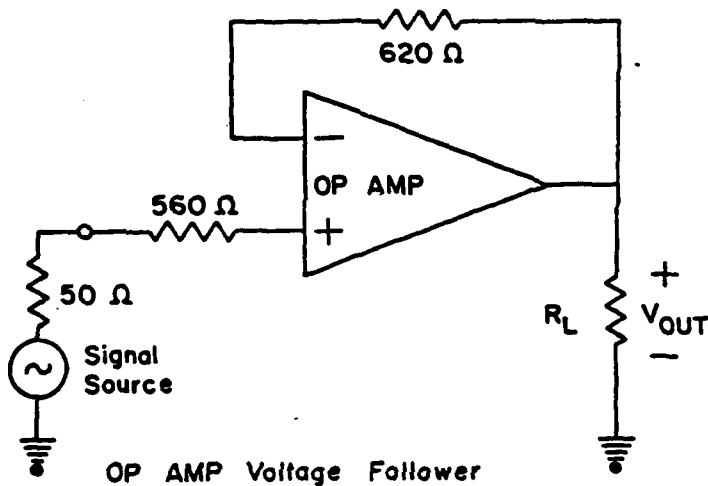


Fig. 3 Schematic illustrating the unity gain op amp voltage follower circuit investigated. The desired signals (unmodulated CW) and the EMI signals (AM modulated RF) were connected directly to the noninverting input terminal.

encies between predicted and measured second-order node voltages. For this reason considerable effort was expended in developing an accurate linear equivalent circuit for the voltage follower circuit shown in Fig. 3 (ref.8). Shown in Fig. 4 is the NCAP coding circuit diagram for the voltage follower circuit with the op amp complete model from ref.8. Shown in Fig. 5 is the same circuit with the op amp macromodel substituted for the op amp complete model. NCAP predictions made for the circuits shown in Figs. 4 and 5 will be compared to measured results in the next section.

4. Comparison of Experimental and Predicted RFI Results

The purpose of the investigation is to determine how well the op amp macromodel can predict the demodulation of RF signals in an op amp. This will be accomplished by comparing NCAP predictions made using the op amp macromodel to NCAP predictions made using the op amp complete model and to experimental results. The experimental results were obtained using the measurement system shown in Fig. 6. The op amp voltage follower was excited by amplitude modulated (AM) sinusoidal RF signals. The RF carrier frequency f_{RF} was varied over the range .050 to 100 MHz. The AM modulation index m was 0.5. The AM modulation frequency f_{AF} was 400 Hz. The voltage follower output voltage V_M at 400 Hz was measured on a tuned audio frequency (AF) voltmeter. The AF voltage V_M is related to the voltage follower second-order transfer function $H_2(f_1, -f_2)$ by

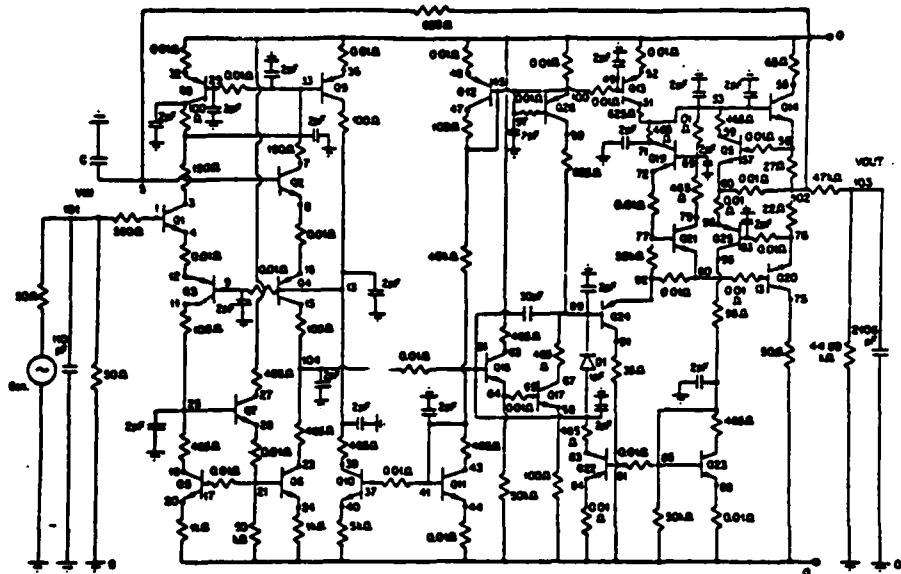


Fig. 4 NCAP coding circuit diagram for the voltage follower circuit with op amp complete model. The circuit shown corresponds to the experimental system shown in Fig. 6.

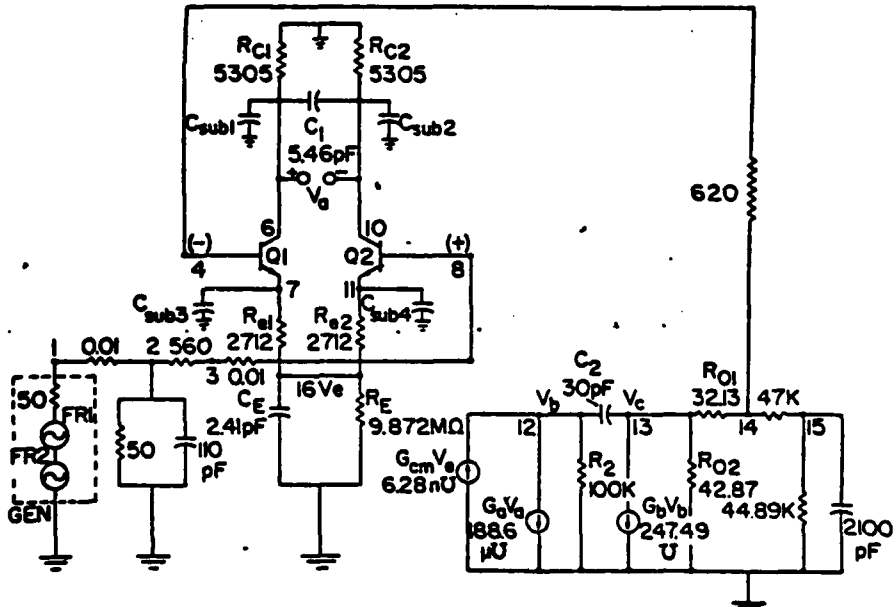
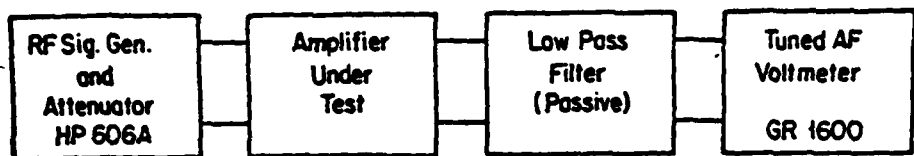


Fig. 5 NCAP coding circuit diagram for the voltage follower circuit with op amp macromodel. The circuit shown corresponds to the experimental system shown in Fig. 6.



$$f_1 = f_{RF}$$

f_{RF} = RF frequency

$$f_2 = f_{RF} - f_{AF}$$

f_{AF} = AF frequency

Modulation: 50% AM at f_{AF}

Fig. 6 Experimental system for measuring the second-order transfer function $H_2(f_1, -f_2)$.

$$V_M(\text{rms}) = (0.707)mA^2 H_2(f_1, -f_2) \quad (1)$$

where m is the modulation index, A the voltage amplitude of the RF signal generator, f_1 the RF carrier frequency f_{RF} , and f_2 the lower sideband frequency ($f_{RF} - f_{AF}$). In obtaining Eq. (1) it was assumed that the upper and lower sidebands contributed equally (ref.11). The voltage amplitude A can be calculated using

$$A = (8 \times P_{\text{gen}} \times R_{\text{gen}})^{0.5} \quad (2)$$

where P_{gen} is the available power from an RF signal generator with internal impedance R_{gen} . Using Eqs. (1) and (2), experimental values for the second-order transfer function $H_2(f_1, -f_2)$ can be determined in a manner that now will be described.

Shown in Fig. 7 is a plot of the tuned AF voltmeter rms voltage reading V_M versus the generator available RF power P_{gen} . For $P_{\text{gen}} < +5 \text{ dBm}$ the V_M values increase 10 dB for each 5 dB increase in P_{gen} , and Equation (1) is valid. For $P_{\text{gen}} > +5 \text{ dBm}$, the V_M values begin to increase more rapidly, and Equation (1) is no longer valid. Also shown on Fig. 7 is a dashed line which corresponds to the V_M values predicted by NCAP for second-order nonlinearities in the op amp voltage follower circuit. Higher-order nonlinear effects which may be important for $P_{\text{gen}} > +5 \text{ dBm}$ have not been considered in this investigation. The second-order transfer function $H_2(f_1, -f_2)$ may be interpreted as a normalized nonlinear (demodulation) response for the op amp voltage follower circuit at sufficiently low RF power levels (i.e. $P_{\text{gen}} < +5 \text{ dBm}$). Experimental values for $H_2(f_1, -f_2)$ can be determined at any point on the straight

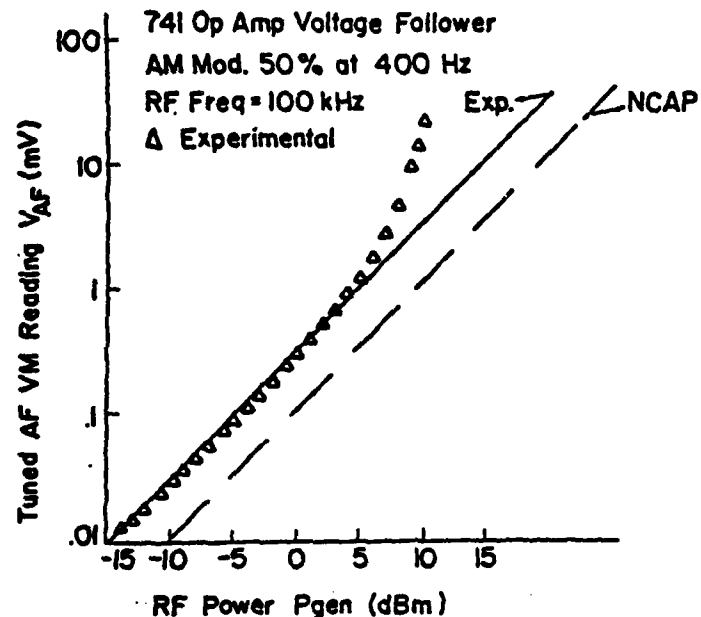


Fig. 7 Measured values for the rms audio frequency (AF) output voltage V_M vs RF input power P_{gen} for the op amp voltage follower circuit.

line drawn through the data for $P_{gen} < +5$ dBm. Using Eq. (1) and Eq. (2) with $R_{gen} = 50$ ohms and the V_M value at $P_{gen} = -10$ dBm, experimental values for $H_2(f_1, -f_2)$ were determined. These values are given in Table 2 and are plotted in Fig. 8.

Also shown in Fig. 8 are values for $H_2(f_1, -f_2)$ predicted by NCAP for the voltage follower circuit. One set of predicted values were obtained using the op amp complete model shown in Fig. 4; all parasitic substrate capacitances were assigned values of 2 pF. The other set of predicted values were obtained using the op amp macromodel shown in Fig. 5; all parasitic substrate capacitances were assigned values of 4 pF. The NCAP input coding list for Fig. 4 is given in ref. 8. The NCAP input coding list for Fig. 5 is given in Table 3. It is observed that the $H_2(f_1, -f_2)$ values predicted using the op amp macromodel agree well with the $H_2(f_1, -f_2)$ values predicted using the op amp complete model. For values of $H_2(f_1, -f_2) > -40$ dB, the differences are less than 5 dB. For values of $H_2(f_1, -f_2) < -40$ dB (a low value), the differences increase but are still less than 10 dB. The agreement between the op amp macromodel predictions and the op amp complete model predictions is very good. The

TABLE 2

SECOND-ORDER TRANSFER FUNCTION MEASUREMENT
WAT741 UNITY GAIN BUFFER WITH
 $P_{\text{out}} = -10 \text{ dBm}$ and $f_{\text{AF}} = 400 \text{ Hz}$

RF Freq. $f_{\text{RF}}(\text{Hz})$	AF VM Read. VM (rms mV)	$H_2(f_1, -f_2)$ ^a (dB)
50 k	0.008	-64.94
60 k	0.011	-62.17
70 k	0.015	-59.48
80 k	0.019	-57.42
90 k	0.0235	-55.58
100 k	0.029	-53.75
150 k	0.064	-46.08
200 k	0.112	-42
250 k	0.18	-37.9
300 k	0.27	-34.37
400 k	0.925	-28.6
500 k	0.92	-23.724
600 k	1.5	-19.48
700 k	2.2	-16.15
800 k	3.0	-13.46
900 k	3.85	-11.29
1 M	4.7	-9.56
1.5 M	7.1	-5.97
2 M	6.4	-6.88
3 M	6.4	-6.88
4 M	7.0	-6.2
5 M	7.9	-6.2
6 M	7.4	-5.6
7 M	8.2	-4.72
8 M	9.0	-3.92
9 M	9.8	-3.18
10 M	10.5	-2.58
15 M	13.5	-0.393
20 M	13.5	-0.393
30 M	14.5	-0.23
40 M	13.5	-0.393
50 M	12.0	-1.42
60 M	11.0	-2.17

^a The frequency $f_1 = f_{\text{RF}}$, and the frequency
 $f_2 = f_{\text{RF}} - f_{\text{AF}}$ where $f_{\text{AF}} = 400 \text{ Hz}$.

agreement between measured and predicted results shown in Fig. 8 may also be characterized as being quite good.

Shown in Fig. 9 are three sets of predicted values for $H_2(f_1, -f_2)$ obtained using the op amp macromodel shown in Fig. 5. The values assigned to the parasitic substrate capacitance C_{sub} are 0 pF, 2 pF, and 4 pF. It is apparent that the value assigned to C_{sub} has a major effect upon the $H_2(f_1, -f_2)$ values predicted as shown in Fig. 9. The value $C_{\text{sub}} = 4 \text{ pF}$ yields the best agreement between predicted and measured results.

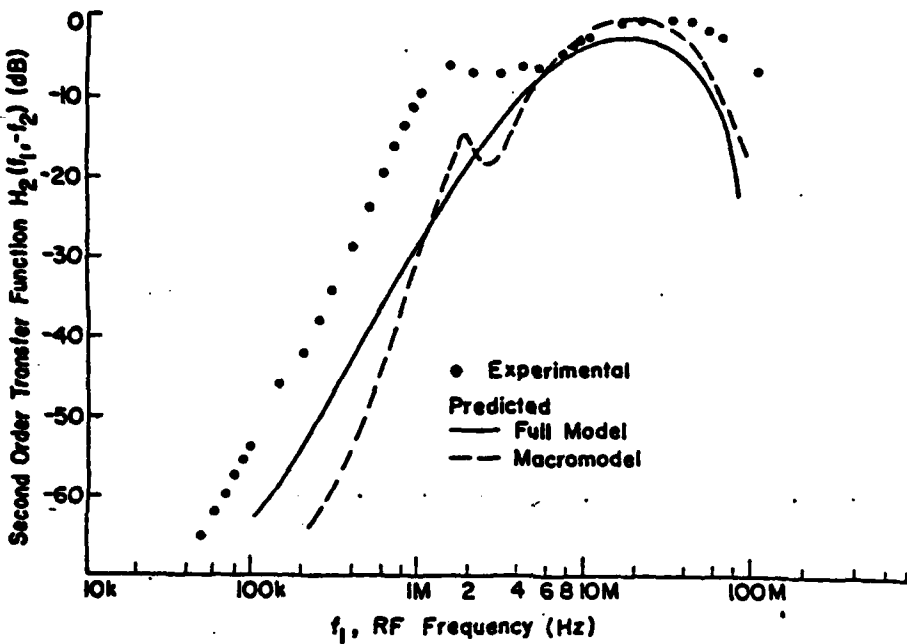


Fig. 8 Measured and predicted values for the second-order transfer function $H_2(f_1, -f_2)$ vs RF frequency for the op amp voltage follower. The measured values are from Table 2. One set of predicted values were obtained using the op amp complete model shown in Fig. 4 with all parasitic substrate capacitance values set at 2 pF. The other set of predicted values were obtained using the op amp macromodel shown in Fig. 5 with all parasitic substrate capacitance values set at 4 pF.

5. Conclusion

A macromodel has been used to predict RFI effects in a μ A741 op amp circuit. Specifically, the computer program NCAP was used to calculate how amplitude modulated RF signals incident upon the input terminals are demodulated in an op amp voltage follower circuit to produce undesired low frequency responses related to the modulation envelope of the RF carrier. A comparison between predicted and experimental values indicates that the macromodel can be used quite successfully to predict the demodulation RFI effects in an op amp circuit for RF frequencies up to 100 MHz. The op amp complete model can be used for RF incident upon any op amp terminal. The use of the op amp macromodel is restricted to the situation in which the RF is incident upon the op amp input terminals. This usually is the most susceptible case. When the RF signals are incident upon the op amp input terminals, the use of the macromodel (instead of the full model) leads to a substantial reduction in computer time and expense.

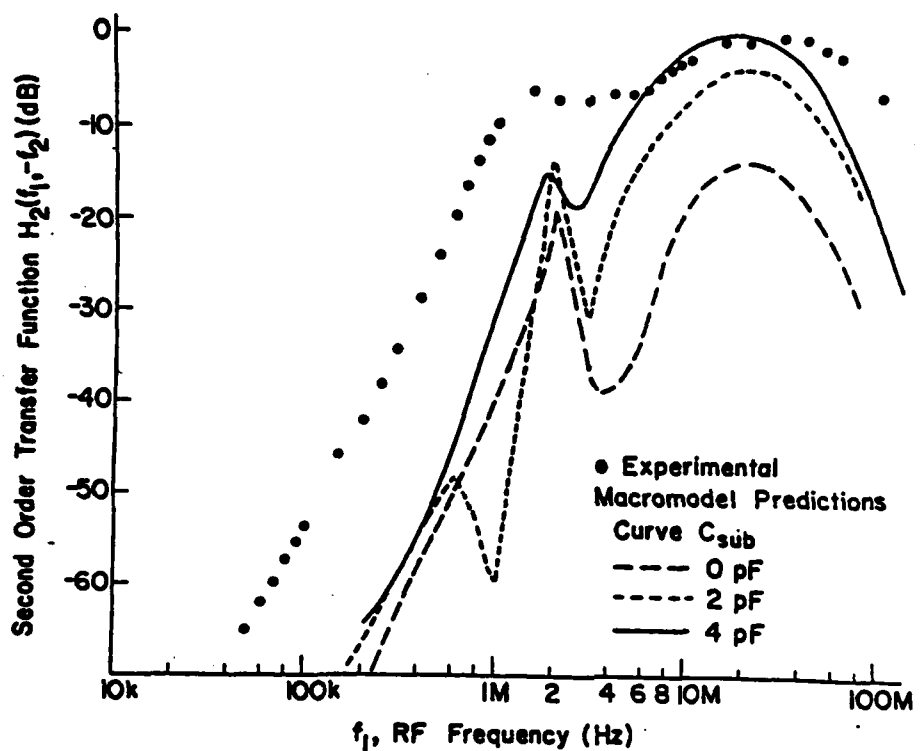


Fig. 9 Measured and predicted values for the second-order transfer function $H_2(f_1, -f_2)$ vs RF frequency for the op amp voltage follower. The measured values are from Table 2. The predicted values were obtained using the op amp macromodel shown in Fig. 5 with all parasitic substrate capacitance values set at 0, 2, or 4 pFs.

An important point is that the op amp macromodel developed by Boyle et al. has to be modified for RFI predictions at RF frequencies greater than 1 MHz. Four capacitors C_{sub} are added to account for parasitic capacitances associated with the pn-junctions used to provide isolation between transistors in the integrated circuit op amp. If these capacitors are omitted ($C_{sub} = 0$ pF), the RFI effects are underestimated by more than 10 dB. The value $C_{sub} = 4$ pF yields good agreement between predicted and measured RFI results.

TABLE 3
NCAP CODING FOR VOLTAGE FOLLOWER WITH MACROMODEL

```

** MACROMODEL OF 741 OP AMP          C 2 0 1.1E-10
** ANALYZED BY NCAP FOR H2          C 6 10 5.460E-12
** SUBMITTED AT SUNY BUFFALO        C 16 0 2.41E-12
** GNDH OUTPUT NODE IS 15          C 12 13 3.0E-11
** WITH SUBSTRATE CAPACITANCES    C 15 0 2.106E-9
** ADJUSTED PARAMETER TO SUIT      ** SUBSTRATE CAPACITANCES
** LM741 MACROMODEL BETA PARAMETER C 6 0 4.0E-12
* START CIRCUIT                  C 10 0 4.0E-12
* GENERATOR                      C 7 0 4.0E-12
NODE 1 0                          C 11 0 4.0E-12
FR 1 6.0E6 80.0E6 5 LIN          * TRANSISTOR
AMP 1 0.0                         NODE 4
FR 2 -7.9996E6 -79.999E6 5 LIN  4.34 14.57 20 0.165 10.05E-6 0.5E-3
AMP 1 0.0                         0.90 400 1.23E-12 1.091 1.23E-12
IMP 50 0                          9.09E-9 830 5.33E6 0.1E-12 0.1E-12
* LINEAR COMPONENTS
R 2 1 0.01                         * TRANSISTOR
R 2 3 560                          NODE 8
R 3 8 0.01                         4.34 14.57 20 0.165 10.05E-6 0.5E-3
R 2 0 50                           0.62 400 1.23E-12 1.091 1.23E-12
R 0 6 5305                         9.09E-9 830 5.33E6 0.1E-12 0.1E-12
R 7 10 2712                        * LINEAR DEPENDENT SOURCE
R 0 10 5305                        NODE 6 10 0 12
R 11 16 2712                       VC 1.886E-4 0.0
R 16 0 9.872E6                     * LINEAR DEPENDENT SOURCE
R 12 0 1.0E5                        NODE 16 0 12 0
R 13 0 42.87                        VC 6.28E-9 0.0
R 13 14 32.13                       * LINEAR DEPENDENT SOURCE
R 14 15 4.7E4                        NODE 12 0 0 13
R 15 0 4.489E4                      VC 247.49 0.0
R 14 4 620                          * END CIRCUIT
* END

```

References

1. J. W. Graham and L. Ehrman, "Nonlinear System Modeling and Analysis with Applications to Communications Receivers," Technical Report RADC-TR-73-178, Rome Air Development Center, Griffiss Air Force Base, New York 13441, June 1973.
2. J. J. Bussgang, L. Ehrman and J. W. Graham, "Analysis of Nonlinear Systems with Multiple Inputs," Proc. IEEE, vol. 62, pp. 1088-1119, August 1974.
3. D. D. Weiner and J. F. Spina, "The Modeling and Analysis of Weakly Nonlinear Systems," 1980. (to be published by Van Nostrand)
4. J. Valente, "The Nonlinear Circuit Analysis Program NCAP," 1977 IEEE International Electromagnetic Compatibility Symposium Record, pp. 461-466, Seattle, Washington, August 2-4, 1977.
5. J. Valente, S. Stratakos, J. F. Spina, D. D. Weiner, C. A. Paludi, Jr. and J. J. Whalen, "Nonlinear Circuit Analysis Program (NCAP) Documentation," Vols. I, II and III, Technical Report RADC-TR-79-245, Rome Air Development Center, Griffiss Air Force Base, New York 13441, September 1979.

6. J. J. Whalen, C. A. Paludi and T. F. Fang, "Applications of the Nonlinear Circuit Analysis Program NCAP," 1977 IEEE International Electromagnetic Compatibility Symposium Record, pp. 467-474, Seattle, Washington, August 2-4, 1977.
7. T. F. Fang and J. J. Whalen, "Application of the Nonlinear Circuit Analysis Program NCAP to Predict RFI Effects in Linear Bipolar Integrated Circuits," Proceedings of the 3rd Symposium and Technical Exhibition on Electromagnetic Compatibility, pp. 263-268, Rotterdam, May 1-3, 1979.
8. T. F. Fang, J. J. Whalen and G. K. Chen, "Using NCAP to Predict RFI Effects in Operational Amplifiers," 1977 IEEE International Electromagnetic Compatibility Symposium Record, pp. 96-103, San Diego, California, October 9-11, 1979.
9. G. R. Boyle, B. M. Cohn, D. O. Pederson and J. E. Solomon, "Macro-modelling of Integrated Circuit Operational Amplifiers," IEEE J. Solid-State Circuits, vol. SC-9, pp. 353-363, December 1974.
10. J. G. Tront, J. J. Whalen, C. E. Larson and J. M. Roe, "Computer-Aided Analysis of RFI Effects in Operational Amplifiers," IEEE Trans. on Electromagnetic Compatibility, vol. EMC-21, pp. 297-306, November 1979.
11. T. F. Fang, "Nonlinear System Analysis In Bipolar Integrated Circuits," Ph.D. dissertation, State University of New York at Buffalo, Amherst, New York 14226, USA, February 1979. A copy of the dissertation can be obtained from University Microfilm, 300 N. Zeeb Road, Ann Arbor, Michigan, 48106. (Also to be published as a Technical Report by RADC, Griffiss Air Force Base, New York 13441.)

Appendix B

LM10 Op Amp and Voltage Reference Data Sheets



DECEMBER 1978

LM10/LM10B(L)/LM10C(L) Op Amp and Voltage Reference

general description

The LM10 series are monolithic linear ICs consisting of a precision reference, an adjustable reference buffer and an independent, high quality op amp.

The unit can operate from a total supply voltage as low as 1.1V or as high as 40V, drawing only 270 μ A. A complementary output stage swings within 15 mV of the supply terminals or will deliver \pm 20 mA output current with \pm 0.4V saturation. Reference output can be as low as 200 mV. Some other characteristics of the LM10 are

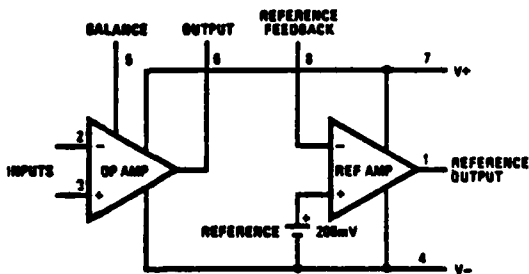
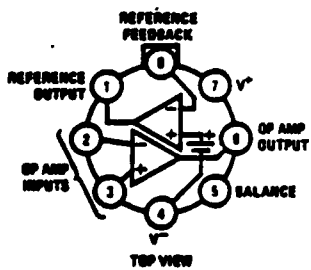
■ input-offset voltage	2.0 mV (max)
■ input-offset current	0.7 nA (max)
■ input-bias current	20 nA (max)
■ reference regulation	0.1% (max)
■ offset-voltage drift	2 μ V/ $^{\circ}$ C
■ reference drift	0.002%/ $^{\circ}$ C

The circuit is recommended for portable equipment and is completely specified for operation from a single power cell. In contrast, high output-drive capability, both voltage and current, along with thermal overload protection, suggest it in demanding general-purpose applications.

The device is capable of operating in a floating mode, independent of fixed supplies. It can function as a remote comparator, signal conditioner, SCR controller or transmitter for analog signals, delivering the processed signal on the same line used to supply power. It is also suited for operation in a wide range of voltage- and current-regulator applications, from low voltages to several hundred volts, providing greater precision than existing ICs.

This series is available in the three standard temperature ranges, with the commercial part having relaxed limits. In addition, a low-voltage specification (suffix "L") is available in the limited temperature ranges at a cost savings.

connection and functional diagrams



absolute maximum ratings

	LM10/LM10B/LM10C	LM10BL/LM10CL
Total supply voltage	48V	7V
Differential input voltage (note 1)	±40V	±7V
Power dissipation (note 2)		Internally limited
Output short-circuit duration (note 3)		Indefinite
Storage-temperature range	-55°C to +150°C	
Lead temperature (soldering, 10s)	300°C	

electrical characteristics (T_j = 25°C, T_{MIN} ≤ T_j ≤ T_{MAX}, note 4)

(Boldest type refers to limits over temperature range.)

PARAMETER	CONDITIONS	LM10/LM10B			LM10C			UNITS
		MIN	TYP	MAX	MIN	TYP	MAX	
Input offset voltage			0.3	2.0		0.5	4.0	mV
				3.0			5.0	mV
Input offset current (note 5)			0.25	0.7		0.4	2.0	nA
				1.5			3.0	nA
Input bias current			10	20		12	30	nA
				30			40	nA
Input resistance		250	500		150	400		kΩ
		150			115			kΩ
Large signal voltage gain	V _S = ±20V, I _{OUT} = 0 V _{OUT} = ±19.95V	120	400		80	400		V/mV
		80			50			V/mV
	V _S = ±20V, V _{OUT} = ±19.4V I _{OUT} = ±20 mA (±15 mA)	50	130		25	130		V/mV
		20			15			V/mV
	V _S = ±0.6V (0.65V), I _{OUT} = ±2 mA V _{OUT} = ±0.4V (±0.3V), V _{CM} = -0.4V	1.5	3.0		1.0	3.0		V/mV
		0.5			0.75			V/mV
Short gain (note 6)	1.2V (1.3V) ≤ V _{OUT} ≤ 40V; R _L = 1.1 kΩ 0.1 mA ≤ I _{OUT} ≤ 5 mA	14	33		10	33		V/mV
		6			6			V/mV
	1.5V ≤ V ⁺ ≤ 40V, R _L = 250Ω 0.1 mA ≤ I _{OUT} ≤ 20 mA	8	25		6	25		V/mV
		4			4			V/mV
Common-mode rejection	-20V ≤ V _{CM} ≤ 19.15V (19V) V _S = ±20V	93	102		90	102		dB
		87			87			dB
Supply-voltage rejection	-0.2V ≥ V ⁺ ≥ -38V V ⁺ = 1.0V (1.1V)	90	98		87	98		dB
		84			84			dB
	1.0V (1.1V) ≤ V ⁺ ≤ 38.8V V ⁻ = -0.2V	26	106		23	106		dB
		20			20			dB
Offset voltage drift			2.0			5.0		µV/°C
Offset current drift			2.0			6.0		pA/°C
Bias current drift	T _C < 100°C	60			90			pA/°C
Line regulation	1.2V (1.3V) ≤ V _S ≤ 40V 0 ≤ I _{REF} ≤ 1.0 mA, V _{REF} = 200 mV	0.001	0.003		0.001	0.008		%/V
			0.006			0.01		%/V
Load regulation	0 ≤ I _{REF} ≤ 1.0 mA V ⁺ = V _{REF} ≥ 1.0V (1.1V)	0.01	0.1		0.01	0.15		%
			0.15			0.2		%
Amplifier gain	0.2V ≤ V _{REF} ≤ 38V	50	75		25	70		V/mV
		23			18			V/mV
Feedback sense voltage	195	200	205	190	200	210		mV
	194		208	189		211		mV
Feedback current		20	50	65	22	75	90	nA
Reference drift			0.002			0.003		%/°C
Supply current		270	400	500	300	500	570	µA
Supply current change	1.2V (1.3V) ≤ V _S ≤ 40V	15	75		15	75		µA

electrical characteristics (T_j = 25°C, T_{MIN} ≤ T_j ≤ T_{MAX}, note 4)

(Boldface type refers to limits over temperature range.)

PARAMETER	CONDITIONS	LM108L			LM10C(L)			UNITS
		MIN	Typ	MAX	MIN	Typ	MAX	
Input offset voltage			0.3	2.0		0.5	4.0	μV
				3.0			5.0	μV
Input offset current (note 5)			0.1	0.7		0.2	2.0	nA
				1.5			3.0	nA
Input bias current			10	20		12	30	nA
				30			40	nA
Input resistance		250	500		150	400		kΩ
		150			115			kΩ
Large signal voltage gain	V _g = ±3.25V, I _{OUT} = 0 V _{OUT} = ±3.2V	60	300		40	300		V/mV
	V _g = ±3.25V, I _{OUT} = 10 mA V _{OUT} = ±2.78V	40			25			V/mV
	V _g = ±0.8V (0.65V), I _{OUT} = ±2 mA V _{OUT} = ±0.4V (±0.3V), V _{CM} = -0.4V	10	25		5	25		V/mV
	V _g = ±0.8V (0.65V), I _{OUT} = ±2 mA V _{OUT} = ±0.4V (±0.3V), V _{CM} = -0.4V	4			3			V/mV
Shunt gain (note 6)	1.5V ≤ V ⁺ ≤ 6.5V, R _L = 500Ω 0.1 mA ≤ I _{OUT} ≤ 10 mA	1.5	3.0		1.0	3.0		V/mV
		0.5			0.75			V/mV
Common-mode rejection	-3.25V ≤ V _{CM} ≤ 2.4V (2.25V) V _g = ±3.25V	80	102		80	102		dB
		83						dB
Supply-voltage rejection	-0.2V ≥ V ⁻ ≥ -0.4V V ⁺ = 1.0V (1.2V)	80	96		80	96		dB
	1.0V (1.1V) ≤ V ⁺ ≤ 6.3V V ⁻ = 0.2V	94	108		80	108		dB
		98						dB
Offset voltage drift			2.0			5.0		μV/°C
Offset current drift			2.0			5.0		pA/°C
Bias current drift			60			90		pA/°C
Line regulation	1.2V (1.3V) ≤ V _g ≤ 6.5V 0 ≤ I _{REF} ≤ 0.5 mA, V _{REF} = 200 mV	0.001	0.01		0.001	0.02		%/V
			0.02			0.03		%/V
Load regulation	0 ≤ I _{REF} ≤ 0.8 mA V ⁺ - V _{REF} ≥ 1.0V (1.1V)	0.01	0.1		0.01	0.15		%
			0.15			0.2		%
Amplifier gain	0.2V ≤ V _{REF} ≤ 5.5V	30	70		20	70		V/mV
		29			15			V/mV
Feedback series voltage		195	200	205	190	200	210	μV
		194		206	189		211	μV
Feedback current	C	20	50		22	75		nA
			65			90		nA
Reference drift			0.002			0.003		%/°C
Supply current		200	400		280	500		μA
			500			570		μA

Note 1: The input voltage can exceed the supply voltages provided that the voltage from the input to any other terminal does not exceed the maximum differential input voltage and excess dissipation is accounted for when V_{IN} < V⁻.

Note 2: The maximum operating-junction temperature is 150°C for the LM10, 100°C for the LM108(L) and 85°C for the LM10C(L). At elevated temperatures, devices must be derated based on package thermal resistance.

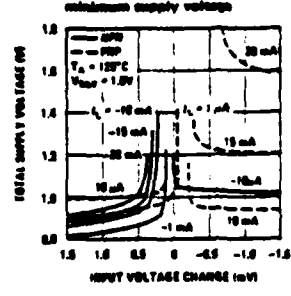
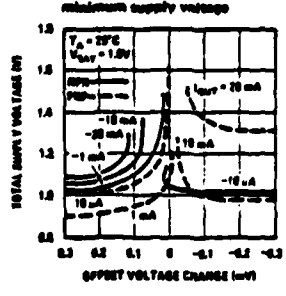
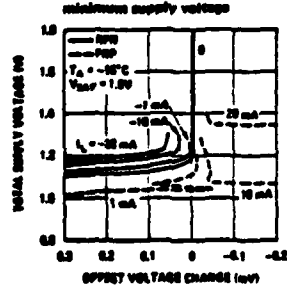
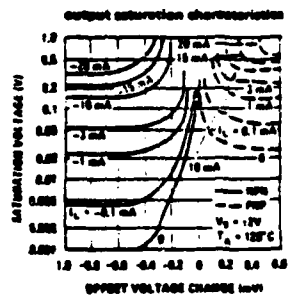
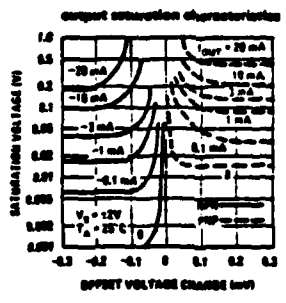
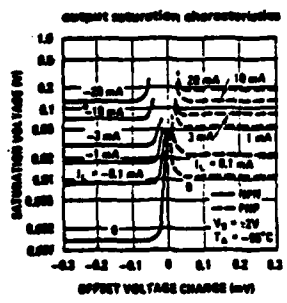
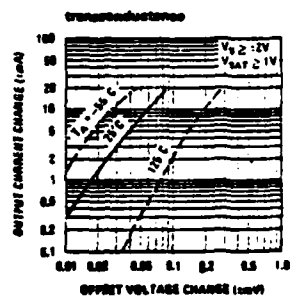
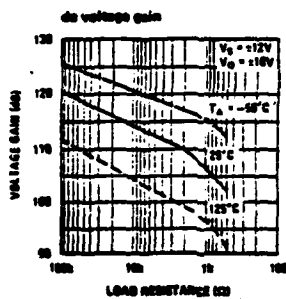
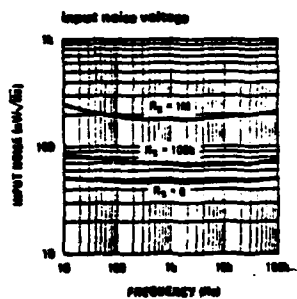
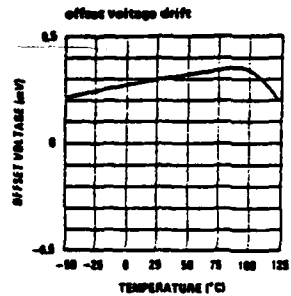
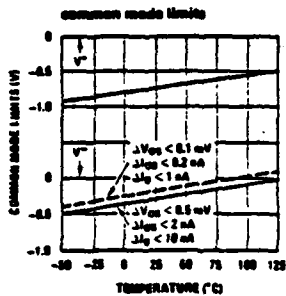
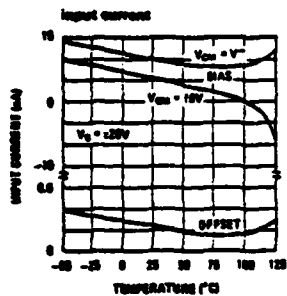
Note 3: Internal thermal limiting prevents excessive heating that could result in sudden failure, but the IC can be subjected to accelerated stress with a shorted output and worst-case conditions.

Note 4: These specifications apply for V⁻ ≤ V_{CM} ≤ V⁺ - 0.85V (1.0V), 1.2V (1.3V) ≤ V_g ≤ V_{MAX}, V_{REF} = 0.2V and 0 ≤ I_{REF} ≤ 1.0 mA, unless otherwise specified: V_{MAX} = 40V for the standard part and 6.5V for the low voltage part. Normal typeface indicates 25°C limits. Boldface type indicates limits and altered test conditions for full-temperature-range operation; this is -55°C to 125°C for the LM10, -25°C to 85°C for the LM108(L) and 0°C to 70°C for the LM10C(L). The specifications do not include the effects of thermal gradients (r_θ = 20 m²/W, die heating (r_θ = 0.23) or package heating. Gradient effects are small and tend to offset the electrical error (see curves).

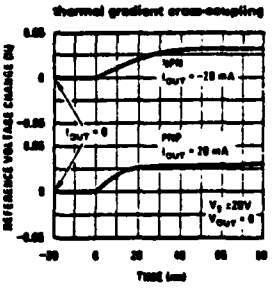
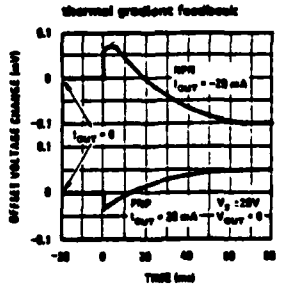
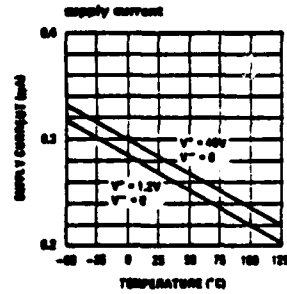
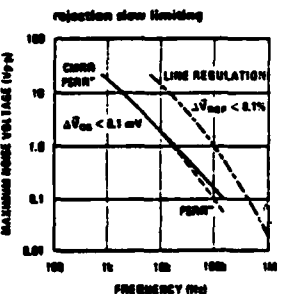
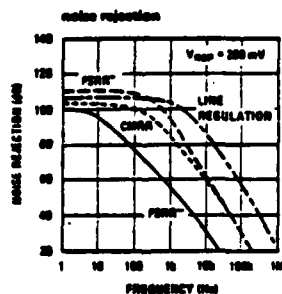
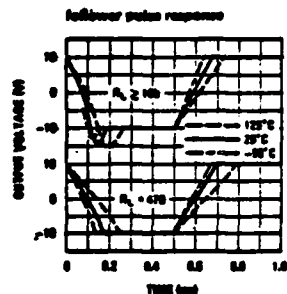
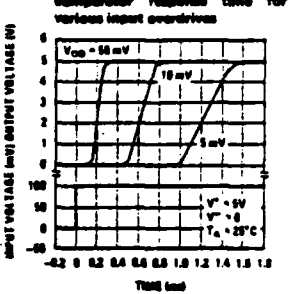
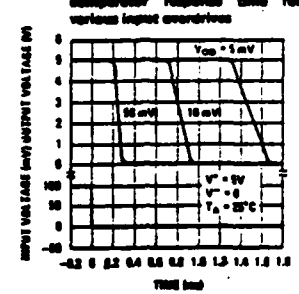
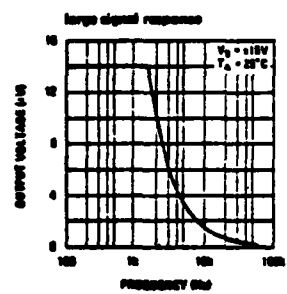
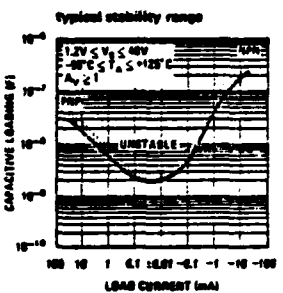
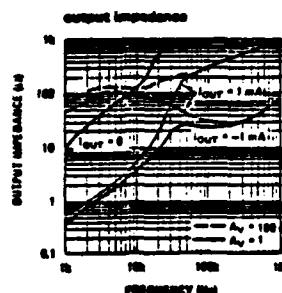
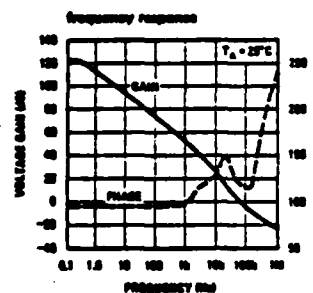
Note 5: For T_j > 80°C, I_{OG} may exceed 1.8 nA for V_{CM} = V⁻. With T_j = 125°C and V⁻ ≤ V_{CM} ≤ V⁺ + 0.1V, I_{OG} ≤ 5 nA.

Note 6: This defines operation in floating applications such as the bootstrapped regulator or two-wire transmitter. Output is connected to the V⁺ terminal of the IC and input common mode is referred to V⁻ (see typical applications). Effect of larger output-voltage swings with higher load resistances can be accounted for by adding the positive-supply rejection error.

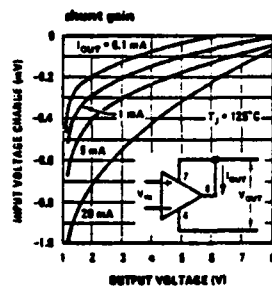
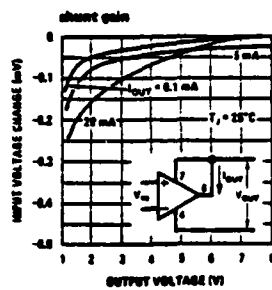
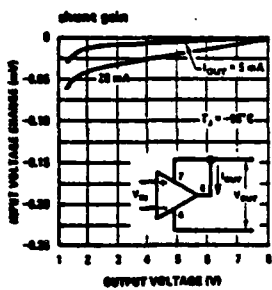
typical performance characteristics (op amp)



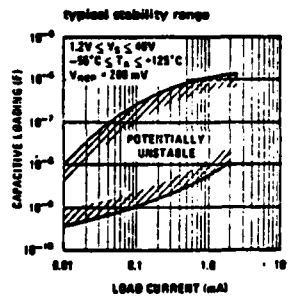
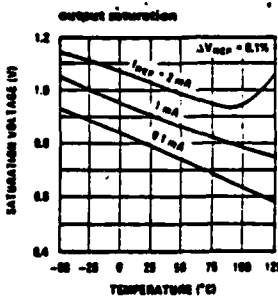
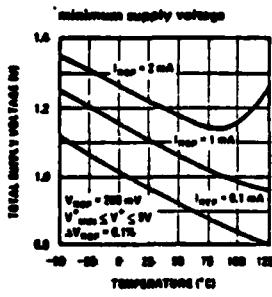
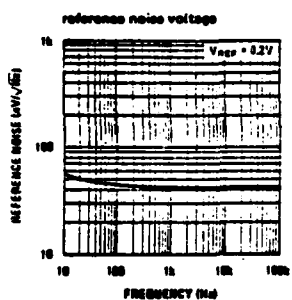
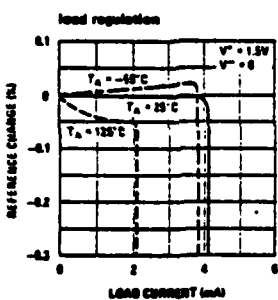
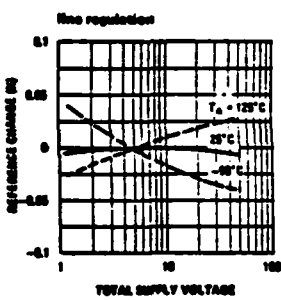
typical performance characteristics (op amp)



typical performance characteristics (op amp)



typical performance characteristics (reference)



definition of terms

Input offset voltage: That voltage which must be applied between the input terminals to bias the unloaded output in the linear region.

Input offset current: The difference in the currents at the input terminals when the output is unloaded in the linear region.

Input bias current: The absolute value of the average of the two input currents.

Input resistances: The ratio of the change in input voltage to the change in input current on either input with the other grounded.

Large signal voltage gain: The ratio of the specified output voltage swing to the change in differential input voltage required to produce it.

Shunt gain: The ratio of the specified output voltage swing to the change in differential input voltage required to produce it with the output tied to the V^+ terminal of the IC. The load and power source are connected between the V^+ and V^- terminals, and input common-mode is referred to the V^- terminal.

Common-mode rejection: The ratio of the input voltage range to the change in offset voltage between the extremes.

Supply-voltage rejection: The ratio of the specified supply-voltage change to the change in offset voltage between the extremes.

Line regulation: The average change in reference output voltage over the specified supply voltage range.

Load regulation: The change in reference output voltage from no load to that load specified.

Feedback sense voltage: The voltage, referred to V^- , on the reference feedback terminal while operating in regulation.

Reference amplifier gain: The ratio of the specified reference output change to the change in feedback sense voltage required to produce it.

Feedback current: The absolute value of the current at the feedback terminal when operating in regulation.

Supply current: The current required from the power source to operate the amplifier and reference with their outputs unloaded and operating in the linear range.



National Semiconductor
Corporate Headquarters
2900 Semiconductor Drive
Santa Clara, California 95051
Tel. (408) 727-5000
Telex (408) 325-2246

National Semiconductor Sales
Europe Headquarters 617/6
8800 Velpseweg 21
5500 GM Utrecht
The Netherlands
Tel. (030) 578000
Telex 65-23772

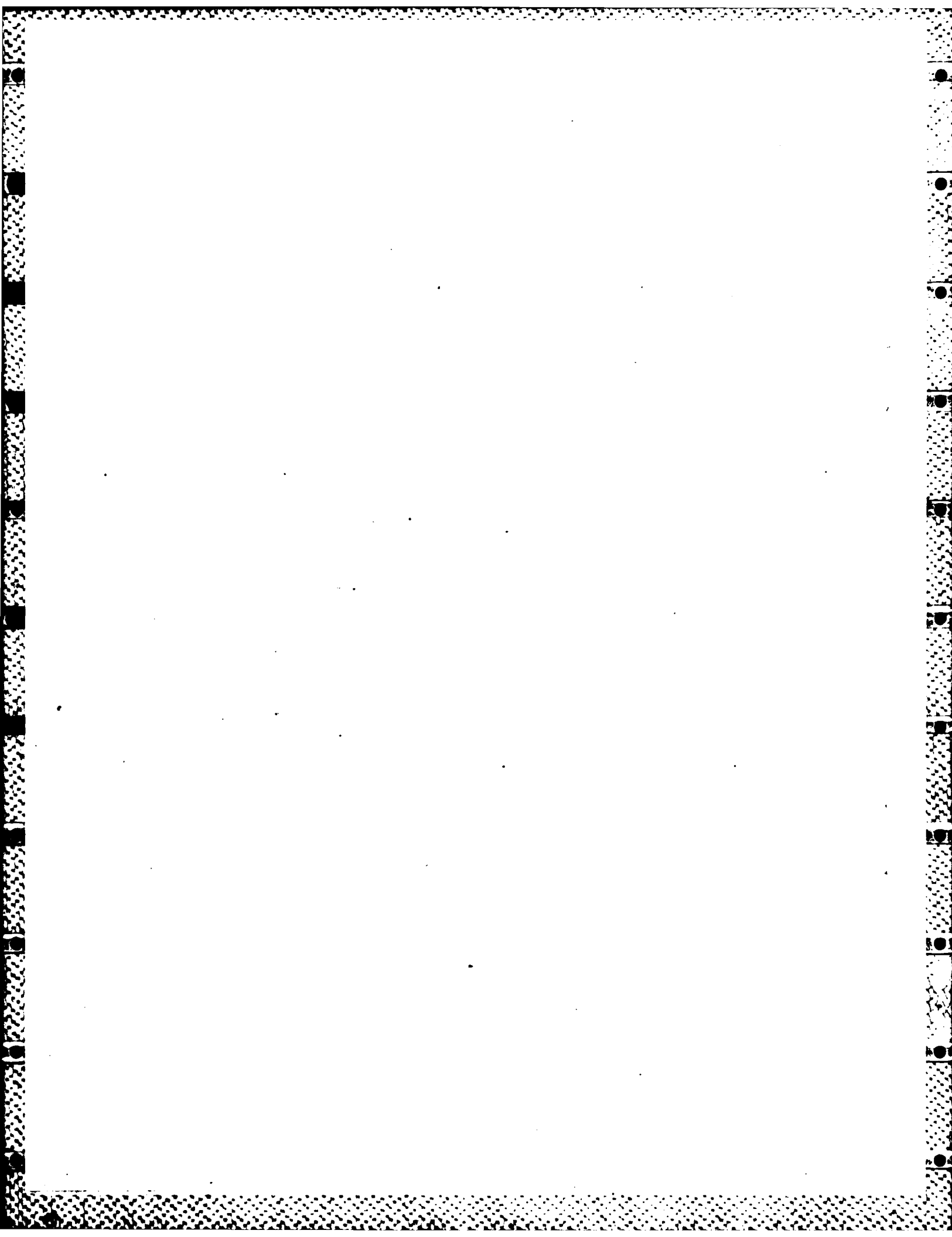
National Semiconductor
Nagoya Subsidiary
1-3 Yodogawa, Showan-cho 160
Nagoya, Japan
Tel. (052) 255-3711
Telex 232-2813 NSCJ-J

National Semiconductor
Hong Kong Ltd.
8/F, Pacific Building
100 Queen's Road East
Central, Hong Kong
4 Hung To Street
Kwai Chung
Hong Kong
Tel. (852) 557-2200
Telex 212000 CAGBIS SAB PHALD

National Semiconductor
India Operations, P.O. Box 644
11 Andheri (Connaught) 400 054
Mumbai, India
Japan Operations
8-12, 1-chome, Nishi-Shinjuku
Shinjuku-ku, Tokyo 160
Tel. (03) 334-6333
Telex 32096

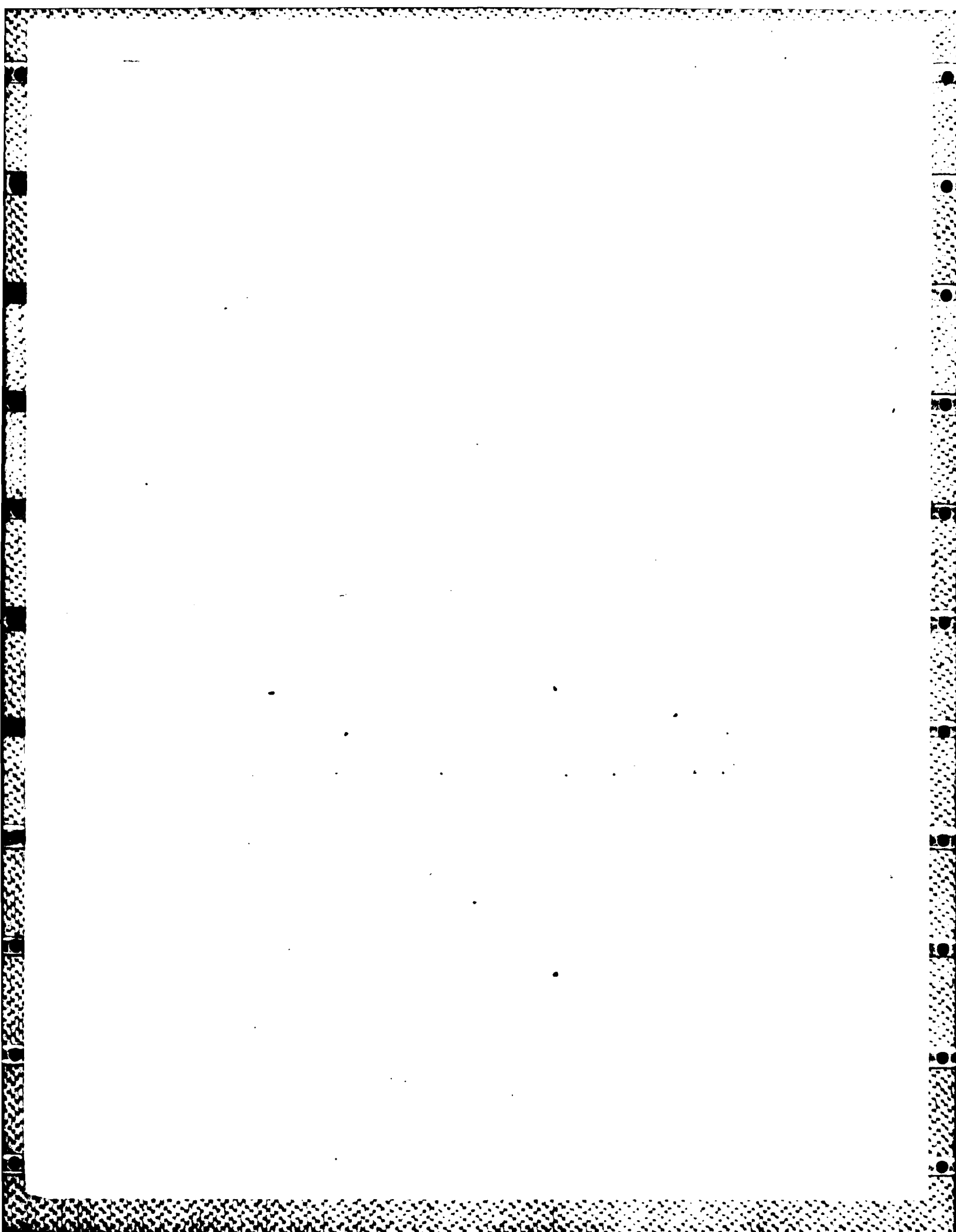
National Semiconductor
Caribbean Sales & Service 2193
Apex-ester, Victoria 2193
Barbados
Tel. (809) 427-6333
Telex 32096

National does not assume any responsibility for use of any circuitry described, no circuit patent licenses are implied, and National reserves the right at any time without notice, to change said circuitry.



MISSION
of
Rome Air Development Center

RADC plans and executes research, development, test and selected acquisition programs in support of Command, Control Communications and Intelligence (C³I) activities. Technical and engineering support within areas of technical competence is provided to ESD Program Offices (POs) and other ESD elements. The principal technical mission areas are communications, electromagnetic guidance and control, surveillance of ground and aerospace objects, intelligence data collection and handling, information system technology, ionospheric propagation, solid state sciences, microwave physics and electronic reliability, maintainability and compatibility.



SEARCHED

FILED

DISK